AN INVESTIGATION OF SIZE EXCLUSION AND DIFFUSION CONTROLLED MEMBRANE FOULING

by

COLIN MICHAEL HOBBS
BSCE University of Central Florida, 1998
BSEnvE University of Central Florida, 1998
MSEnvE University of Central Florida, 2000

A dissertation submitted in partial fulfillment of the requirements
for the degree of Doctor of Philosophy
in the Department of Civil and Environmental Engineering
in the College of Engineering and Computer Science
at the University of Central Florida
Orlando, Florida

Fall Term
2007

Major Professor: James S. Taylor

ABSTRACT

The reduction of membrane productivity (i.e. membrane fouling) during operation occurs in virtually all membrane applications. Membrane fouling originates from the method by which membranes operate: contaminants are rejected by the membrane and retained on the feed side of the membrane while treated water passes through the membrane. The accumulation of these contaminants on the feed side of the membrane results in increased operating pressures, increased backwashing frequencies, increased chemical cleaning frequencies, and increased membrane replacement frequencies. The most significant practical implication of membrane fouling is increased operating and maintenance costs. As such, membrane fouling must be properly managed to ensure successful and efficient operation of membrane systems. This document presents four independent studies regarding the fouling of size exclusion and diffusion controlled membranes. A brief description of each study is presented below.

The first study systematically investigated the fouling characteristics of various thin film composite polyamide reverse osmosis (RO) and nanofiltration (NF) membranes using a high organic surficial groundwater obtained from the City of Plantation, Florida. Prior to bench-scale fouling experiments, surface properties of the selected RO and NF membranes were carefully analysed in order to correlate the rate and extent of fouling to membrane surface characteristics, such as roughness, charge and hydrophobicity. More specifically, the surface roughness was characterized by atomic force microscopy, while the surface charge and hydrophobicity of the membranes were evaluated through zeta potential and contact angle measurements, respectively. The results indicated that membrane fouling became more severe with increasing surface

roughness, as measured by the surface area difference, which accounts for both magnitude and frequency of surface peaks. Surface roughness was correlated to flux decline; however, surface charge was not. The limited range of hydrophobicity of the flat sheet studies prohibited conclusions regarding the correlation of flux decline and hydrophobicity.

Mass loading and resistance models were developed in the second study to describe changes in solvent mass transfer (membrane productivity) over time of operation. Changes in the observed solvent mass transfer coefficient of four low pressure reverse osmosis membranes were correlated to feed water quality in a 2,000 hour pilot study. Independent variables utilized for model development included: temperature, initial solvent mass transfer coefficient, water loading, ultraviolet absorbance, turbidity, and monochloramine concentration. Models were generated by data collected throughout this study and were subsequently used to predict the solvent mass transfer coefficient. The sensitivity of each model with respect to monochloramine concentration was also analyzed.

In the third study, mass loading and resistance models were generated to predict changes in solvent mass transfer (membrane productivity) with operating time for three reverse osmosis and nanofiltration membranes. Variations in the observed solvent mass transfer coefficient of these membranes treating filtered secondary effluent were correlated to the initial solvent mass transfer coefficient, temperature, and water loading in a 2,000 hour pilot study. Independent variables evaluated during model development included: temperature, initial solvent mass transfer coefficient, water loading, total dissolved solids, orthophosphorous, silica, total organic carbon, and turbidity. All models were generated by data collected throughout this study. Autopsies performed on membrane elements indicated membranes that received microfiltered

water accumulated significantly more dissolved organic carbon and polysaccharides on their surface than membranes that received ultrafiltered water.

Series of filtration experiments were systematically performed to investigate physical and chemical factors affecting the efficiency of backwashing during microfiltration of colloidal suspensions in the fourth study. Throughout this study, all experiments were conducted in dead-end filtration mode utilizing an outside-in, hollow-fiber module with a nominal pore size of 0.1 μm. Silica particles (mean diameter ~ 0.14 μm) were used as model colloids. Using a flux decline model based on the Happel's cell for the hydraulic resistance of the particle layer, the cake structure was determined from experimental fouling data and then correlated to backwash efficiency. Modeling of experimental data revealed no noticeable changes in cake layer structure when feed particle concentration and operating pressure increased. Specifically, the packing density of the cake layer (l-cake porosity) in the cake layer ranged from 0.66 to 0.67, which corresponds well to random packing density. However, the particle packing density increased drastically with ionic strength. The results of backwashing experiments demonstrated that the efficiency of backwashing decreased significantly with increasing solution ionic strength, while backwash efficiency did not vary when particle concentration and operating pressure increased. This finding suggests that backwash efficiency is closely related to the structure of the cake layer formed during particle filtration. More densely packed cake layers were formed under high ionic strength, and consequently less flux was recovered per given backwash volume during backwashing.

ACKNOWLEDGMENTS

I would like to extend my sincere gratitude to the following individuals and organizations, without whose help I could not have completed this work. First and foremost, I would like to thank my advisor, Dr. James S. Taylor for the guidance and support he has given to me throughout my academic and professional career. I would also like to thank Dr. C. David Cooper, Dr. Debra Reinhart, Dr. Steven Duranceau, and Dr. Sudipta Seal for taking time out of their schedules to serve on my committee. Their knowledge and experience was invaluable in the process of completing this document.

In addition to my committee members, I would also like to thank the following individuals and organizations for their generous contributions throughout these four studies. Significant contributions made during each study are acknowledged below:

Acknowledgments for the study regarding the effect of surface roughness of reverse osmosis and nanofiltration membranes during the filtration of a high organic surficial groundwater include: my co-authors Dr. Seungkwan Hong and Dr. James S. Taylor; the American Water Work Association Research Foundation (AWWARF) for their financial support; the City of Plantation's Central Water Treatment Facility for their assistance in gathering both the operating data and source water; and the Advanced Material Processing and Analysis Center (AMPAC) at University of Central Florida and Dr. Amy Childress from the University of Nevada, Reno for their assistance in membrane surface characterization.

Significant contributions to the study of monochloramine degradation of thin film composite low pressure reverse osmosis membranes included: funding by the St. Johns River

Water Management District (SJRWMD) and the consulting engineering firm CH2MHill; and analytical, interpretative, and modeling efforts by the University of Central Florida.

Contributions to the performance modeling of nanofiltration and reverse osmosis membranes during the treatment of filtered secondary wastewater effluent and foulant identification were made by the following individuals and organizations: the Water Environment Research Foundation (WERF) and the consulting engineering firm Camp Dresser & McKee, Inc. (CDM) provided financial support; Ms. Barbara Hicks and the operations staff of the North Buffalo Water Reclamation Facility for their assistance during pilot testing; Dr. Francis DiGiano and the University of North Carolina at Chapel Hill for performing organic analyses; Meritech Environmental Laboratory, Inc. for performing inorganic analyses; and Membrane Forensics for conducting autopsies on the fouled membranes.

Acknowledgments for the study regarding variations in backwash efficiency during colloidal filtration of hollow-fiber microfiltration membranes include: my co-authors Dr. Seungkwan Hong, Praveen Krishna, Dohee Kim, and Dr. Jaeweon Cho; the American Water Works Association Research Foundation (AWWARF) and Brain Korea 21 (BK21) for funding this study; SK Chemicals for providing the hollow-fiber microfiltration membrane module; and Nissan Chemical Industries, Ltd. for providing the model silica colloids.

Finally, I would like to acknowledge the following journals for granting me permission to reproduce and reprint copyrighted material. Chapter 3 of this document was reprinted from Journal of Water Supply: Research and Technology – AQUA, volume 55, issue number 7-8, pages 559-570, with permission from the copyright holders, IWA Publishing. Chapter 6 of this

document was reprinted from Desalination – The International Journal on the Science and Technology of Desalting and Water Purification, volume 173, pages 257-268, by permission.

TABLE OF CONTENTS

LIST OF FIGURES

LIST OF TABLES

CHAPTER 1
INTRODUCTION

1.1 Background

Increases in population and development have increased potable water demands throughout the world and have stressed traditional, high quality sources of potable water. As a result, numerous potable water suppliers have resorted to utilizing alternative water sources of lesser quality, such as brackish groundwaters, highly turbid and organic surface waters, and wastewater effluent, to augment existing potable water supplies to meet potable water demands. However, treatment of these alternative water sources for immediate or future potable water supplies requires advanced processes capable of removing contaminants unaffected by conventional processes. Membrane separation processes represent one such advanced treatment technology that has been successfully utilized to treat alternative water sources for direct and indirect potable water uses.

Microfiltration (MF), ultrafiltration (UF), nanofiltration (NF), and reverse osmosis (RO) represent the four major classifications of membrane processes commonly utilized in water and wastewater treatment applications and are generally classified by contaminant removal mechanisms and pore size. Microfiltration and ultrafiltration membranes rely on size exclusion mechanisms to sieve contaminants from the source water. Microfiltration membranes are capable of removing contaminants as small as 0.1 μm to 10 μm, while the removal of contaminants as small as 0.01 μm to 0.1 μm is possible with ultrafiltration membranes. In contrast, nanofiltration and reverse osmosis membranes rely on size exclusion and diffusion

controlled mechanisms to remove contaminants from the source water. The removal of contaminants as small as 0.001 μm to 0.01 μm is possible with nanofiltration membranes, while reverse osmosis membranes are capable of removing contaminants as small as 0.0001 μm to 0.001 μm.

During normal operation, the contaminants removed by these membranes accumulate on the surface of the membrane and increase the resistance to water flow through the membrane, which ultimately results in the reduction of membrane productivity. These contaminants remain on the surface of the membrane until they are removed by an outside force, such as backwashing, in the case of microfiltration and ultrafiltration membranes; crossflow velocity, in the case of nanofiltration and reverse osmosis membranes; and chemical cleaning, in the case of all membranes. The reduction of membrane productivity (i.e. fouling) is a significant concern for all membrane applications and must be successfully controlled and/or managed to ensure efficient operation of facilities utilizing membrane separation processes.

1.2 Membrane Fouling

The significance of membrane fouling to the membrane community is evident from the attention this topic has received from numerous researchers. Membrane fouling is generally classified into one of the following four categories: scaling, biological fouling, organic matter fouling, and particulate fouling. Each of these categories is briefly discussed below.

The crystallization of sparingly soluble inorganic compounds on membrane surfaces and the subsequent reduction in membrane productivity during the operation of a membrane system is referred to as scaling. Scaling is affected by several factors, however, source water quality,

operating conditions (i.e. recovery rates), and membrane properties (i.e. solute rejection) are perhaps the most significant factors affecting the precipitation of sparingly soluble inorganic compounds. Nevertheless, inorganic compounds commonly associated with scaling include: carbonate, sulfate, and phosphate salts of calcium, barium, strontium, and aluminum; iron hydroxides; and silica. Current methods of controlling and managing the scaling of inorganic compounds include: pretreatment (i.e. pH adjustment and/or antiscalant addition); maintaining reasonable recovery rates; and the selection of appropriate membranes for treatment requirements.

Biological fouling of a membrane system is described as the reduction in membrane productivity due to the attachment and proliferation of microorganisms, including bacteria, algae, and fungi, on the surface of the membrane or within the pores of the membrane. Similarly, biological degradation of a membrane system is described as the reduction in the contaminant rejection capabilities of membranes due to damage caused by biological processes. Factors such as source water quality (i.e. microbial activity and nutrient concentrations) and operating conditions (i.e. permeation velocity, crossflow velocity, and operating time between cleaning events) greatly affect the extent of biological fouling and degradation. Current methods of inhibiting the biological fouling and degradation of membranes include: pretreatment (i.e. biocide addition); optimization of periodic membrane cleaning events (i.e. chemical cleaning agents, frequency, and duration); and the removal of macro and micro nutrients (i.e. carbon, phosphorous, nitrogen, etc.) from the source water.

The adsorption and accumulation of organic matter on membrane surfaces and within membrane pores and the resulting decrease in membrane productivity is referred to as organic

matter fouling. Organic matter includes a wide variety of components and can vary greatly with the source water. For example, surface water and surficial groundwater sources generally contain natural organic matter, of which a majority is comprised of humic substances, while wastewater sources contain a wide range of organic matter, including effluent organic matter, polysaccharides, extracellular polymeric substances, and soluble microbial products. Organic matter fouling is affected by numerous factors, including: source water quality (i.e. organic matter concentration), membrane characteristics (i.e. surface roughness, surface charge, and hydrophobicity), organic matter characteristics (i.e. hydrophobicity, composition, molecular weight, and charge), and operating conditions (i.e. permeation velocity and crossflow velocity). Currently, the selection of appropriate pretreatment processes and their subsequent optimization remains the only viable method of reducing organic matter fouling. Pretreatment processes including coagulation, sedimentation, and filtration and activated carbon have been successfully utilized to reduce organic matter fouling.

Particulate fouling of a membrane system is described as the reduction in membrane productivity due to the deposition and accumulation of particles on the membrane surface and/or within the membrane pores. Factors affecting the fouling of membranes by particulates include: membrane characteristics (i.e. surface roughness, surface charge, hydrophopicity, and pore size), particulate characteristics (i.e. size, charge, and concentration), operating conditions (i.e. permeation velocity and crossflow velocity), and source water quality. Appropriate pretreatment process selection and optimization currently remain the only feasible methods of reducing the particulate fouling of membranes.

1.3 Project Scope

The use of membrane separation processes to treat alternative water sources for direct and indirect potable uses have increased dramatically in recent years. However, the reduction of membrane productivity during long-term operation presents a significant concern for all facilities utilizing membrane processes and the control and/or management of membrane fouling is of paramount importance. As such, membrane fouling has been the subject of numerous bench-scale and pilot-scale studies.

The purpose of this document is to further the understanding of the causes of and factors affecting the reduction of membrane productivity during operation. Four independent studies were conducted to investigate the fouling of size exclusion and diffusion controlled membranes. The objectives of each of these studies are as follows:

Study 1: Thoroughly characterize the surface of various reverse osmosis and nanofiltration membranes in terms of surface roughness, surface charge, and hydrophobicity and relate the surface properties of the membranes to the decline in membrane productivity as determined from bench-scale studies using a highly organic groundwater.

Study 2: Develop accurate models to predict the productivity of low pressure reverse osmosis membranes treating a highly organic and turbid surface water as a function of operating time and water quality. In addition, evaluate the effect of monochloramine presence and concentration on the performance of low pressure reverse osmosis membranes.

Study 3: Develop accurate models to predict the productivity of nanofiltration and low pressure reverse osmosis membranes treating filtered secondary wastewater effluent as a function of operating time and water quality. In addition, identify the foulants accumulated on

the membrane surfaces through the destructive analysis of fouled membranes, often referenced as membrane autopsies.

Study 4: Examine the effect of feed water quality and operational parameters on the backwashing efficiency of hollow-fiber microfiltration membranes during the filtration of colloidal silica suspensions and relate the backwashing efficiency to the structure of the cake layer formed during filtration.

CHAPTER 2
LITERATURE REVIEW AND METHODOLOGY

2.1 Literature Review

The significance of membrane fouling to the membrane community is evident from the attention this topic has received from numerous researchers. However, the understanding of membrane fouling is compounded by the variety of substances that contribute to the reduction in membrane productivity. These substances include dissolved inorganic material, biological materials, organic matter, and particulates. Membrane fouling resulting from each of these substances is discussed in the following subsections.

2.1.1 Scaling

The rejection of ionic components contained in the feed stream by nanofiltration and/or reverse osmosis membranes may result in the supersaturation of sparingly soluble salts during high recovery operation. Should ionic concentrations exceed the solubility product of one or more salts, membrane fouling by salt crystallization will result (Stumm and Morgan, 1996; Okazaki and Kimura, 1984; Snoeyink and Jenkins, 1980). The scale generated from the crystallization of sparingly soluble salts on membrane surfaces results in the rapid and severe reduction of membrane productivity (Gilron and Hasson, 1987).

Current methods of controlling membrane fouling due to scaling include the adjustment the pH of the feed stream and the addition of antiscalants (WERF, 2005; Benefield et. al.,1982). While the adjustment of the pH of the feed stream is generally effective in preventing the formation of calcium carbonate scale, the addition of commercially available antiscalants is

generally effective in preventing the formation of a wide range of scales. The type and dosage of antiscalant required for a given application can be determined from a detailed analysis of the water quality of the feed stream or through the use of proprietary software packages available from membrane manufacturers. Limiting the operating recovery is also an effective method of controlling scaling, however, the practical implications of reducing the operating recovery make this method undesirable to municipal membrane systems.

Antiscalants are generally classified into one of two categories: polyelectrolytes (i.e. polyacrylic acids) and phosphorous-containing molecules (i.e. phosphates and phosphonates). Polyelectrolytes are effective antiscalants and are described as non-crystalline long chain polymers with carboxyl functional groups. While the detailed atomic configurations of polyelectrolyte antiscalants are proprietary, several researchers have proposed that this category of antiscalants consist of alternating carboxylic functional groups arranged in a three-fold helix (Austin et. al., 1975). Furthermore, these researchers hypothesized the carboxylic groups bond with calcium ions which prevent the formation of calcium scales. The configurations of phosphorous-containing antiscalants are also proprietary, however, it is hypothesized that phosphonates bond with calcium ions to prevent the scaling of calcium salts.

2.1.2 Biological Fouling

The fouling of membranes by biological means can occur in virtually any membrane system and occurs through the attachment and growth of microorganisms on the surface of the membrane. Microbial attachment occurs through the approach of the microbe to the membrane surface and the bonding of the microbe to the membrane surface. Once attached, microbial

growth occurs through the assimilation of nutrients, such as assimilable organic carbon, contained in the feed stream (Van der Kooij, 1992; Huck, 1990). The continual transport of nutrients to the attached microbes and the concentration of these nutrients by the membrane process allow for the maintenance and the proliferation of the biofilm under very limited nutrient concentrations (Bryers, 1993).

Common methods of controlling the biological fouling of membranes include: the addition of biocides, periodic chemical cleaning events, and the removal of nutrients. The addition of biocides upstream of membrane treatment has proven to be effective in the prevention of biological fouling (Brandt et. al., 1993; Flemming, 1993; LeChevallier, 1987, 1991). Both monochloramine and sodium bisulfite have been used as biological inhibitors during membrane treatment due to their biocidal properties and their compatibility with a variety of membrane materials (Reiss et. al., 1999; Ridgeway and Flemming, 1996). The periodic chemical cleaning of membrane systems represents another effective method of controlling the biological fouling of membranes. The effectiveness of these cleaning events is affected by the composition of the cleaning solution and the cleaning frequency. While the composition of cleaning solutions vary, most solutions utilized to clean biologically fouled membranes contain one or more surfactants which aid in the decomposition of the biofilm structure (Ridgeway and Flemming, 1996). The removal of nutrients from the feed stream is also an effective method of controlling the biological fouling of membranes, however, complexities and expenses associated with nutrient removal limit the practicality of this method of biofouling control.

2.1.3 Organic Matter Fouling

Virtually all natural sources of water contain organic matter that can reduce the productivity of membrane systems during operation. A significant fraction of dissolved organic matter in natural aquatic environments is attributed to the presence of humic substances, anionic macromolecules of low to moderate molecular weight. In contrast, wastewater supplies contain a wide range of organic matter including effluent organic matter, polysaccharides, extracellular polymeric substances, and soluble microbial products (WERF, 2005). The rejection and subsequent accumulation of these organic compounds on the surface of membranes results in the organic fouling of membranes. The mechanisms by which organic matter fouls membranes are complex and are affected by various chemical and physical factors including membrane characteristics, properties of organic matter, and feed solution chemistry (Hobbs, 2000).

Organic fouling and the factors that affect the organic fouling of membranes have been studied extensively by the membrane community. Research has indicated that the adsorption of humic substances onto hydrophobic membranes is more pronounced than adsorption onto hydrophilic membranes (Cho et. al., 1999; Jucker and Clark, 1994). Additional studies revealed hydrophobic fractions of natural organic matter resulted in more prominent membrane fouling when compared to hydrophilic fractions (Nilson and DiGiano, 1996).

The effect of feed solution chemistry on the extent of organic fouling was investigated in several studies. A significant decline in membrane productivity was observed by Braghetta et. al. (1997) during the nanofiltration of a high ionic strength, low pH solution containing aquatic natural organic matter. Additional studies conducted by Bonner (1993) and Lahoussine-Turcaud et. al. (1990) revealed membrane fouling by humic acid was exacerbated in the presence of

divalent cations. Furthermore, a series of studies conducted by Hong and Elimelech (1997) confirmed the fouling of membranes by natural organic matter was intensified as the solution pH decreased and the ionic strength and the presence of divalent cations increased.

2.1.4 Particulate Fouling

The reduction in membrane productivity due to the deposition and accumulation of particles on the surface and/or within the pores of a membrane is referenced as particulate fouling. There are three major modes of particulate fouling: cake formation (Huang et. al., 1998; Huisman et. al., 1998; Hong et. al, 1997), pore blocking (Madaeni, 1998; Timmer, et. al., 1997), and particle adsorption (Boyd and Zydney, 1998; Carlsson et. al., 1998; Lindau et. al., 1998), however, membrane fouling due to cake formation is typically the dominant mode of long term particulate fouling (Belfort et. al., 1994).

A qualitative description of the various modes of particulate fouling can be derived from a consideration of the relative sizes of the membrane pore, and the colloidal particle, (Belfort et. al., 1994). Particles considerably larger than membrane pores can not enter the pores and accumulate on the surface of the membrane, resulting in cake formation. In contrast, particles smaller than membrane pores can result in additional modes of particulate fouling, including the physical blocking of membrane pores and the adsorption of particles to the pore walls. In most membrane filtration operations, the mean membrane pore diameter is selected in such a way that a vast majority of the particles targeted for separation are larger than the pore size. However, due to the inherent broad distribution of pore sizes in commercial membranes (Ohya et. al., 1998;

Bowen et. al., 1997), intrusion of particles into the membrane matrix can not be completely precluded.

An important distinction between cake formation and the other two modes of particulate fouling is the reversibility of the former (Maartens et. al., 1998; Lindau and Jonsson, 1994). Generally, the quantity of particles deposited on the surface of the membrane can be minimized during operation through the adjustment of the crossflow velocity and other operating conditions (Chellam et. al., 1998; Faibish et. al., 1998). Should the accumulation of particles on the membrane surface result in excessive reductions in membrane productivity, cake deposits can be virtually completely removed through a high crossflow velocity flush. Contrary to cake formation, particulate fouling by pore blocking or adsorption is generally irreversible and can partially be removed by backwashing (Kennedy et. al., 1998) or aggressive chemical cleaning.

2.2 Methodology

The causes of and factors affecting the reduction of membrane productivity during operation were examined through four independent studies. The methodology used throughout each of these studies is presented below. Additional details regarding the methodology of each study are presented in subsequent chapters of this document.

Study 1: The source water used in this study was an organic rich groundwater from the surficial Biscayne Aquifer. The molecular weight distribution of the natural organic matter present in this source water was determined by high performance liquid chromatography-size exclusion chromatography which allowed a separation range of 1.0 kDa to 30.0 kDa. The structure of the organic matter was resolved through fractionation using XAD-8 and XAD-4

resins; hydrophobic organic matter was adsorbed by the XAD-8 resin, transphilic organic matter was adsorbed by the XAD-4 resin, and hydrophilic organic matter was not absorbed by either resin. Organic material adsorbed onto the XAD-8 and XAD-4 resins were removed with a sodium hydroxide solution and the mass fractions of each structure were determined through measurement of the dissolved organic carbon of each sodium hydroxide solution and the resin effluent.

The surfaces of three reverse osmosis membranes (BW-30FR, Dow/FilmTec; LFC-1, Hydranautics; and X-20, Trisep) and three nanofiltration membranes (NF-70, Dow/FilmTec; TFC-ULP, Koch/Fluid Systems; and HL, Osmonics) were thoroughly characterized in terms of roughness, charge (zeta potential), and hydrophobicity (contact angle), such that the fouling observed during subsequent fouling experiments could be related to surface properties. The roughness of each membrane surface was determined directly through atomic force microscopy. The Digital Instruments NanoScope™ scanned the surface of each membrane with an oscillating cantilever during which the vertical position of the cantilever was recorded at each (x, y) position. These data made it possible to determine a host of parameters, including the average roughness and the three-dimensional surface area. The surface charge of each membrane was estimated through the analysis of the streaming potential measured by the Brookhaven Instruments BI-EKA. In order to avoid ionic interference, the acid and base legs of each titration, referenced to the initial pH, were titrated with separate membrane samples in order to generate zeta potential curves for each membrane from pH 3 to 11. The hydrophobicity of each membrane was estimated through the measurement of contact angles with a Rame-Hart Goniometer.

Bench scale fouling studies were conducted for each membrane using the organic rich groundwater from the Biscayne Aquifer. The bench scale membrane filtration unit consisted of two stainless steel test cells with backpressure regulators and permeate and concentrate flowmeters, a positive displacement feed pump, and a feed reservoir with a stainless steel heat exchange coil for temperature control. Prior to each 48-hr fouling study, the membrane was stabilized with a 10^{-3} M sodium bicarbonate solution for 18 hrs to 24 hrs. The initial flux rates for both the stabilization period and the fouling study was set at 17 gallons per square foot per day (gfd). Variations in permeate flux were monitored and recorded to assess the performance of each membrane.

Study 2: The source water used throughout this study was a highly organic and turbid surface water with moderate dissolved solids from the St. Johns River at Lake Monroe. Advanced pretreatment was provided by two distinct processes: ultrafiltration with in-line ferric sulfate coagulation and ferric sulfate coagulation with ballasted flocculation and dual media filtration. Following the advanced pretreatment processes, a commercially available antiscalant, as well as ammonium hydroxide and sodium hypochlorite, were added to each process stream to control scaling and biological activity in the subsequent membrane treatment units. Low pressure reverse osmosis membrane treatment was provided for each pretreated water by four different thin film composite membranes, the Hydranautics LFC1, the Trisep X20, the Osmonics SG, and the Dow/FilmTec BW30FR.

Simultaneous pilot scale membrane testing was conducted for each advanced pretreatment train using a total of eight modified Osmonics E-2200 single element pilot units. Each test unit contained a 5 μm cartridge filter, a high pressure feed pump, a pressure vessel, one

4-inch diameter, 40-inch long membrane element, a concentrate recirculate loop, and various pressure gauges and flow meters for the monitoring and recording of operating conditions. Constant operating conditions were maintained for all single element pilot units through the manipulation of feed, recycle, concentrate, and permeate control valves. Target recovery and flux values were 70 percent and 12 gfd, respectively. Operating conditions were measured and recorded twice daily during the study.

Raw, feed, permeate, and concentrate samples were collected from each single element pilot unit on a weekly basis. All samples were transported to the Environmental Systems Engineering Institute (ESEI) at the University of Central Florida for storage and analysis. Water quality parameters of interest included chloride, sulfate, bromide, and silicon, measured by ion chromatography; sodium, calcium, magnesium, strontium, iron, and barium, measured by atomic absorption spectrometry; non-purgable dissolved organic carbon, measured by a total organic carbon analyzer; UV-254, measured by a spectrophotometer with a 1-cm path length; total dissolved solids, measured by summing the concentrations of seven major inorganic ions (calcium, magnesium, sodium, bicarbonate, sulfate, chloride, and silicon); and alkalinity, measured by titration.

Mass loading and resistance models were developed to predict solvent mass transfer through each thin film composite membrane evaluated in this study as a function of time and several independent variables. Independent variables of interest included: temperature, the initial solvent mass transfer coefficient, water loading, ultraviolet absorbance, turbidity, and monochloramine concentration. All models were evaluated using non-linear regression techniques. Sensitivity analyses were performed for all models to determine the responsiveness

of the solvent mass transfer coefficient predicted by each model to monochloramine concentration and run time.

Study 3: The source water used throughout this study was filtered secondary effluent from the North Buffalo Water Reclamation Facility in Greensboro, North Carolina. Advanced pretreatment was provided by two different processes: microfiltration and ultrafiltration with in-line ferric sulfate coagulation. No further physical or chemical pretreatment was provided prior to subsequent membrane treatment. Low pressure reverse osmosis and nanofiltration membrane treatment was provided for each pretreated water by three different thin film composite membranes, the Hydranautics ESPA2, the Dow/FilmTec NF90, and the Trisep X20.

Pilot scale membrane testing was conducted simultaneously for each advanced pretreatment train using two multi-train skid mounted test units. Each test unit contained a multi-stage centrifugal feed pump equipped with a variable frequency drive, three membrane trains, and various pressure gauges, flow meters, and valves to monitor and control the operation of each train. Each membrane train contained six 4-inch diameter, 40-inch long membrane elements arranged in series and configured to operate in a single stage. Constant operating conditions were maintained for all single stage membrane trains through the manipulation of the speed of the feed pumps and feed and concentrate control valves. The desired flux and recovery rates for all membrane trains were 8 gfd and 50 percent, respectively.

Samples of the feed, permeate, and concentrate streams were collected from each multi-train skid mounted unit on a bi-weekly basis. All samples were delivered to Meritech Inc. Environmental Laboratory and the University of North Carolina at Chapel Hill for analysis. the analysis of all inorganic parameters of interest, ammonia nitrogen, calcium, chloride,

nitrate/nitrite nitrogen, orthophosphate, silica, sodium, and total dissolved solids, were performed by Meritech. The University of North Carolina at Chapel Hill determined the total organic carbon concentration of all samples. Autopsies were performed on membrane elements removed from each train for both pilot units upon the completion of the operational portion of this study. Membrane Forensics of San Diego California performed loss on ignition tests and targeted energy dispersive X-ray analyses to determine the relative percentages of organic and inorganic foulants on the surface of the membranes and to identify the composition of the inorganic fractions, respectively. The University of North Carolina at Chapel Hill quantified both the amount of dissolved organic carbon and the amount of polysaccharides that had accumulated on the surface of the membranes during operation.

Mass loading and resistance models were developed to predict solvent mass transfer through each thin film composite membrane evaluated in this study as a function of time and several independent variables. Independent variables of interest included: temperature, the initial solvent mass transfer coefficient, water loading, total dissolved solids concentration, orthophosphorous concentration, silica concentration, total organic carbon concentration, and turbidity. All models were evaluated using non-linear regression techniques.

Study 4: A series of fouling and backwashing studies were conducted with a bench scale microfiltration unit and synthetic source waters containing various concentrations of colloidal silica particles. The colloidal silica particles were provided by Nissan Chemical Industries and were monodispersed with a mean particle diameter of 140 nm. Furthermore, these particles had a zeta potential ranging from -27 mV to -30 mV at a pH of 8 and a background sodium chloride concentration of 10^{-2} M.

The bench scale membrane filitration unit consisted of a hollow fiber microfiltration module, a positive displacement feed pump, a feed pressure gauge, permeate and concentrate flow meters, various control valves, and a feed reservoir with a stainless steel heat exchange coil for temperature control. The hollow fiber microfiltration membrane used throughout this study was provided by SK Chemicals and had the following specifications: nominal pore size of 0.1 μm, an inside fiber diameter of 0.7 mm, and outside fiber diameter of 1.0 mm, and a fiber length of 520 mm. Containing a total of 150 hollow fibers, the module contained approximately 0.25 m^2 of surface area.

Initial clean water tests were performed to determine the membrane productivity prior to each fouling experiment. Each clean water test was conducted in a dead-end mode of operation at a feed pressure of 6 psi with a background electrolyte solution identical to that which would be used for the subsequent fouling study (i.e. 10^{-3} M $NaHCO_3$ and 10^{-2} M NaCl). A total of 5 L of filtrate was collected, and a stopwatch was used to measure the collection times associated with 1, 2, 3, 4, and 5 L of filtrate accumulated.

Following the initial clean water test, feed, concentrate, and bypass valves were manipulated to achieve the desired initial operating conditions for the fouling study. Once stable operation was attained, the predetermined volume of concentrated silica particles was added to the feed solution to achieve the desired particle concentration. Immediately following the addition of silica particles, 5 L of filtrate was collected, and collection times were measured and recorded for 1, 2, 3, 4, and 5 L.

Once the fouling study was completed, 1 L of DI water was backwashed through the MF module at a pressure of 68.9 kPa (10 psi), and a final clean water test was conducted. Similar to

the initial clean water test, the final clean water test was conducted in a dead-end mode of operation at a feed pressure of 41.4 kPa (6 psi) with a background electrolyte solution identical to that which was used for the previous fouling study. Again, a total of 5 L of filtrate was collected, and a stopwatch was used to measure the collection times associated with 1, 2, 3, 4, and 5L. Normalized flux values and backwash efficiencies were calculated to assess the membrane performance during each fouling and backwashing study.

2.3 References

1. Austin, A. (1975) Chemical additives for calcium sulfate scale control. Desalination, 16(3):345-357.

2. Belfort, G.; Davis, R.; Zydney, A. (1994) The behavior of suspensions and macromolecular solutions in crossflow microfiltration. Journal of Membrane Science, 96:1-58.

3. Benefield, L.; Judkins, J.; and Weand, B. (1982) Process Chemistry for Water and Wastewater Treatment. Prentice-Hall, Inc., Englewood Cliffs, New Jersey.

4. Bonner, F. (1993) The effects of the dissolved organic matter on ultrafiltration for potable water treatment: experimental studies with natural and model compounds. Doctoral Dissertation, Johns Hopkins University, Baltimore, Maryland.

5. Bowen, W.; Hilal, N.; Lovitt, R.; Sharif, A.; and Williams, P. (1997) Atomic force microscopestudies of membranes: Force measurement and imaging in electrolyte solutions. Journal of Membrane Science, 126:77-89.

6. Boyd, R. and Zydney, A. (1998) Analysis of protein fouling during ultrafiltration using a two-layer membrane model. Biotechnology and Bioengineering, 59:451-460.

7. Braghetta; DiGiano, F.; and Ball, W. (1997) Nanofiltration of natural organic matter: pH and ionic strength effects. Journal of Environmental Engineering, ASCE, 123(7):628-641.

8. Brandt, D.; Leitner, G.; and Leitner, W. (1993) Reverse osmosis membranes state of the art, in Z. Amjad (ed.), Reverse osmosis: membrane technology, water chemistry, and industrial applications. Van Nostrand Reinhold, New York.

9. Bryers, J. (1993) Bacterial biofilms. Current Opinion of Biotechnology, (4):197-204.

10. Carlsson, D.; Dalcin, M.; Black, P.; and Lick, C. (1998) A surface spectroscopic study of membranes fouled by pulp mill effluent. Journal of Membrane Science, 142:1-11.

11. Chellam, S.; Jacangelo, J.; and Bonacquisti, T. (1998) Modeling and experimental verification of pilot-scale hollow fiber direct flow microfiltration with periodic backwashing. Environmental Science and Technology, 32:75-81.

12. Cho, J.; Amy, G.; and Pellegrino, J. (1999) Membrane filtration of natural organic matter: Initial comparison of rejection and flux decline characteristics with UF and NF membranes. Water Research, 33(11):2517-2526.

13. Faibish, R.; Elimelech, M.; and Cohen, Y. (1998) Effect of interparticle electrostatic double layer interactions on permeate flux decline in crossflow membrane filtration of colloidal suspensions – an experimental investigation. Journal of Colloid Interface Science, 204:77-86.

14. Flemming, H. (1993) Mechanistic aspects of reverse osmosis membrane biofouling and prevention, in Z. Amjad (ed.), Reverse osmosis: membrane technology, water chemistry, and industrial applications. Van Nostrand Reinhold, New York.

15. Gilron, J. and Hasson, D. (1987) Calcium sulfate fouling of reverse osmosis membranes – Flux decline mechanism. Chemical Engineering Science, 42(10):2351-2360.

16. Hobbs, C. (2000) Effect of membrane properties on fouling in RO/NF membrane filtration of high organic groundwater. Master's Thesis, University of Central Florida, Orlando, Florida.

17. Hong, S. and Elimelech, M. (1997) Chemical and physical aspects of natural organic matter (NOM) fouling of nanofiltration membranes. Journal of Membrane Science, 132:159-181.

18. Hong, S.; Faibish, R.; and Elimelech, M. (1997) Kinetics of permeate flux decline in crossflow membrane filtration of colloidal suspensions. Journal of Colloid Interface Science, 196:267-277.

19. Huang, L. and Morrissey, M. (1998) Fouling of membranes during microfiltration of surimi wash water – Roles of pore blocking and surface cake formation. Journal of Membrane Science, 144:113-123.

20. Huck, P. (1990) Measurement of biodegradable organic matter and bacterial growth potential in drinking water. Journal of American Water Works Association, 82:78-86.

21. Huisman, I.; Elzo, D.; Middelink, E.; and Tragardh, A. (1998) Properties of the cake layer formed during crossflow microfiltration. Colloids and Surfaces Physiochemical and Engineering Aspects, 138:265-281.

22. Jucker, C. and Clark, M. (1994) Adsorption of aquatic humic substances on hydrophobic ultrafiltration membranes. Journal of Membrane Science, 97:37-52.

23. Kennedy, M.; Kim, S.; Mutenyo, I.; Broens, L.; ad Schippers, J. (1998) Intermittent crossflushing of hollow fiber ultrafiltration systems. Desalination, 118:175-187.

24. Lahoussine-Turcaud, V.; Wiesner, M.; and Bottero, J. (1990) Fouling in tangential-flow filtration: The effect of colloid size and coagulation treatment. Journal of Membrane Science, 52:173-190.

25. LeChevallier, M. (1987) Disinfection of bacterial biofilms. Proceedings of the Sixth Conference on Water Disinfection: Environmental Impact and Health Effects, May 3-8, 1-20.

26. LeChevallier, M. (1991) Biocides and the current status of biofouling control in water systems, in H. Flemming and G. Geesey (eds.), Biofouling and Biocorrosion in Industrial Water Systems. Springer-Verlag, Berlin.

27. Lindau, J. and Jonsson, A. (1994) Cleaning of ultrafiltration membranes after treatment of oily wastewater. Journal of Membrane Science, 87:71-78.

28. Lindau, J.; Jonsson, A.; and Bottino, A. (1998) Flux reduction of ultrafiltration membranes with different cut-off due to adsorption of low-molecular weight hydrophobic solute – correlation between flux decline and pore size. Journal of Membrane Science, 149:11-20.

29. Maartens, A.; Swart, P.; and Jacobs, E. (1998) Humic membrane foulants in natural brown water – Characterization and removal. Desalination, 115:215-227.

30. Madaeni, S. (1998) Ultrafiltration of very dilute colloidal mixtures. Colloids and Surfaces Physiochemical and Engineering Aspects, 131:109-118.

31. Nilson, J. and DiGiano, F. (1996) Influence of NOM composition on nanofiltration. Journal of American Water Works Association, 88:53-66.

32. Ohya, H.; Kim, J.; Chinen, A.; Aihara, M.; Semenova, S.; Negishi, Y.; Mori, O.; and Yasuda, M. (1998) Effects of pore size on separation mechanisms of microfiltration of oily water using porus glass tubular membrane. Journal of Membrane Science, 145:1-14.

33. Okazaki, M. and Kimura, S. (1984) Scale formation on reverse osmosis membranes. Journal of Chemical Engineering of Japan, 17(2):145-151.

34. Reiss, C.; Hong, S.; and Taylor, J. (1999) Successful nanofiltration of 20 mg/L TOC river water. Proceedings of the 1999 AWWA Membrane Specialty Conference, Long Beach, California.

35. Ridgeway, H. and Flemming, H. (1996) Membrane biofouling, in J. Mallevialle, P. Odendaal; and M. Wiesner (eds.), Water Treatment Membrane Processes. McGraw Hill, New York.

36. Snoeyink, V. and Jenkins, D. (1980) Water Chemistry. John Wiley & Sons, New York.

37. Stumm, W. and Morgan, J. (1996) Aquatic Chemistry. John Wiley & Sons, New York.

38. Timmer, J.; Vanderhorst, H.; and Labbe, J. (1997) Cross-flow microfiltration of beta-lactoglobulin solutions and the influence of silicates on the flow resistance. Journal of Membrane Science, 136:41-56.

39. Van der Kooij, D. (1992) Assimilable organic carbon as an indicator of bacterial regrowth. Journal of American Water Works Association, 84:57-65.

40. Water Environment Research Foundation (2005) Membrane treatment of secondary effluent for subsequent use, Water Environment Research Foundation, Alexandria, Virginia.

CHAPTER 3
EFFECT OF SURFACE ROUGHNESS ON FOULING OF RO AND NF MEMBRANES DURING FILTRATION OF A HIGH ORGANIC SURFICIAL GROUNDWATER

3.1 Introduction

The use of membrane technology in drinking water treatment has increased dramatically in recent years (AWWA 1999; Van Der Bruggen *et al.* 2003). Membrane separation processes, such as reverse osmosis (RO) and nanofiltration (NF), are becoming more popular for several reasons, some of which include their ability to produce a superior quality of water, to reduce the size of the treatment facilities, and to simplify water treatment processes (Taylor and Jacobs 1996; Wilbert *et al.* 1993). The declining quality of source waters and increasingly stringent drinking water standards are further expanding the utilization of these treatment alternatives in full-scale water utilities (Beverly *et al.* 2000; Taylor and Hong 2000).

Operational problems, such as membrane fouling have hampered the acceptance of RO and NF technologies as a treatment of choice for low quality source waters (Hong and Elimelech 1997). Source waters with high fouling potentials require extensive feed water pretreatment to maintain membrane productivity (Taylor and Jacobs 1996). In addition, frequent chemical cleaning is often required to remove foulants adsorbed onto the surface of the membrane (Li and Elimelech 2004). Despite rigorous pretreatment and cleaning, membranes often suffer irreversible losses in productivity. Irreversible fouling results in the gradual deterioration of membrane performance and will inevitably lead to the replacement of the membrane elements in the system.

In order to minimize the costs associated with fouling control and membrane replacement, it is of paramount importance to select RO and NF membranes that possess properties that inherently resist fouling. Membrane surface characteristics, regardless of fouling types, are major factors affecting the rate and extent of membrane fouling. Among such factors are surface roughness (Elimelech *et al.* 1997; Vrijenhoek *et al.* 2001; Hoek *et al.* 2003; Myung *et al.* 2005; Zhao *et al.* 2005), charge (Hong and Elimelech 1997; Childress and Elimelech 2000; Zhan *et al.* 2004; Myung *et al.* 2005; Wang *et al.* 2005) and hydrophobicity (Jucker and Clark 1994; Nilson and DiGiano 1996; Cho *et al.* 2002; Laine *et al.* 2003) for RO and NF membranes. Presently, the selection of new or replacement membranes for full-scale membrane water treatment facilities is typically based on either bench-scale or pilot-scale evaluation of several membranes commercially available at the time of testing (Fu *et al.* 1994). A more fundamental approach, based on membrane surface properties, is not commonly explored for the selection of membranes. In order to achieve this goal, a correlation between membrane properties and membrane fouling potential must be established.

In this study, RO/NF membrane film characteristics were characterized using atomic force microscopy (AFM) for surface roughness, streaming potential analysis (SPA) for surface charge, and contact angle measurements for hydrophobicity. These characteristics were then related to membrane productivity as determined from flat sheet tests using a high organic groundwater taken from a surficial aquifer that served as the drinking water source for the City of Plantation, Florida. The impact of surface properties on membrane performance was assessed using these results.

3.2 Materials and Methods

3.2.1 Source Water Quality

The source water used in this study was an organic rich groundwater used by the City of Plantation's Central Water Treatment Facility, a 45,400 m^3 day^{-1} (12 mgd) membrane softening plant located in south Florida. This water originated from the surficial Biscayne Aquifer and had very consistent water quality year-round. The pH of this water was near neutral, and both hardness and alkalinity values were high. Both iron and total organic carbon values were relatively high at approximately 1.5 mg l^{-1} and 22 mg l^{-1}, respectively. Finally, the temperature of this water was typical of south Floridian groundwaters, measuring 25 °C (77 °F).

Water samples were collected from the City of Plantation's Central Water Facility on 28 July 1999 for testing purposes. These samples were taken from one of eight wells that feed the Central Water Facility with water from the Biscayne Aquifer. These samples were immediately analysed to determine a host of water quality parameters. The average values of the measured parameters followed relatively closely to the values reported by the utility, as shown in Table 1, with few exceptions. Both the measured pH and total dissolved solids values of the samples averaged slightly higher, at 7.9 and 427 mg l^{-1}, respectively, than the reported values of 7.1–7.2 and 349 mg l^{-1}. Total organic carbon measured slightly less than the value reported by the utility at 17.5 mg l^{-1}. Hardness and alkalinity values of 333 mg l^{-1} as $CaCO_3$ and 281 mg l^{-1} as $CaCO_3$, respectively, agreed very well with the reported values of 307 mg l^{-1} as $CaCO_3$ and 276 mg l^{-1} as $CaCO_3$.

Table 1: Plantation City Source Water Quality

Parameter	Annual Average	Measured Values
pH	7.2	7.9
Total Dissolved Solids (mg/L)	349	427
Hardness (mg/L as $CaCO_3$)	307	333
Alkalinity (mg/L as $CaCO_3$)	276	281
Iron (mg/L)	1.5	N/A
Turbidity (NTU)	N/A	3.4
Total Organic Carbon (mg/L)	22	17.5
Temperature (°C)	25	20

The molecular weight distribution of the natural organic matter (NOM) present in the source water was determined by high performance liquid chromatography-size exclusion chromatography (HPLC-SEC, Waters) with a protein-pak column and a 20 μL sample loop (Shimadzu) (Amy *et al*. 1992), which allowed a separation range of 1.0–30.0 kDa. The lower detection limit of 58 Da was identified and verified using an acetone solution. Standards for the molecular weight calibration curve were prepared with sodium polystyrene sulfonate (0.25, 1.8, 4.6 and 8.0 kDa) with the lower range values confirmed by acetone and salicylic acid solutions, with molecular weights of 58 and 138 Da, respectively.

The structure (hydrophobicity, transphilicity and hydrophilicity) of the organic matter was resolved through fractionation (Aiken *et al*. 1992). XAD-8 and XAD-4 resins (Rohm and Haas, Philadelphia, Pennsylvania) were used for NOM fractionation into hydrophobic NOM (XAD-8 adsorbable), transphilic NOM (XAD-4 adsorbable), and hydrophilic NOM (neither XAD-8 nor XAD-4 adsorbable) components. Clean resins were transferred to a resin column and subsequently rinsed with 0.1 N NaOH and HCl solutions until the dissolved organic carbon

measurements of the column effluent were identical to the measurements of the distilled water (Milli-Q) used to prepare the solutions. Prior to fractionation, all samples were filtered with a 0.45 μm filter and acidified to pH ≤ 2 with 5 N HCl. NOM fractions adsorbed to the resins were eluted by passing a 0.1 N NaOH solution through each column. Mass fractions of each NOM component were then determined through dissolved organic carbon measurements of each eluted solution and the XAD-8/4 effluent.

Lastly, the charge density of the organic matter was determined through a potentiometric micro-titration. An autotitrator (Metrohm 702SM Titrino, Switzerland), capable of titration increments of 0.025 ml, was used in conjunction with a pH meter (Fisher Scientific) and probe (8104BN, Orion) to perform all titrations. Prior to titration, all inorganic carbon species were removed by acidification to pH ≤ 3 with 5 N HCl and nitrogen gas sparging. Data were gathered and titration curves were plotted such that carboxylic and phenolic acidity could be determined.

3.2.2 RO/NF Membranes

The BW-30FR (Dow-FilmTec), LFC-1 (Hydranautics) and X-20 (Trisep), were the tested RO membranes, and the NF-70 (Dow-FilmTec), TFC-ULP (Koch-Fluid System) and HL (Osmonics) were the tested NF membranes in this study. The manufacturer stated water mass transfer coefficients (MTCs) of the RO membranes were 0.0123 to 0.0369 lmh/kPa (0.05 to 0.15 gfd/psi), and were considered to be low pressure RO membranes. The manufacturer MTCs for the NF membranes ranged from 0.0492 to 0.1723 lmh/kPa (0.2 to 0.7 gfd/psi).

3.2.3 Membrane Filtration Unit

The membrane filtration unit consisted of two identical, low foulant, stainless steel test cells (Sepa CF, Osmonics Inc.) operated in parallel and with both feed and permeate spacers. Each cell had channel dimensions of 14.5 cm (5.7 in) in length, 9.4 cm (3.7 in) in width, and 0.86 mm (0.034 in) in height, which provided an effective membrane area of 1.361×10^{-2} m^2 (21.1 in^2). The feed solution for these cells was contained in a 20-l (5-gal) HDPE Nalgene Cylindrical Tank and was mechanically agitated by a magnetic stirring plate. The temperature of the feed solution was maintained at 20°C (68°F) by a stainless steel heat exchange coil used in conjunction with a refrigerated recirculator (Neslab CFT-33). The solution was pumped out of the reservoir and pressurized by a Hydracell pump (Wanner Engineering), which was capable of delivering 4.2 lpm (1.1 gpm) at a maximum pressure of 3.4 MPa (500 psi). The concentrate flow (crossflow velocity) was monitored via a floating disk flowmeter (Blue White Industries) and could be adjusted by a by-pass valve (Swagelok). The feed pressure was manipulated through a back pressure regulator (US Paraplate) located immediately downstream of the test cell concentrate exit. Through careful adjustment of the by-pass valve and the back pressure regulator, the crossflow velocity and feed pressure could be finely controlled. The permeate flow, operation time and cumulative volume of permeate were continuously monitored and recorded by two digital flowmeters (Humonics) interfaced with two Dell PCs.

3.2.4 Membrane Filtration Experiments

The fouling behaviour of each membrane was assessed through bench-scale filtration experiments. Prior to fouling experiments, the membrane filtration unit was cleaned thoroughly

using sodium dodecyl sulphate and sodium laurel sulphate (SDS and SLS), sodium hydroxide, and citric acid solutions. The membrane sections were then placed in each test cell and sealed via a hydraulic press, per manufacturer instructions. All filtration studies were preceded by a stabilization period in which the membranes were equilibrated with deionized (DI) water, which contained 10^{-3} M $NaHCO_3$ (pH ≈ 7.9), for 18–24 h, at a pressure that produced the predetermined initial flux e.g. 29 lmh (17 gfd). After stabilization, the test unit was flushed with 2 l (0.5 gallons) of the testing solution to remove the sodium bicarbonate solution from the hold-up volume. The membranes were then evaluated for the ensuing 48 h with 18 l (4.5 gallons) of the testing solution at an initial flux of 29 lmh (17 gfd). Variations in permeate flux were monitored and plotted against operation time in order to assess the performance of the membranes.

The selectivity of each membrane was also evaluated for each fouling experiment. At the beginning of each fouling test, both feed and permeate samples were collected for TDS and TOC analyses. The conductance of both the feed and permeate streams were measured with a conductance meter (Model 32, YSI) and converted to TDS through the Russell and Langelier approximations presented in Equations 1 and 2 below (Snoeyink and Jenkins 1980). Similarly, TOC data were obtained through the use of a TOC analyser (Phoenix 8000 UV-Persulphate Analyser, Dohrmann).

$$\mu = 1.6 \times 10^{-5} \times (Conductanc\ e) \tag{1}$$

$$TDS = \frac{\mu}{2.5 \times 10^{-5}} \tag{2}$$

where: μ = ionic strength; conductance in micromhos per centimetre

3.2.5 Membrane Surface Characterization

In order to correlate fouling potential to membrane surface properties, the selected RO/NF membranes were thoroughly characterized prior to fouling experiments. The surface roughness was first characterized by atomic force microscopy (AFM) and by scanning electron microscopy (SEM). Furthermore, indicators of membrane surface charge and hydrophobicity were determined through streaming potential analysis (SPA) and contact angle measurements, respectively.

The Digital Instruments (DI) NanoScope™ was selected to analyze the surface roughness for all membrane samples. In order to minimize sample damage and maximize resolution, the DI AFM was operated in tapping mode. This mode operated by scanning a tip attached to the end of an oscillating cantilever, across the surface of the sample, which resulted in the 'tapping' of the tip on the surface of the sample. The vertical position of the scanner at each (x, y) data point was stored by the computer, which formed a topographic image of the sample surface. In addition, the computer analyzed these data, which made it possible to determine a host of parameters, including average roughness and 3-dimensional surface area. In order to ensure representative data, a total of three scans were performed for each membrane, each on a separate membrane section. These data were then tabulated, averaged and analysed to evaluate membrane surface roughness. In addition, SEM photographs (JOEL 6400F Scanning Electron Microscope) were taken of each membrane.

The zeta potential of the membrane surface at the plane of shear was determined using a streaming potential analyser (BI-EKA, Brookhaven Instruments Co.). The zeta potential was calculated from the streaming potential by the relationship presented in Equation 3 (McFadyen

2002). Additional details regarding the development of this relationship can be found elsewhere (McFadyen 2002).

$$\zeta = \frac{V_s}{\Delta p}\frac{\eta}{\varepsilon\varepsilon_0}\frac{L}{A}\frac{1}{R} \tag{3}$$

where: ζ = zeta potential

V_s = streaming potential

Δp = hydrodynamic pressure difference

η = liquid viscosity

ε = liquid permittivity

ε_0 = permittivity of the free space

L = sample length

A = sample cross-sectional area

R = electrical resistance

All measurements were performed at room temperature, approximately 22°C (72°F), with a background electrolyte solution of 10^{-2} M NaCl. Furthermore, to avoid ionic interference, the acid and base legs (referenced to the initial pH) were titrated with separate membrane samples in order to generate a zeta potential curve from pH 3 to 11. Two separate tests were performed for each membrane, and trend lines were developed using the best-fit logarithmic model for both tests, using Microsoft Excel.

The contact angle measurements were obtained through the captive or adhering bubble technique (Goniometer, Rame-Hart). Unlike the sessile drop technique, this technique allowed for the determination of the contact angle in an aqueous phase. In order to complete these

measurements, each membrane sample was mounted on a flat surface with the active layer exposed. The assembly was then inverted, and lowered into a quartz cell, which contained DI water, such that the active layer of the membrane was face down. A submerged syringe with a U-shaped needle attachment delivered a bubble of pre-determined size, which floated up to the membrane surface. Once the air bubble stabilized with the surface of the membrane, the contact angle on each side of the bubble was measured by an automated goniometer. In order to ensure representative results, a total of six contact angle measurements were made for each membrane.

3.3 Results and Discussion

3.3.1 Organic Analysis

The molecular weight distribution of the dissolved organic material or natural organic matter (NOM) in the City of Plantation raw water is presented in Figure 1. As shown, a significant portion of the organic matter was high in molecular weight (above 1,000 g mol^{-1}). The results obtained from the fractionation onto XAD 8/4 resins revealed that the majority (54.9%) of the organic matter was hydrophobic in nature as presented in Figure 2, which may suggest a greater propensity for organic fouling.

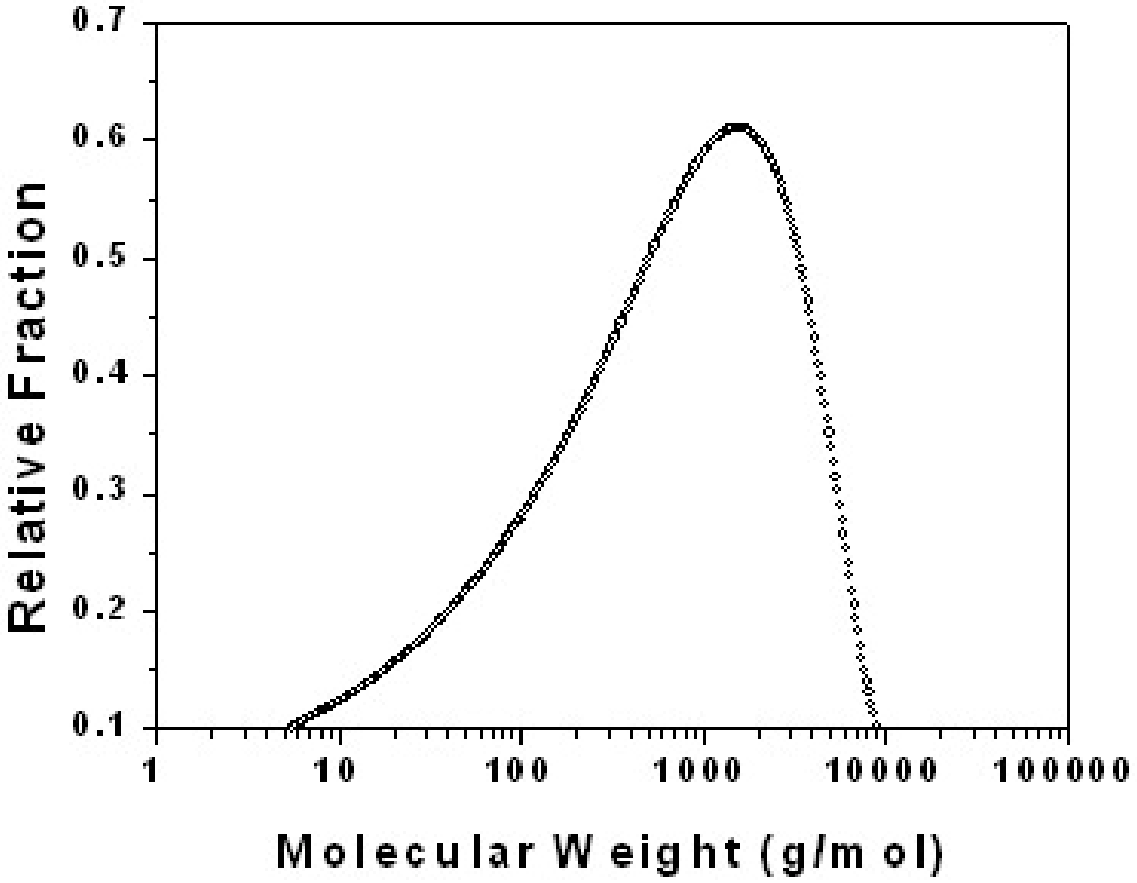

Figure 1: Natural Organic Matter Size Distribution for the City of Plantation's Surficial Groundwater

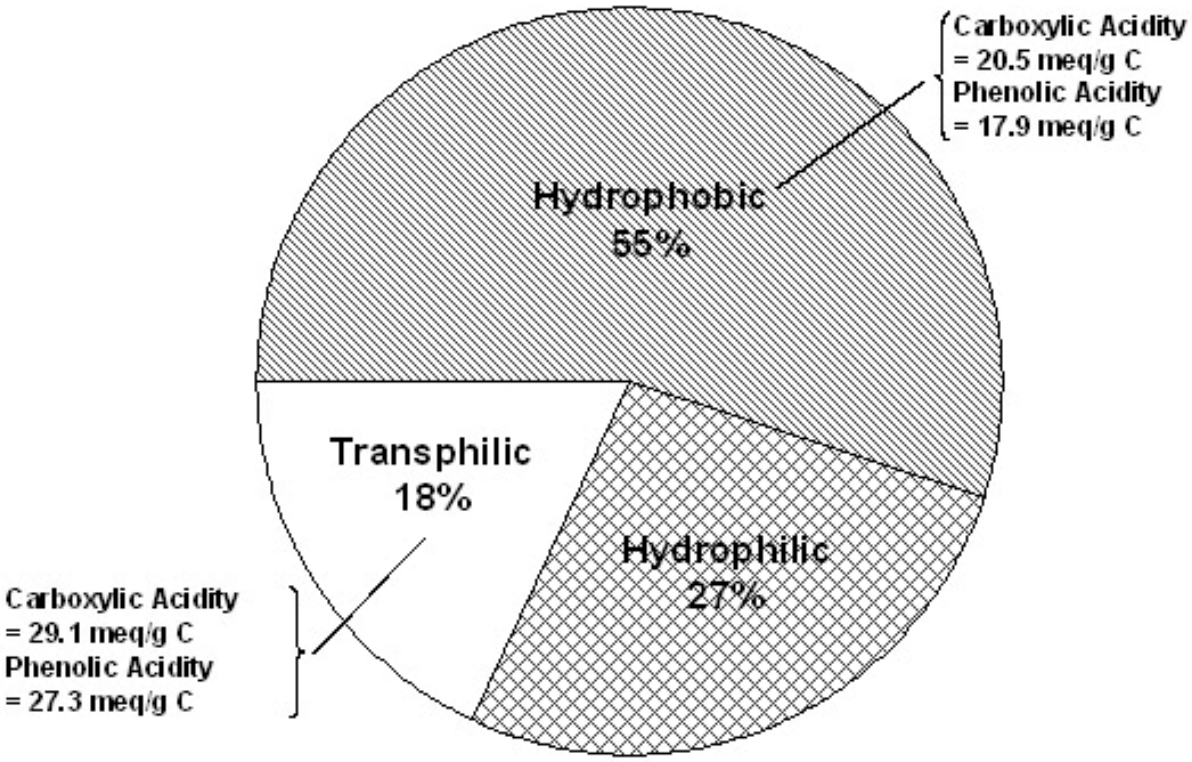

Figure 2: Natural Organic Matter Structure and Functionality for the City of Plantation's Surficial Groundwater

3.3.2 Bench-Scale Membrane Performance

The fouling behaviour of selected RO/NF membranes was first investigated via bench-scale filtration experiments using the highly organic ground water used by the membrane softening plant at the City of Plantation, Florida. Figures 3 and 4 show permeate flux versus operation time for RO and NF membranes tested, respectively, and it should be noted that the permeate flux shown in these figures was the average flux for two fouling test runs. While all membranes suffered a loss of flux, the severity of membrane fouling was different among

membranes. The order of RO membranes in increasing fouling rate was LFC-1, BW-30FR, and X-20; while the order of NF membranes in increasing fouling rate was HL, TFC-ULP, and NF-70. The initial MTCs as determined by flat sheet testing were the same as specified in the literature by manufacturer, which indicated these tests were representative of the membrane films used in the commercially available elements.

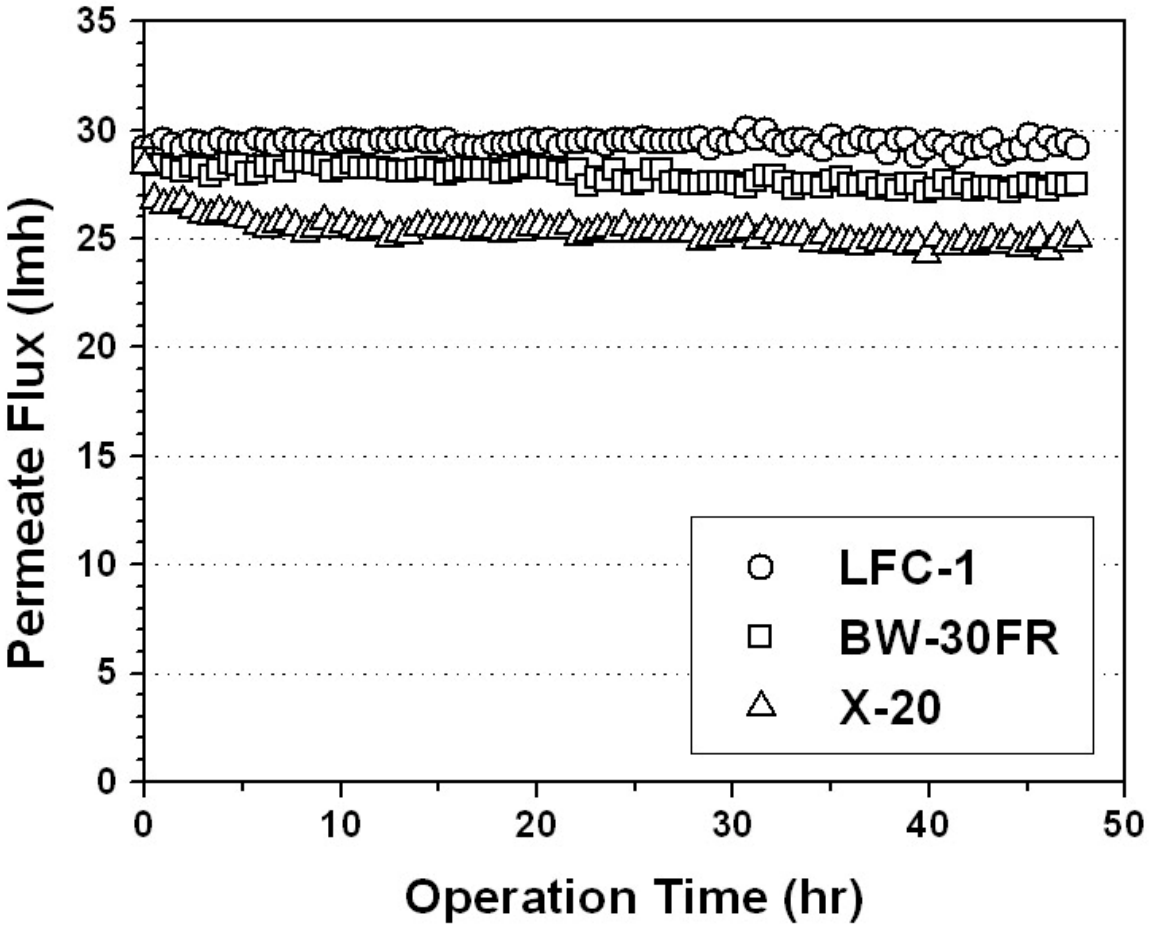

Figure 3: Flux Variations with Respect to Filtration Time for RO Membranes

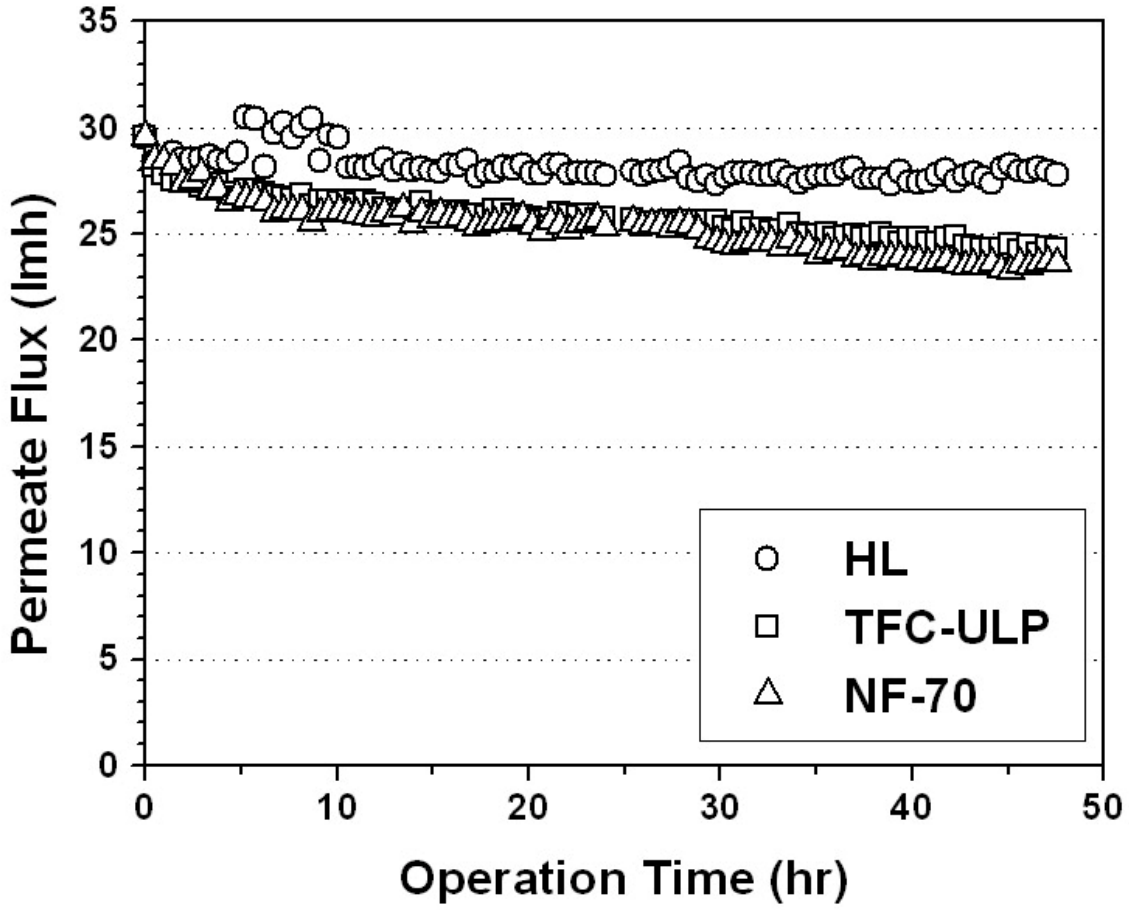

Figure 4: Flux Variations with Respect to Filtration Time for NF Membranes

The TOC and TDS selectivity of each membrane is shown in Table 2, and was evaluated to further verify that the membrane samples were representative of the film in the commercially available elements. As expected, all RO membranes rejected more TDS and TOC than did NF membranes. The higher RO rejection was generally attributed to the 'tightness' of RO membranes, as shown by corresponding lower MTC values.

Table 2: Summary of Bench-Scale Membrane Performance Tests

Membrane	Type	Initial MTC (lmh/kPa)	Flux Decline Ratio (%)	TDS Rejection (%)	TOC Rejection (%)
BW30-FR	RO	0.0271	4.4	98.0	98.1
LFC-1		0.0320	0.0	98.7	98.0
X-20		0.0246	12.6	97.2	97.8
HL	NF	0.0836	6.1	57.7	94.6
NF-70		0.1476	20.1	43.3	71.0
TFC-ULP		0.0590	17.6	86.9	95.6

3.3.3 Surface Roughness

In general, the roughness of any surface is dependent on the size, shape, frequency and distribution of the surface projections. An atomic force microscope was chosen and utilized for the analysis of surface peaks on the RO and NF membranes. This particular instrument was selected for its ability to resolve extremely small surface features, on the order of several nanometres. While AFMs are capable of analyzing a host of descriptive parameters, two criteria were used to quantify membrane surface roughness, average roughness with the associated root mean square and the surface area difference. The average roughness denotes the arithmetic average of the absolute values of the surface height deviations measured from the center plane. The root mean square roughness is the standard deviation of the average roughness. The surface area difference represents the percentage increase of the three-dimensional surface area over the two-dimensional surface area, which accounts for both the magnitude and the frequency of surface features, and provides a good measure of surface roughness.

The AFM scans of the selected membranes are presented in Figures 5 through 10. The majority of the membranes showed a surface that was covered with ‘mountainous peaks’. Visual inspection of the SEM images revealed similar surface features and were in a good agreement with the AFM scans for all of the membranes tested. The statistical analyses of the surfaces of the membranes, as determined by the AFM, are summarized in Table 3. For the six different RO/NF membranes analysed, the average roughness ranged from 10.1 to 56.7 nm. The order of increasing average membrane roughness of RO membranes was X-20, LFC-1 and BW-30FR. The order of increasing average membrane roughness of NF membranes was HL, TFC-ULP and NF-70. The surface area difference for these membranes ranged from 1.2 to 32.7%. The order of increasing surface area difference for RO membranes was LFC-1, BW-30FR and X-20; and HL, TFC-ULP, and NF-70 for NF membranes.

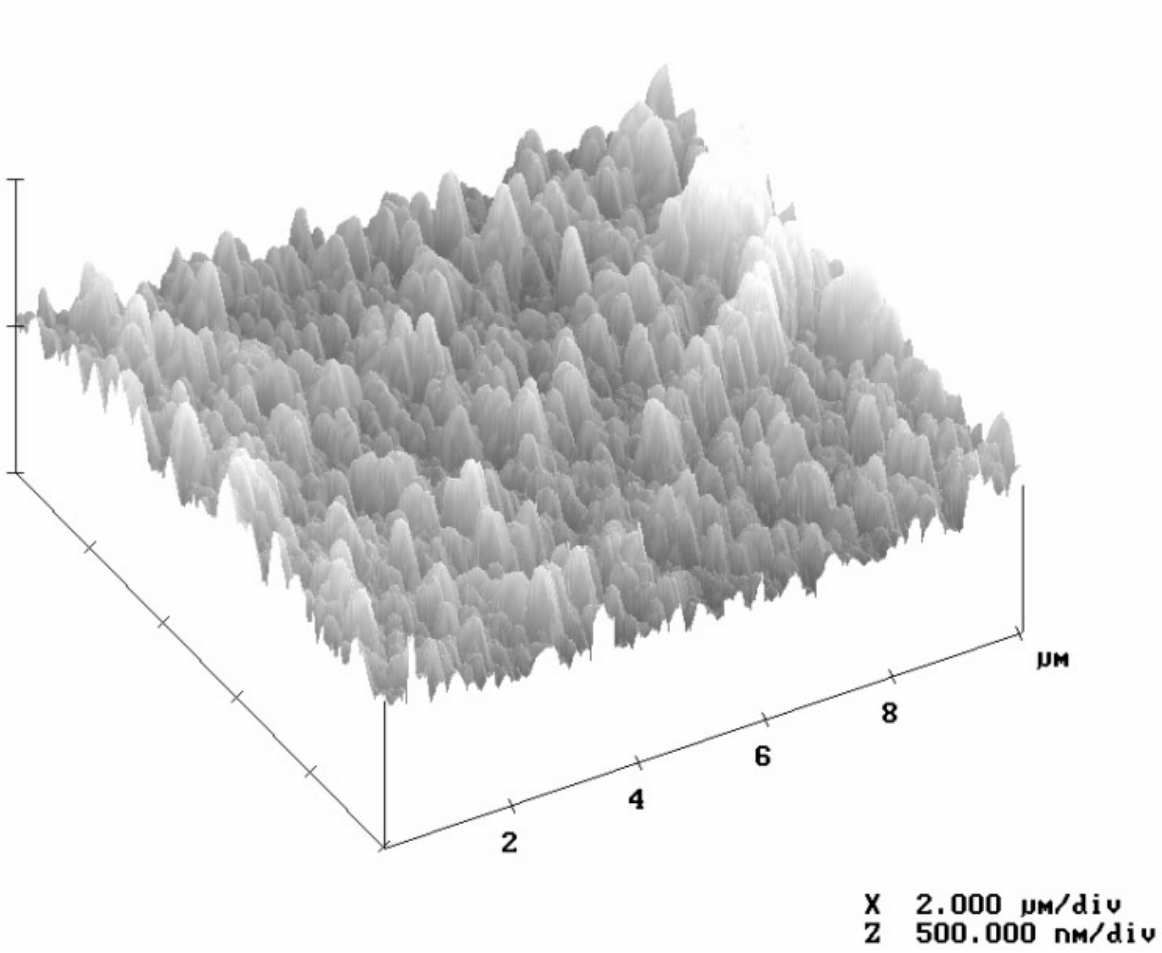

Figure 5: AFM Image of BW30-FR Membrane

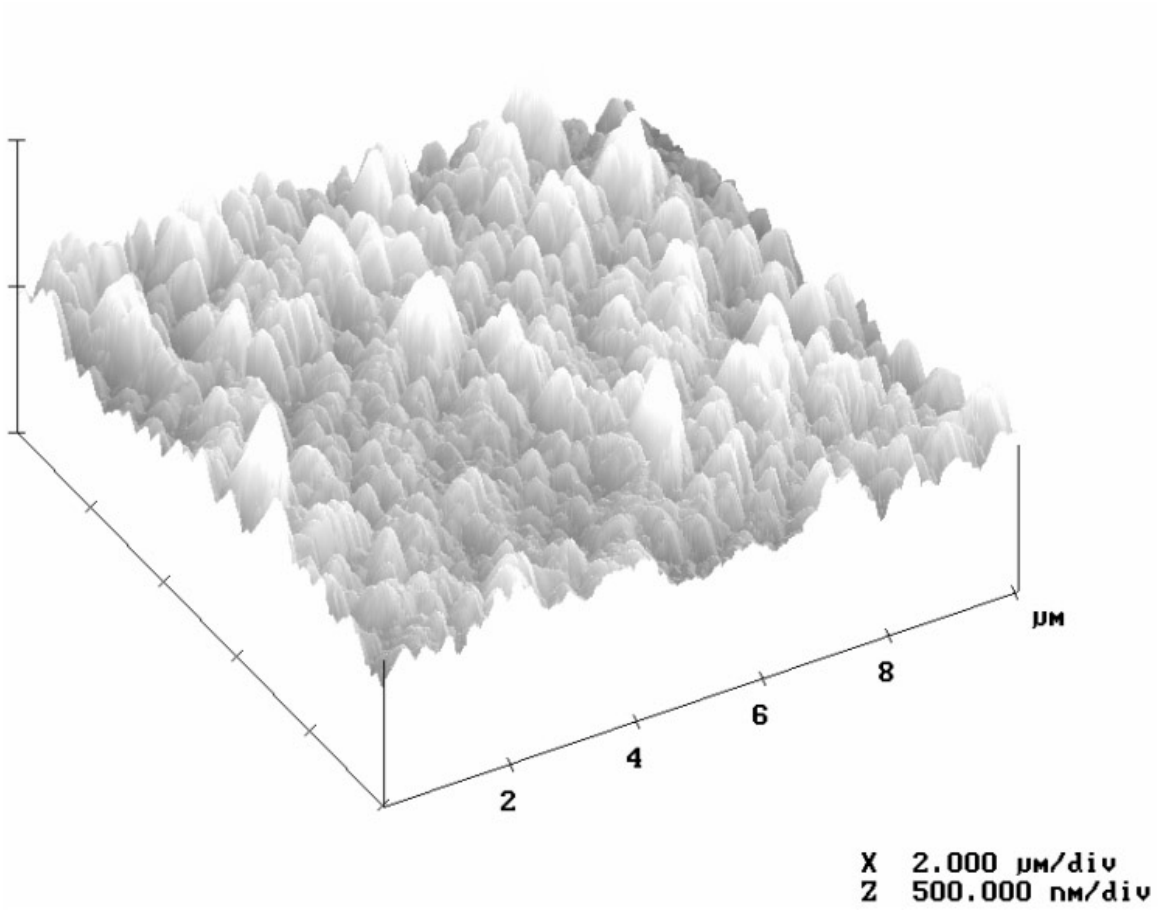

Figure 6: AFM Image of LFC-1 Membrane

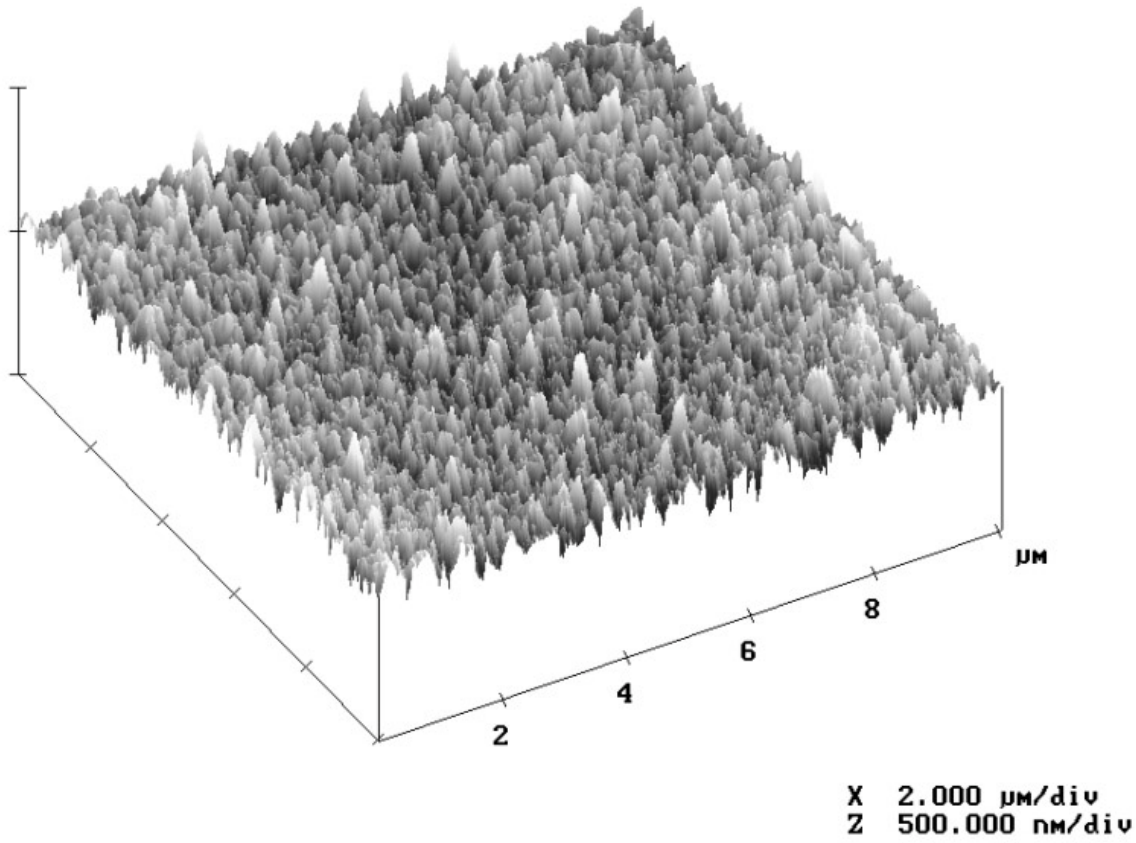

Figure 7: AFM Image of X-20 Membrane

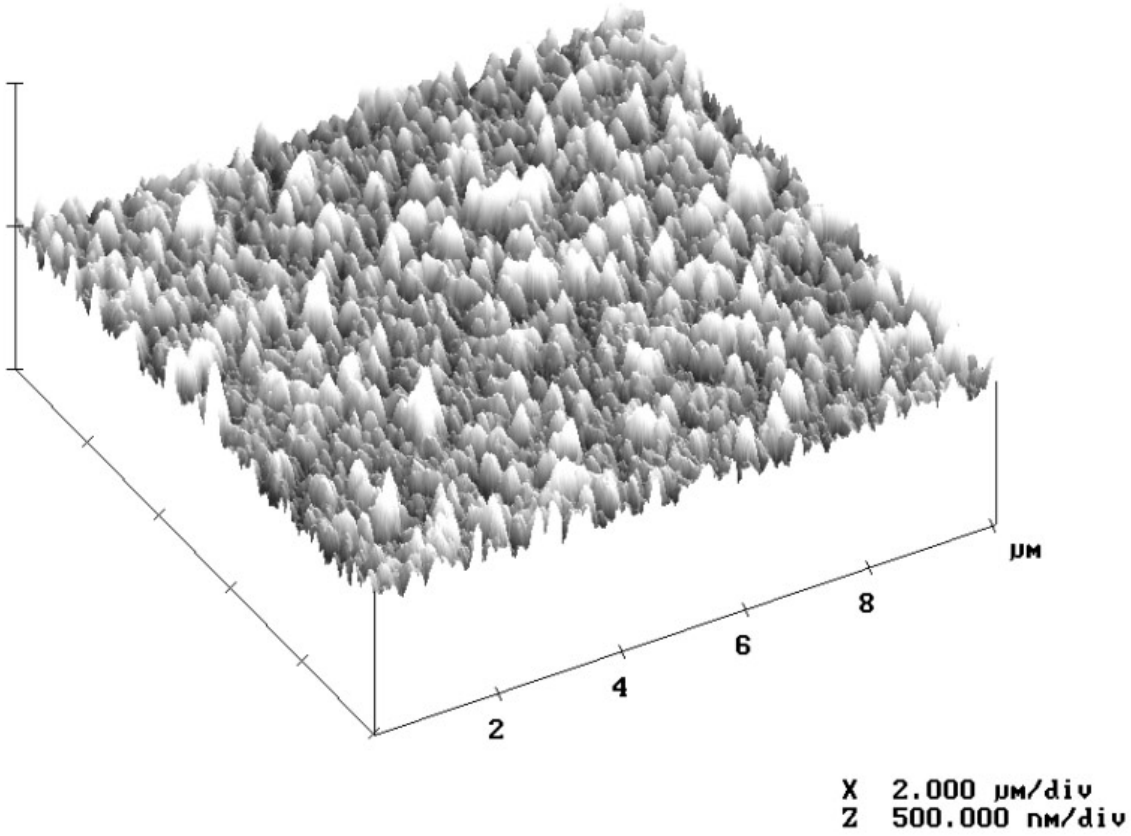

Figure 8: AFM Image of TFC-ULP Membrane

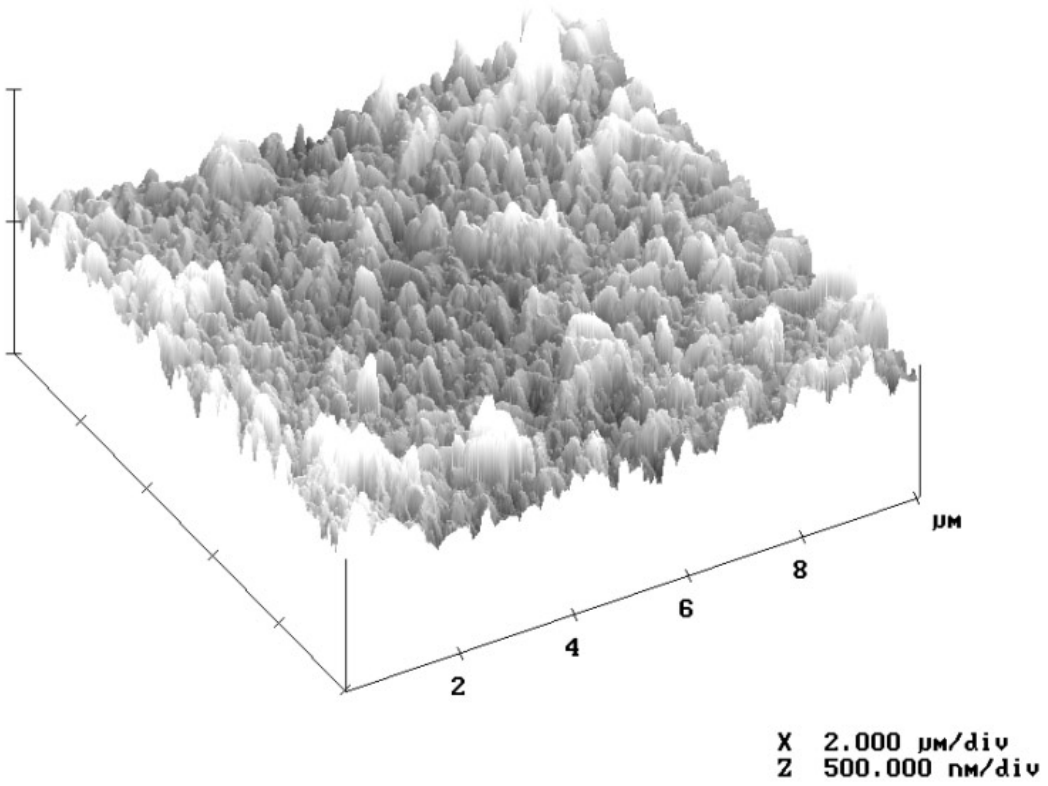

Figure 9: AFM Image of NF-70 Membrane

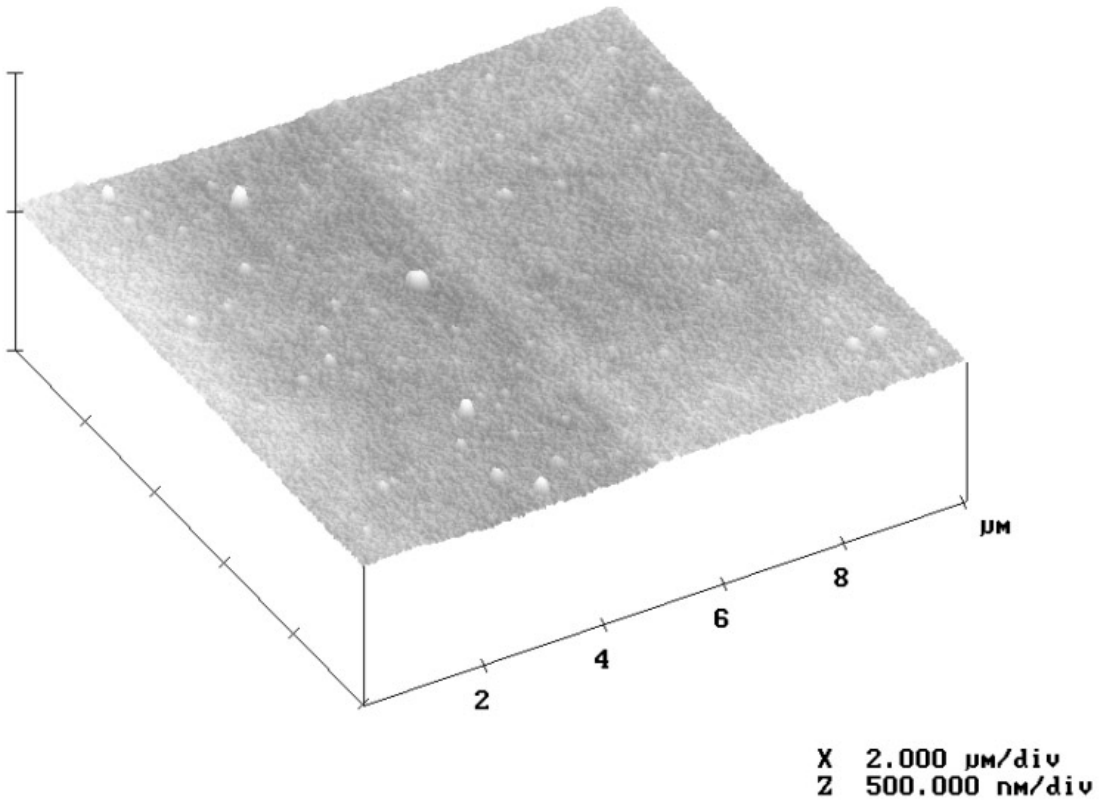

Figure 10: AFM Image of HL Membrane

Table 3: Summary of Membrane Surface Characteristics

Membrane	Type	Average Roughness (nm)	Surface Area Difference (%)	Zeta Potential (mV)	Contact Angle (°)
BW30-FR	RO	56.7 ± 73.2	25.8 ± 0.2	-6.0	55.3 ± 1.2
LFC-1		52.0 ± 67.4	16.9 ± 2.7	-5.4	51.7 ± 1.0
X-20		33.4 ± 41.6	32.7 ± 6.6	-15.0	54.1 ± 1.3
HL	NF	10.1 ± 12.8	1.2 ± 0.2	-7.9	51.9 ± 1.0
NF-70		43.3 ± 56.5	20.7 ± 1.3	-8.3	52.5 ± 0.9
TFC-ULP		30.6 ± 38.9	18.0 ± 1.1	-10.2	51.9 ± 5.3

It is important to understand the difference between average roughness and surface area difference when assessing the roughness of a membrane surface. Depending on the frequency and distribution of surface projections, these parameters can give very different results for the surface roughness. For example, the LFC-1 membrane had an average roughness of 52.0 ± 67.4 nm, as shown in Table 3, and had the second highest average roughness of the RO membranes tested. However, owing to few peak counts, LFC-1 exhibited only 16.9% surface area difference, the lowest surface area difference measured for the RO membranes tested. The X-20 membrane, on the other hand, possessed numerous smaller peaks averaging 33.4 ± 41.6 nm (Table 3) and had the lowest average roughness of the RO membranes tested. Due to the high peak frequency, the surface area difference of the X-20 membrane was 32.7%, the highest surface area difference measured for the RO membranes tested. While an increase in peak count may not significantly affect the average roughness, it can dramatically increase the surface area difference, as was the case with X-20.

3.3.4 Surface Charge

RO and NF membranes often acquire a charge on their surface when brought into contact with an aqueous solution. The surface charge was quantified by assessing the zeta potential at the plane of shear from the measured streaming potential using the Helmholtz-Smoluchowski relationship. The zeta potentials of the selected membranes were measured at various solution pHs and their results are presented in Figures 11 and 12. The experimental results clearly demonstrate that the zeta potential of each membrane becomes more negative as the value of pH increases, which is consistent with previous investigations (Nyström *et al.* 1995). This trend

arises in thin-film composite membranes from the dissociation of various functional groups (typically carboxyl) located on the surface of the membrane with increasing pH and pendant amino groups (Childress and Elimelech 1996). The zeta potential of the membranes at a pH value of 7.9 (i.e. pH of Plantation City groundwater) ranged from -5.4 to -15.0 mV, based on the exponential trend lines developed under the given solution chemistry (Table 3). The membranes in order of increasing magnitude of surface charge are LFC-1, BW-30FR and X-20 for RO membranes and HL, NF-70 and TFC-ULP for NF membranes.

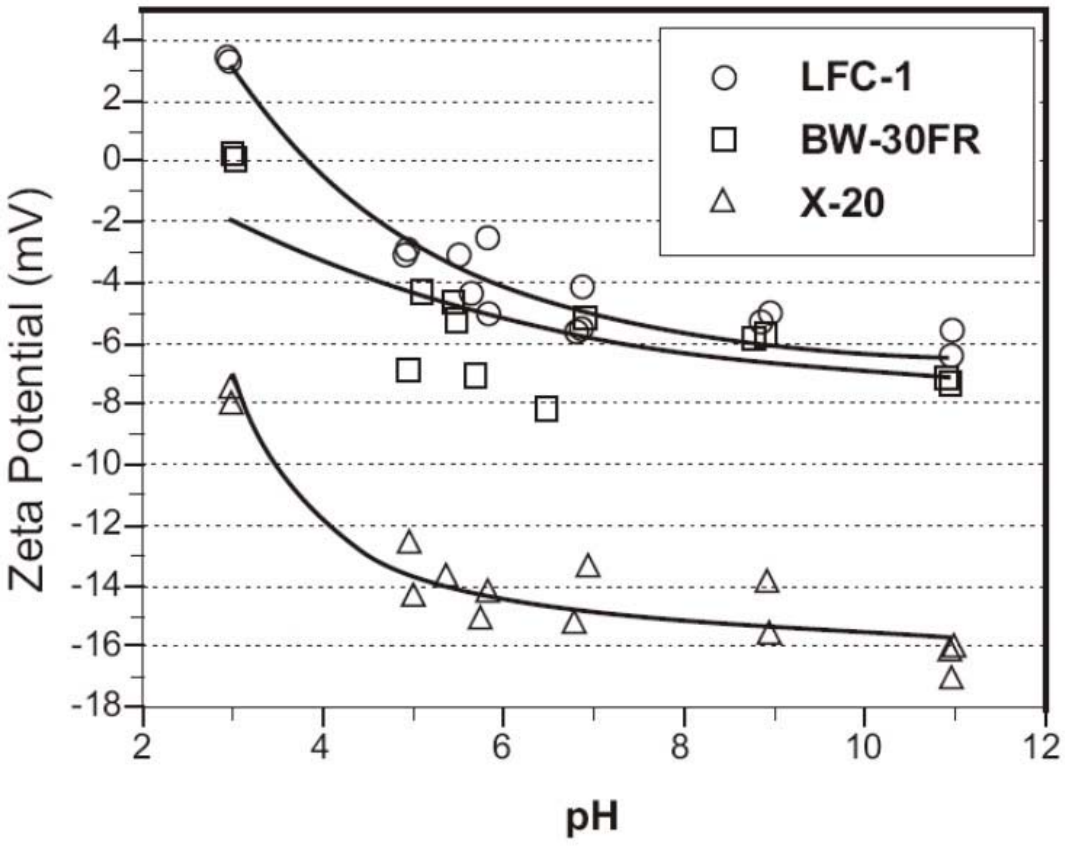

Figure 11: Zeta Potential Measurements at Various pH Values for RO Membranes

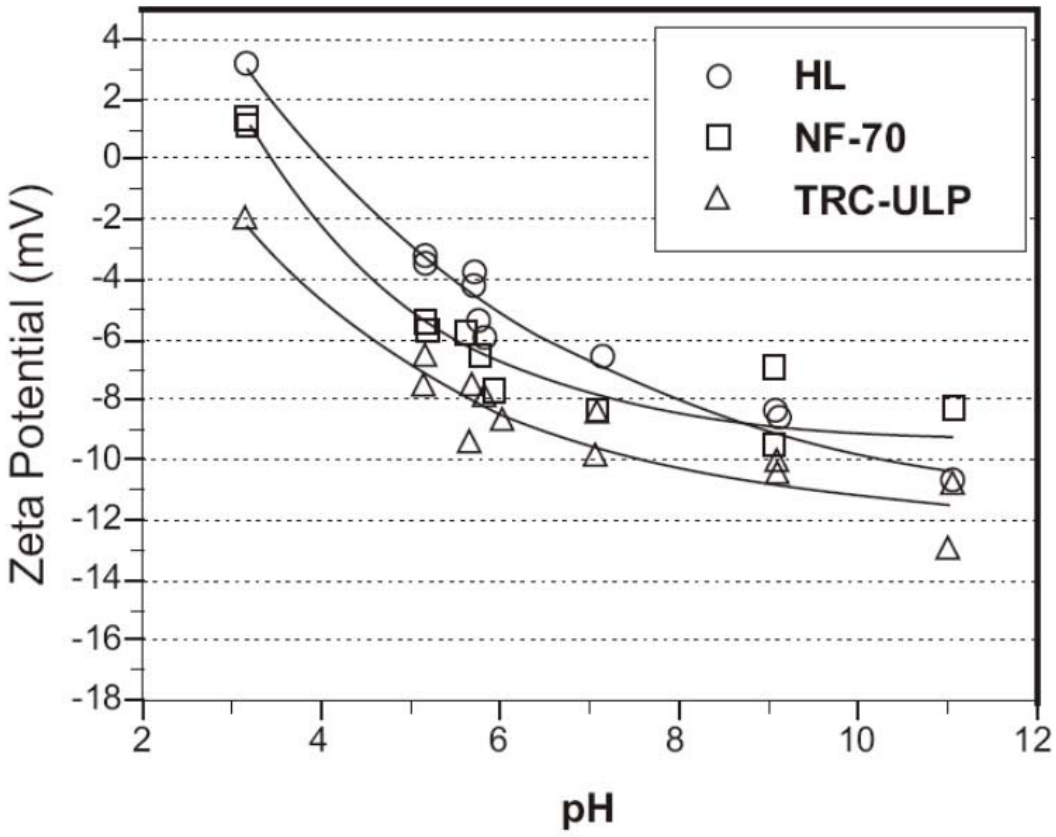

Figure 12: Zeta Potential Measurements at Various pH Values for NF Membranes

3.3.5 Hydrophobicity

Contact angle measurements are often utilized as an indication of the hydrophobicity of a membrane surface. The origin of contact angles lies in the interactions between the solid–liquid, solid–gas and liquid–gas interfaces. The difference between the attractive forces of molecules in each phase and the attractive forces between neighbouring phases results in an interfacial energy. The distribution of this energy causes one fluid to contract, which results in the formation of the contact angle (Gourley *et al.* 1994; Marmur 1996). Figure 13 and Table 3 show the results of the

contact angle measurements for each of the six selected membranes. The contact angle of the membranes were within a narrow range of 51.7° to 55.3°. Based on accepted interpretations of contact angle measurements, all six RO/NF membranes tested were hydrophilic (contact angles between 0° and 90°), with varying degrees of hydrophobicity. The membranes in order of increasing membrane hydrophobicity were LFC-1, X-20 and BW-30FR for the RO membranes and HL, TFC-ULP and NF-70 for the NF membranes.

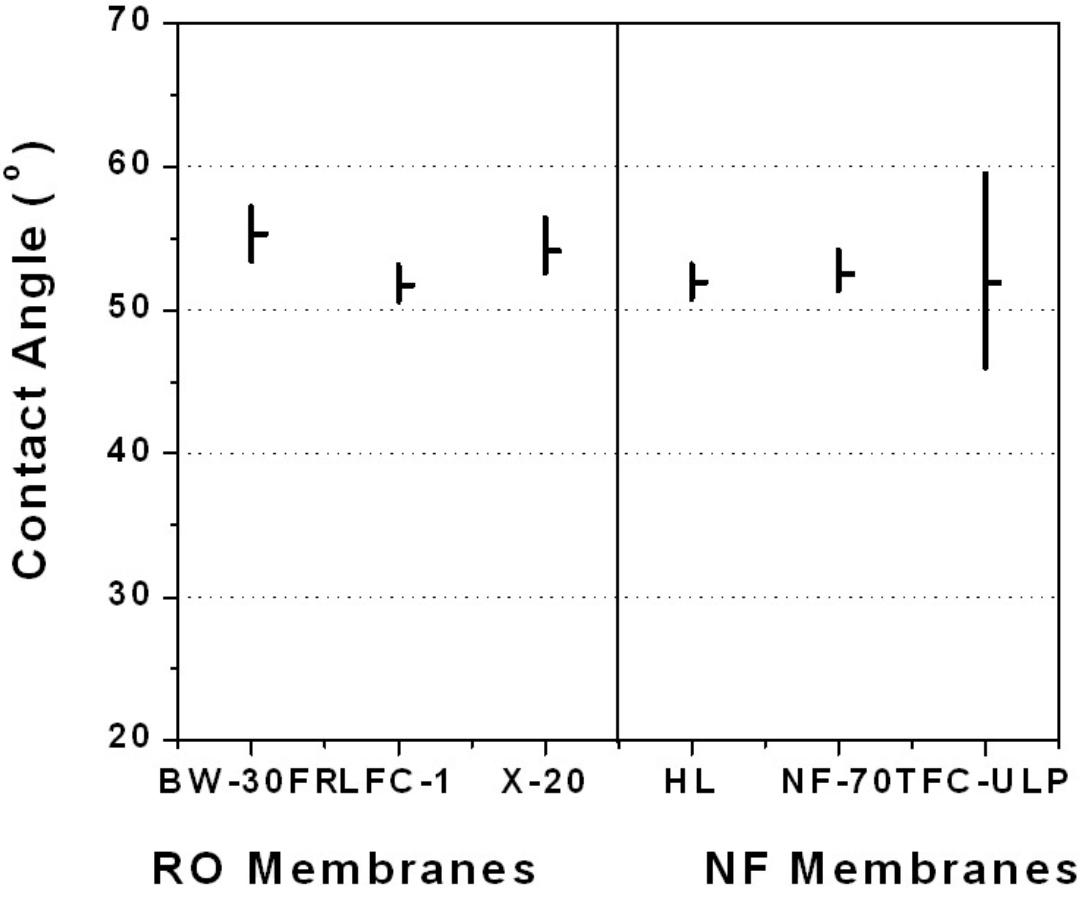

Figure 13: Contact Angle Measurements for RO and NF Membranes

3.3.6 Correlation Between Surface Properties and Fouling

The effects of surface roughness on membrane fouling are graphically presented in Figures 14 through 17. The data presented in Figures 14 and 15 showed a reasonable visual correlation between average roughness and flux decline ratio for the NF membranes. However, the flux decline ratio for the RO membranes was not visually well correlated to average roughness. Plots of surface area difference versus flux decline ratio appear visually related as shown by the consistent positive slopes for both RO and NF membranes as shown in Figures 16 and 17. Although there is not adequate data for statistical interpretation, the R^2 (also known as the square of the Pearson product moment correlation coefficient and an interpretation of the proportion of the variance in the dependent variable that is attributable to the variance in the independent variable) shown in Table 4 provides a relative comparison of the relationships between surface area difference and flux decline ratio, and average roughness and flux decline ratio. The R^2 values in Table 4 show that the flux decline ratio is more dependent on surface area difference than average roughness. More specifically, X-20 with a smaller average roughness suffered more flux decline than LFC-1, because it had more surface features and thus more surface area. These findings, combined with source water quality data indicating high organic content, suggest that the surface area difference is a superior indicator for organic fouling than average roughness, because only surface area difference accounts for increased surface area, which is available for adsorption.

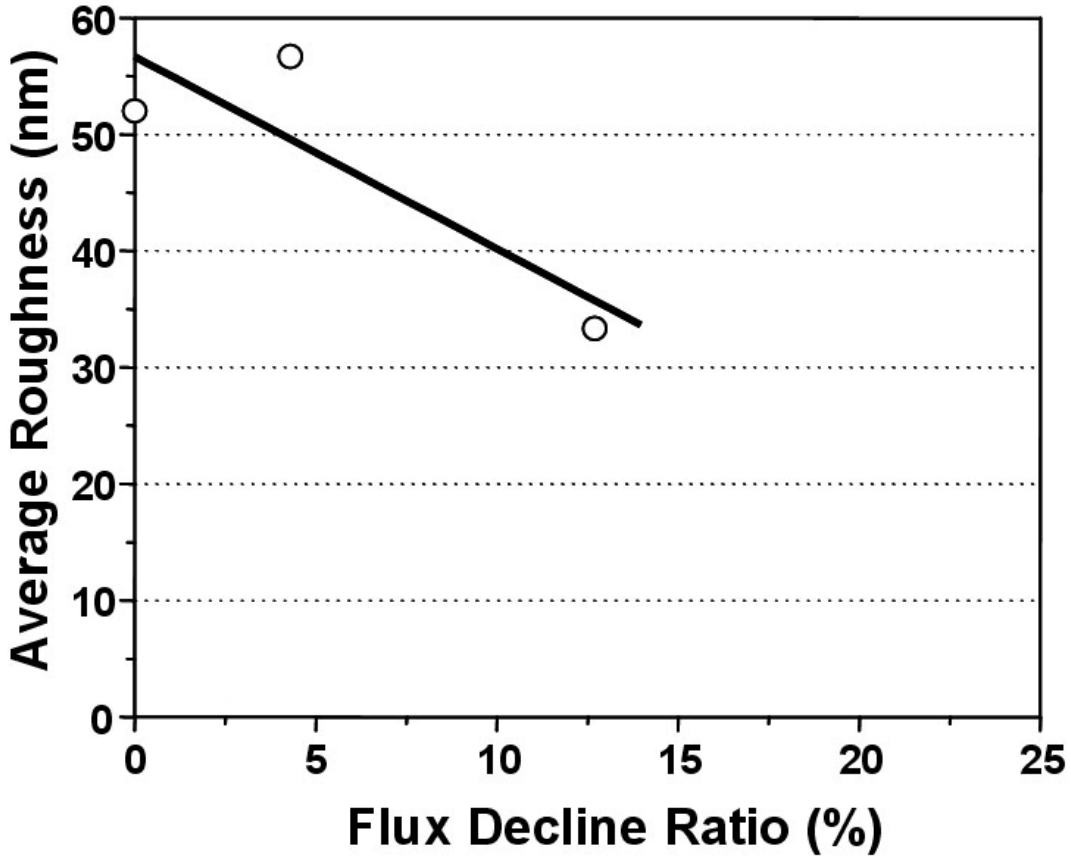

Figure 14: Correlation Between Average Surface Roughness and Flux Decline Ratio for RO Membranes

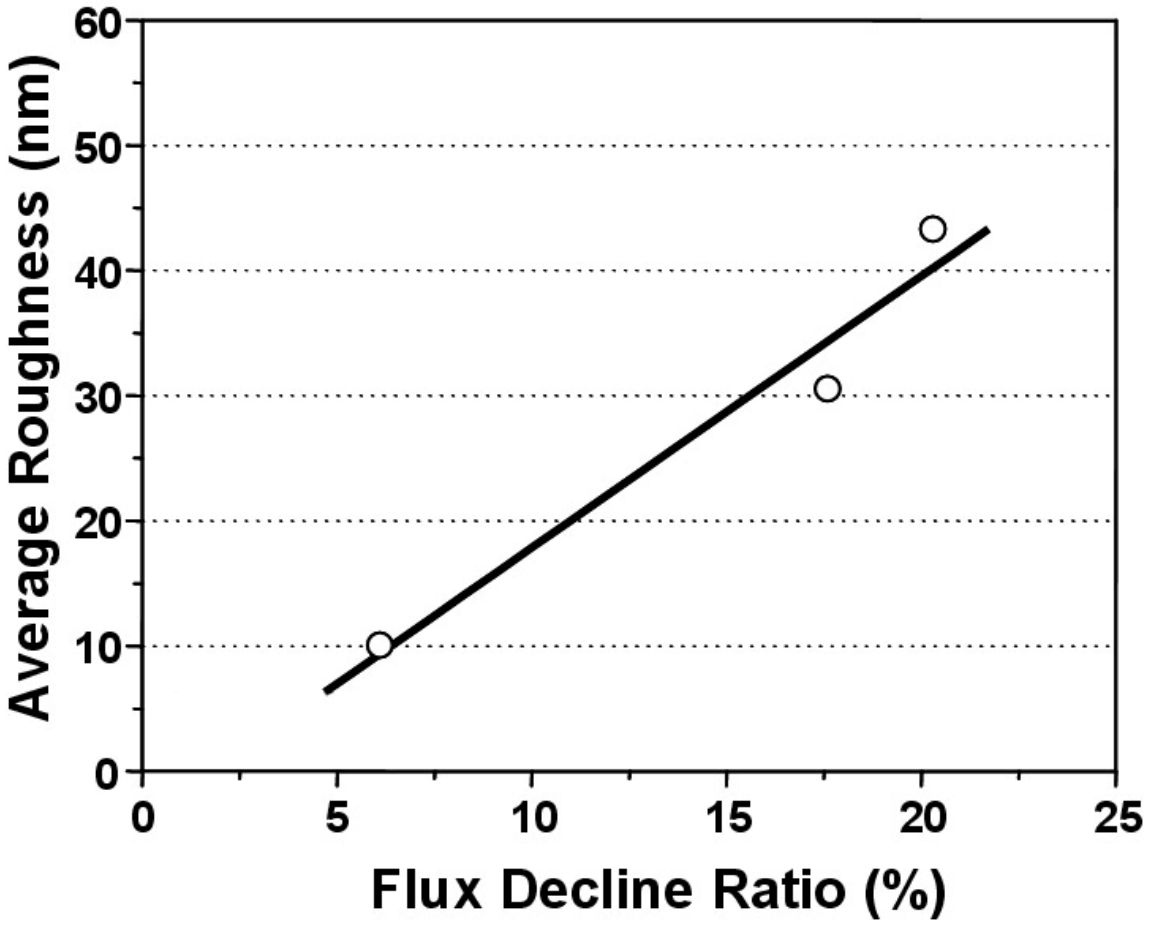

Figure 15: Correlation Between Average Surface Roughness and Flux Decline Ratio for NF Membranes

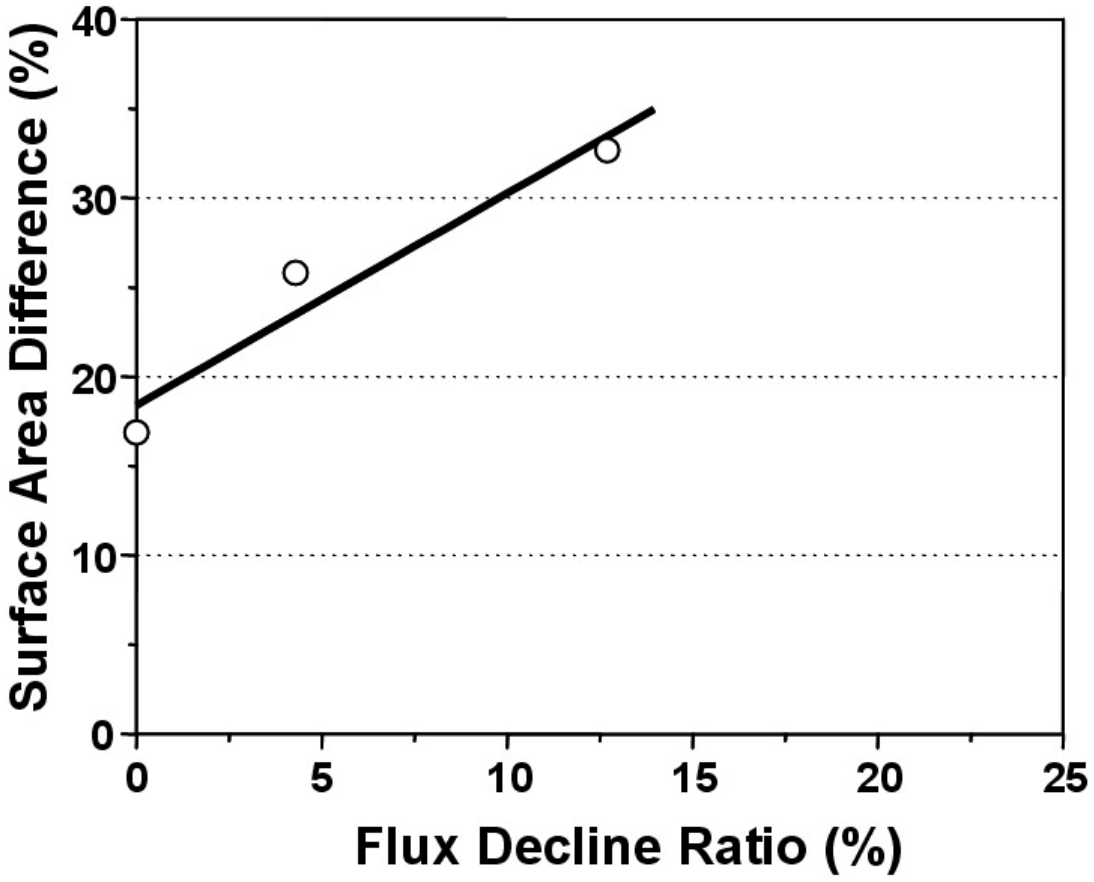

Figure 16: Correlation Between Surface Area Difference and Flux Decline Ratio for RO Membranes

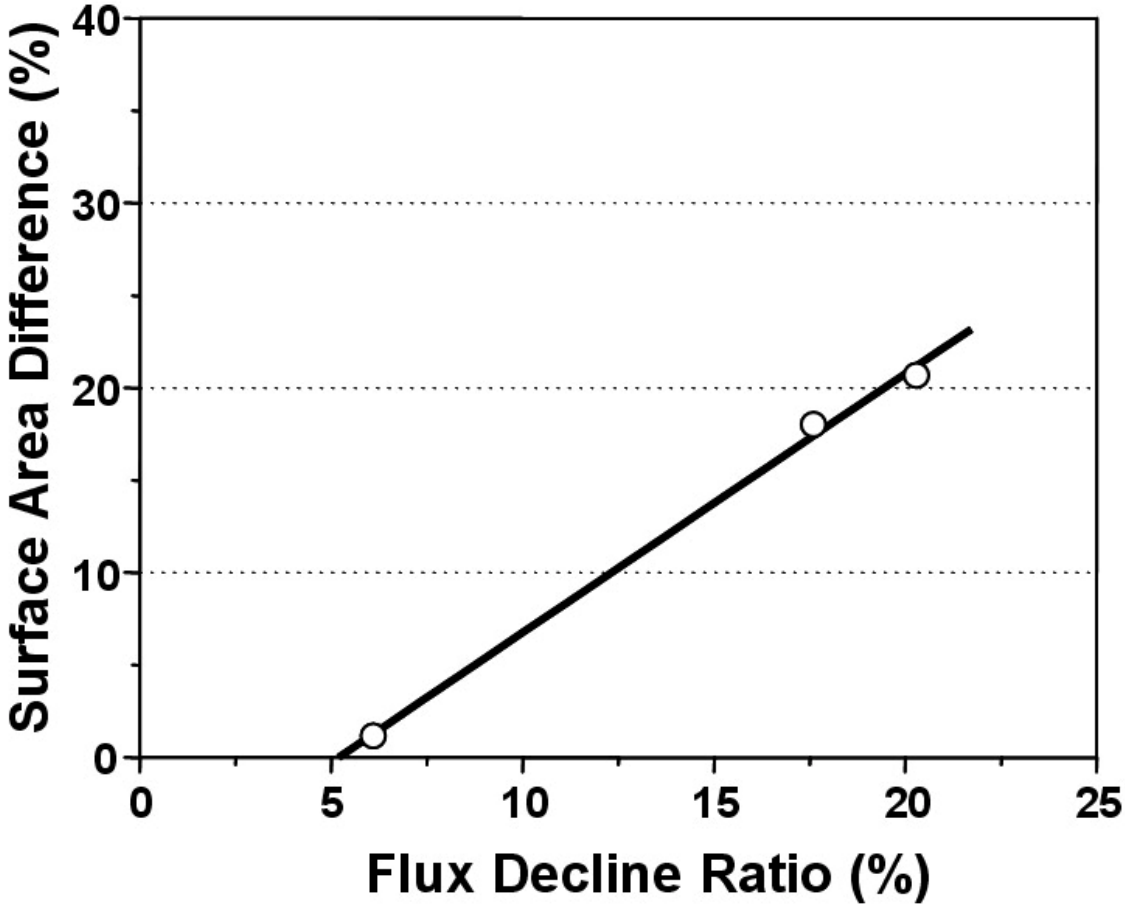

Figure 17: Correlation Between Surface Area Difference and Flux Decline Ratio for NF Membranes

Table 4: Summary of Statistical Analyses

Membrane Type	Statistical Parameter	Average Roughness	Surface Area Difference	Zeta Potential	Contact Angle
NF	R^2	0.952	0.998	0.246	0.407
	P-Value	0.140	0.026	0.670	0.560
RO	R^2	0.733	0.941	0.915	0.266
	P-Value	0.346	0.156	0.188	0.655

In addition to surface roughness, membrane surface charge and hydrophobicity values were plotted against the corresponding flux decline ratios. The results revealed that both parameters were poorly related to flux decline ratio for the given experimental conditions. Specifically, there was no clear trend observed for the NF membranes investigated. Furthermore, an inverse relationship between zeta potential and flux decline ratio was even noted for the RO membranes although the correlation coefficient was relatively low. This finding may indicate that the source water tested was composed of a multitude of foulants with various electrokinetic properties. No clear correlation was established between the contact angle (i.e. hydrophobicity) and flux decline ratio. This is not surprising since the range of membrane hydrophobicity studied was very narrow, which hindered the development of any discernable trends (refer to Figure 13). Poor correlation of charge and hydrophobicity with membrane fouling suggest that surface roughness plays a dominant role in the initial stage of membrane fouling relative to other surface properties. Similar results were also observed in a study conducted by Vrijenhoek *et al*. (2001) who investigated the mechanisms of colloidal fouling using similar membranes. The lack of correlation with charge and hydrophobicity can be attributed to the degree of ionization of the film surface and organic foulants in the bulk water. Natural organic solutes could well adsorb onto the surface and increase resistance of the mass transfer of water though the film, which would appear independent of charge.

3.4 Conclusions

During RO/NF filtration of a high organic surficial groundwater, membrane fouling clearly increased with increasing surface roughness, as measured by the surface area difference.

Based on visual correlations and relative statistical analyses utilizing R^2 and probability values (also known as P-values, which represent the probability of samples that could have been drawn from test populations assuming the null hypothesis was true), it was determined that this parameter provided a better indicator of fouling potential especially for organic adsorption than average surface roughness which is normally used to represent surface roughness, because of its inherent inclusion of both magnitude and frequency of peaks. Membrane charge and hydrophobicity were, on the other hand, loosely related to permeate flux decline, suggesting that surface roughness is a dominating factor affecting initial fouling rate.

3.5 References

1. Aiken G.R., McKnight D.M., Thorn K.A., and Thurman E.M. (1992) Isolation of hydrophilic organic acids from water using nonionic macroporous resins. Org. Geochem. 18(4):567-573.

2. Amy, G.L., Sierka R.A., Bedessem J., Price D., and Tan L. (1992) Molecular size distribution of dissolved organic matter. Journal American Water Works Association, 84(6):67-75.

3. American Water Works Association, (1999). Reverse Osmosis and Nanofiltration: Manual. AWWA, Denver, Colorado.

4. Beverly, S.; Seal, S.; and Hong, S. (2000) Identification of surface chemical functional groups correlated to failure of reverse osmosis polymeric membranes. Journal of Vacuum Science and Technology, 18(4):1107-1113.

5. Childress, A.; and M. Elimelech. (1996). Effect of Solution Chemistry on the Surface Charge of Polymeric Reverse Osmosis and Nanofiltration Membranes. Journal of Membrane Science, 119:253-268.

6. Childress, A. and Elimelech, M. (2000) Relating nanofiltration membrane performance to membrane charge characteristics. Environmental Science and Technology 34:3710-3716.

7. Cho, J.; Sohn, J.; Choi, H.; Kim, I.; and Amy, G. (2002) Effects of molecular weight cutoff, f/k ratio (a hydrodynamic condition), and hydrophobic interactions on natural organic matter rejection and fouling in membranes. Journal of Water Supply: Research and Technology - AQUA, 2:109-123.

8. Elimelech, M.; Zhu, X.; Childress, A.; and Hong, S. (1997) Role of surface morphology in colloidal fouling of cellulose acetate and composite polyamide RO membranes. Journal of Membrane Science, 127:101-109.

9. Fu, P.; Ruiz, H.; Thompson, K.; and Spangenberg, C. (1994) Selecting membranes for removing NOM and DBP precursors. Journal American Water Works Association, 86(12):55-72.

10. Gourley, L.; Britten, M.; Gauthier, S.F.; and Pouliot, Y. (1994) Characterization of adsorptive fouling on ultrafiltration membranes by peptides mixtures using contact angle measurements. Journal of Membrane Science, 97:283-289.

11. Hoek, E.; Bhattacharjee, S.; and Elimelech, M. (2003) Effect of membrane surface roughness on colloid-membrane DLVO interactions. Langmuir, 19(11):4836-4847.

12. Hong, S. and Elimelech, M. (1997) Chemical and physical aspects of natural organic matter (NOM) fouling of nanofiltration membranes. Journal of Membrane Science, 132:159-181.

13. Jucker, C. and Clark, M. (1994) Adsorption of aquatic humic substances on hydrophobic ultrafiltration membranes. Journal of Membrane Science, 97:37-52.

14. Laine, J.; Campos, C.; Baudin, I.; and Janex, M. (2003) Understanding membrane fouling: A review of over a decade of research. Water Science and Technology, 3(5-6):155-164.

15. Li, Q. and Elimelech, M. (2004) Organic fouling and chemical cleaning of nanofiltration membranes: measurements and mechanisms. Environmental Science and Technology, 38(17):4683-4693.

16. Marmur, A. (1996) Equilibrium contact angles: theory and measurement. Colloid Surface, 116:55-61.

17. McFadyen, P. (2002) Zeta Potential of Macroscopic Surfaces from Streaming Potential Measurements. Brookhaven Instruments Limited, New York.

18. Myung, S.; Choi, I.; Lee, S.; Kim, I.; and Lee, K. (2005) Use of fouling resistant nanofiltration and reverse osmosis membranes for dyeing wastewater effluent treatment. Water Science and Technology, 51(6-7):159-164.

19. Nilson, J. and DiGiano, F. (1996) Influence of NOM composition on nanofiltration. Journal American Water Works Association, 88:53-66.

20. Nystrom, M.; Kaipia, L.; and Luque, S. (1995) Fouling and retention of nanofiltration membranes. Journal of Membrane Science, 98:249-262.

21. Snoeyink, V. and Jenkins, D. (1980) Water Chemistry. John Wiley & Sons, New York.

22. Taylor, J. and Hong, S. (2000) Potable Water Quality and Membrane Technology, Journal of Laboratory Medicine, 31(10):563-568.

23. Taylor, J. and Jacobs, E. (1996) Reverse osmosis and nanofiltration. in Water Treatment: Membrane Processes (Mallevaille, J.; Odendaal, P. E.; and Wiesner, M. R., editors). American Water Works Association Research Foundation, McGraw Hill, New York.

24. Van Der Bruggen, B.; Vandecasteele, C.; Van Gestel, T.; Doyen, W.; and Leysen, R. (2003) A review of pressure-driven membrane processes in wastewater treatment and drinking water production. Environmental Progress, 22(1):46-56.

25. Vrijenhoek, E.; Elimelech, M.; and Hong, S. (2001) Influence of membrane surface properties on initial rate of colloidal fouling of reverse osmosis and nanofiltration membranes. Journal of Membrane Science, 188:115-128.

26. Wang, Z.; Zhao, Y.; Wang, J.; and Wang, S. (2005) Studies on nanofiltration membrane fouling in the treatment of water solutions containing humic acids. Desalination, 178(1-3):171-178.

27. Wilbert, M.; Leitz, F.; Abart, E.; Boegli, B.; and Linton, K. (1993) The Desalting and Water Treatment Membrane Manual: A Guide to Membranes for Municipal Water Treatment. US Department of the Interior, Bureau of Reclamation, Denver, Colorado.

28. Zhan, J.; Liu, Z.; Wang, B.; and Ding, F. (2004) Modification of a membrane surface charge by a low temperature plasma induced grafting reaction and its application to reduce membrane fouling. Separation Science and Technology, 39(13):2977-2995.

29. Zhao, Y.; Taylor, J.; and Hong, S. (2005) Combined influence of membrane surface properties and feed water qualities on RO/NF mass transfer, a pilot study. Water Research, 39(7):1233-1244.

CHAPTER 4
MONOCHLORAMINE DEGRADATION OF THIN FILM COMPOSITE LOW PRESSURE REVERSE OSMOSIS MEMBRANES

4.1 Introduction

The utilization of membrane processes such as microfiltration (MF), ultrafiltration (UF), nanofiltration (NF), and reverse osmosis (RO) in environmental applications has increased dramatically over recent years (Zhao and Taylor, 2005; Zhao et. al., 2005; Chellam et. al., 1998). Despite the increased use of membrane processes in water and wastewater treatment, the reduction of membrane productivity (i.e. membrane fouling) and the deterioration of membrane performance (i.e. membrane degradation) remain significant drawbacks for all membrane systems. Membrane fouling arises through the accumulation of contaminants on the feed side of the membrane and results in an increased resistance to solvent transport through the membrane while membrane degradation arises through the chemical and/or physical deterioration of the membrane and results in increased contaminant transport through the membrane.

The rate and extent of membrane fouling has been documented to be affected by both physical and chemical factors, such as: membrane characteristics, particle characteristics, membrane hydrodynamics, and feed solution chemistry. Membrane characteristics, including hydrophobicity, surface charge, and surface roughness, were examined for their effect on membrane fouling through various studies. The effect of membrane hydrophobicity on membrane fouling was evaluated by Madaeni and Fane (1996). Results of this study indicated that hydrophobic membranes fouled to a greater extent when compared to hydrophilic membranes. Welsh et. al. (1995) and Tarleton and Wakeman (1994) conducted studies to

determine the effect of membrane surface charge on fouling. These studies indicated membrane fouling increased when conditions favoring repulsive electrical interactions between the membrane and foulants existed. Studies were also conducted to evaluate the relationship between membrane surface roughness and fouling. Hobbs et. al. (2006) and Elimelech et. al. (1997) determined membrane fouling increased with increasing surface roughness.

The effects of particle characteristics, including size and concentration, on membrane fouling were evaluated through several studies. Numerous researchers examined the effect of particle size on membrane fouling, including Chellem and Wiesner (1997), Hong et. al. (1997), Jonsson and Jonsson (1996), and Jiao and Sharma (1994). These researchers concluded the severity of membrane fouling increased with decreasing particle size due to the formation of a dense cake layer on the surface of the membrane. Welsch et. al. (1995), Zhu and Elimelech (1995), and Romero and Davis (1991) investigated the effect of particle concentration on membrane fouling through a series of experiments. These experiments clearly demonstrated increased membrane fouling resulted from the filtration of suspensions containing elevated particle concentrations.

Hydrodynamic conditions, including crossflow velocity and permeation velocity, were examined for their effect on membrane fouling. The effect of crossflow velocity on membrane fouling was examined by Chellam and Wiesner (1997), Jonsson and Jonsson (1996), and Jiao and Sharma (1994). These researchers observed an inverse relationship between crossflow velocity and membrane fouling. This observation was attributed to elevated foulant deposition on the membrane surface due to a reduction shear induced lift which resulted in the formation of a foulant layer with increased hydraulic resistance to permeate flow. Similarly, Field et. al.

(1995), Romero and Davis (1991), and Visvanathan and Aim (1989) studied the effect of permeation velocity on membrane fouling. These researchers observed a direct relationship between permeation velocity and membrane fouling. This observation was attributed to increased foulant transport to the membrane surface due to increased permeation drag which resulted in increased membrane fouling.

The effect of feed solution chemistry (i.e. ionic strength) on membrane fouling was studied by several researchers through a series of studies. Studies conducted by Faibish et. al. (1998), Jonsson and Jonsson (1996), and Zhu and Elimelech (1995) indicated membrane fouling increased when the ionic strength of the feed solution was increased. This observation was attributed to two phenomena, both of which relate to electrokinetic interactions. First, the repulsive forces between the foulants and the surface of the membrane are reduced as the ionic strength of the feed solution is increased and results in the increased deposition of foulant material on the membrane surface. Second, the repulsive forces between accumulated foulants on the surface of the membrane are reduced as the ionic strength of the feed solution is increased and results in the formation of a densely packed foulant layer resistant to permeate flow.

These studies have made significant contributions to the membrane community regarding the fundamental mechanics of membrane fouling and degradation. However, short-term laboratory studies using synthetic source waters such as these have limited applicability for predicting long-term fouling and performance for membrane systems using natural source waters. As such, pilot studies are often conducted with natural source waters to evaluate the effects of long-term operation on membrane fouling and degradation.

A multitude of pilot studies have been conducted on a variety of natural source waters, including: seawater, groundwater, and surface water (Gao et. al., 2006 and Gwon et. al., 2003). The main objective of many of these pilot studies was to collect operating data to aid in the design of full-scale facilities. Operating data of interest often include: pretreatment requirements, feed pressure requirements, limitations on flux and recovery rates, product water quality, post-treatment requirements, and cleaning frequency. A handful of pilot studies have been conducted with more fundamental objectives. Researchers including Lovins (2000), Mulford et. al. (1999), and Robert (1999) have conducted fundamental pilot studies to dynamically model the solvent and solute mass transfer across semi-permeable membranes. However, literature surveys indicated the degradation of semi-permeable membranes by chloramines has not yet been addressed.

4.2 Membrane Theory and Model Development

The productivity of each membrane was evaluated by calculating the solvent mass transfer coefficient throughout the study. A simplified diagram of general membrane processes is presented in Figure 18. Flow and mass balances for the membrane process are presented in Equations 4 and 5, respectively.

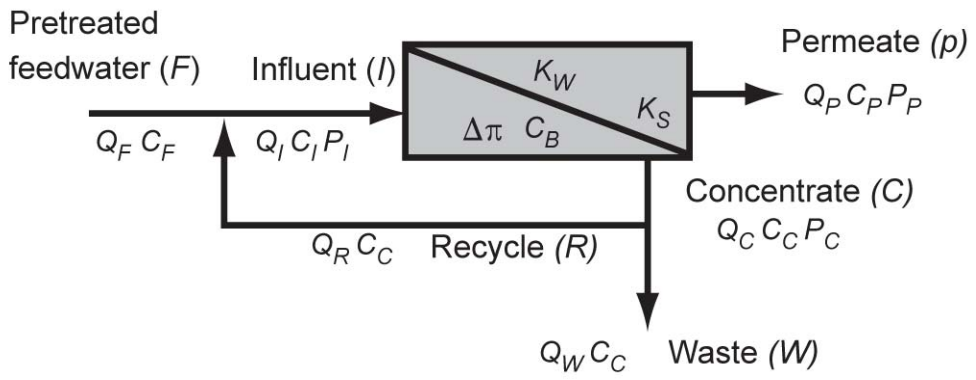

Figure 18: Single Membrane Element Flow Diagram

$$Q_f = Q_p + Q_c \tag{4}$$

$$Q_f C_f = Q_p C_p + Q_c C_c \tag{5}$$

where: Q_f = Feed stream flow rate (L^3/t)

Q_p = Permeate stream flow rate (L^3/t)

Q_c = Concentrate stream flow rate (L^3/t)

C_f = Feed stream solute concentration (M/L^3)

C_p = Permeate stream solute concentration (M/L^3)

C_c = Concentrate stream solute concentration (M/L^3)

The permeate flux was determined by dividing the permeate flow rate by the total available membrane surface area as shown in Equation 6. Due to daily temperature variations, the permeate flux must be normalized to account for changes in solvent viscosity. The calculated permeate flux was normalized with respect to temperature by using Equation 7. The normalized solvent mass transfer coefficient (productivity) was calculated by dividing the normalized permeate flux by the net driving force applied to the system as shown in Equation 8.

$$F_w = \frac{Q_p}{A} \tag{6}$$

$$F_{w_{Noem}} = \frac{F_w}{1.03^{(T-25)}} \tag{7}$$

$$K_{w_{Norm}} = \frac{F_{w_{Norm}}}{\Delta P - \Delta \Pi} = \frac{F_{w_{Norm}}}{NDF} \tag{8}$$

where: F_w = Permeate flux (L/t)

Q_p = Permeate stream flow rate (L^3/t)

A = Membrane surface area (L^2)

F_{wNorm} = Normalized permeate flux (L/t)

T = Temperature (°C)

K_{wNorm} = Normalized solvent mass transfer coefficient (L^2t/M)

ΔP = Pressure gradient (F/L^2)

$\Delta \Pi$ = Osmotic pressure gradient (F/L^2)

NDF = Net driving force (F/L^2)

The solvent mass transfer coefficient of a membrane system varies with time of operation and several researchers have modeled the dynamic nature of membrane productivity using mass loading and resistance models (Lovins, 2000; Mulford et. al., 1999; Robert, 1999; Chellam et. al., 1998). Details of mass loading and resistance model development can be found in the aforementioned references. In this study, mass loading and resistance models were developed to predict solvent mass transfer as a function of time and several independent variables. Independent variables of interest include: temperature, the initial solvent mass transfer coefficient, water loading, ultraviolet absorbance, turbidity, and monochloramine concentration.

Mass loading and resistance models are presented in general terms in Equations 9 and 10, respectively.

$$K_{w_{Norm}} = \Theta^{T-25}\left(K_{w0} + X_1 F_w t + X_2 F_w C_{UVA} t + X_3 F_w C_{Turb} t + X_4 F_w C_{NH_2Cl} t\right) \quad (9)$$

$$K_{w_{Norm}} = \frac{K_{w0}\Theta^{25-T}}{1 - \Theta^{25-T}\left(K_{w0} + X_1 F_w t + X_2 F_w C_{UVA} t + X_3 F_w C_{Turb} t + X_4 F_w C_{NH_2Cl} t\right)} \quad (10)$$

where: K_{wNorm} = Normalized solvent mass transfer coefficient (L^2t/M)

Θ = Temperature correction factor

T = Temperature (°C)

K_{w0} = Initial solvent mass transfer coefficient (L^2t/M)

X_i = Regression coefficient for parameter i

F_w = Permeate flux (L/t)

t = Operation time (t)

C_{UVA} = UV-254 (1/L)

C_{Turb} = Turbidity (NTU)

C_{NH2Cl} = Monochloramine concentration (M/L^3)

Both mass loading and resistance models were evaluated using non-linear regression. Initially, all independent variable data were regressed against the mass loading and resistance models presented above. Independent variables that were determined to be statistically insignificant were removed from the model, one at a time and beginning with the least significant variable and the regression was repeated until all variables were significant.

4.3 Pilot System

4.3.1 Overview

The source water utilized throughout this study originated from the St. Johns River at Lake Monroe located in Sanford, Florida. Advanced pretreatment was provided by two distinct processes. The first advanced pretreatment process consisted of ultrafiltration (UF) with in-line ferric sulfate coagulation. The second advanced pretreatment process consisted of modified up-flow blanket clarification and dual media filtration.

Low pressure reverse osmosis (LPRO) membrane treatment was provided by four different thin film composite membrane elements, the Hydranautics LFC1, the Trisep X20, the Osmonics SG, and the Filmtec BW30FR. In order to test all four membrane elements using both pretreated waters simultaneously, a total of eight single element units were utilized throughout this study. A process flow diagram for the pilot system is presented in Figure 19.

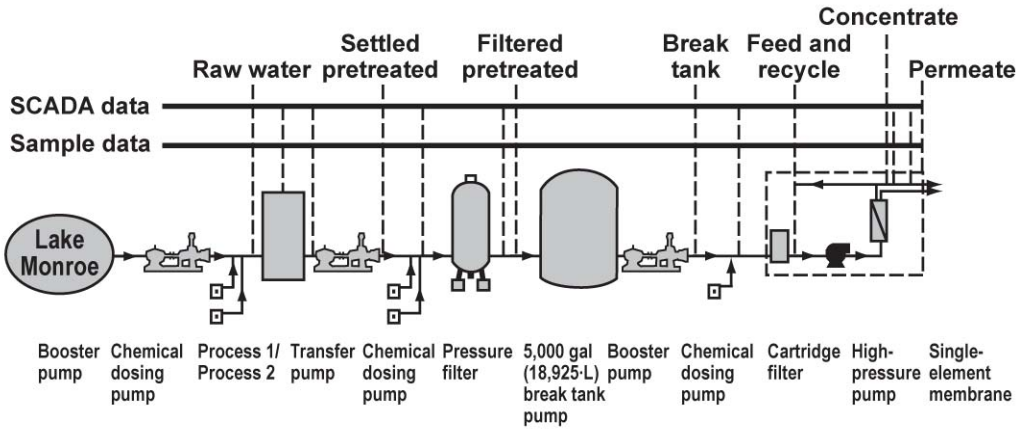

Figure 19: Pilot System Process Flow Diagram

4.3.2 Source Water

The raw source water utilized throughout this study originated from the St. Johns River and was generally characterized as highly organic and turbid surface water with moderate dissolved solids content. However, the quality of this source water varied seasonally due to the effects of frequent rainfall events. During the rainy season (May to September), the total organic carbon (TOC) of the raw source water increased due to runoff while the total dissolved solids (TDS) concentration decreased due to dilution. The TOC and TDS concentrations during the rainy season were approximately 40 mg/L and 300 mg/L, respectively. During the dry season TOC and TDS concentrations were approximately 10 mg/L and 1,500 mg/L respectively.

4.3.3 Advanced Pretreatment

Particulate matter, natural organic matter (NOM), and pathogens were removed by both advanced pretreatment processes. The first advanced pretreatment process consisted of UF membrane treatment with in-line ferric sulfate coagulation. Coagulation was accomplished through the addition of 175 mg/L of ferric sulfate and flocculation occurred in a 250 gallon baffled rectangular tank. The pH during coagulation and flocculation processes was maintained at a value of 6.0 to minimize the residual iron concentration. Ultrafiltration was provided by Zenon ZeeWeed submerged membranes. Three submerged membrane modules provided a total of 700 ft^2 or membrane surface area. Operating flux and recovery values for the Zenon UF process were maintained at approximately 25 gfd and 90 percent, respectively.

The second advanced pretreatment process, described as a modified upflow blanket clarifier (Super Pulsator), utilized powdered activated carbon, coagulation, polymer addition,

flocculation, sedimentation, and dual-media filtration. Coagulation was accomplished through the addition of 150-200 mg/L of ferric sulfate and 20 mg/L of Calgon WPL powdered activated carbon. The pH during the coagulation process was maintained at a value of 4.5 to maximize the removal of organics. A medium charge density cationic polymer (Ciba LT22S) was dosed at a concentration of 0.5-0.6 mg/L to aid in the flocculation process and to increase the cohesion of the sludge blanket. Following flocculation and sedimentation, the pH was increased to 6.0 prior to dual-media filtration to minimize the residual iron concentration.

Following each advanced pretreatment process, ammonium hydroxide and sodium hypochlorite were added to the effluent to provide a monochloramine residual to control biological fouling of the LPRO membranes. A commercially available antiscalant was also added to the LPRO membrane feed to control scale formation.

4.3.4 Single Element Pilot Units

The single element pilot units utilized throughout this study were modified Osmonics E-2200 units and were similar to units described in the Information Collection Rule Manual for Bench- and Pilot-Scale Treatment Studies (USEPA, 1996). Each unit contained a 5-um cartridge filter, a high pressure feed pump, a pressure vessel, a concentrate recirculation loop, and various pressure gauges and flow meters for the monitoring and recording of operating conditions.

A total of four low pressure reverse osmosis membranes were evaluated in this study and included the Hydranautics LFC1 (H), Trisep X20 (T), Osmonics SG (O), and FilmTec BW30FR (F). Simultaneous side-by-side low pressure reverse osmosis membrane treatment was provided by eight single element units. These eight units were arranged in two four-unit trains, each train

received water from one of the advanced pretreatment processes. Low pressure reverse osmosis membranes that received Zenon pretreated water were designated as ZH, ZT, ZO, and ZF while those that received Super Pulsator pretreated water were designated as SH, ST, SO, and SF.

4.3.5 Operation of Single Element Pilot Units

Constant operating conditions were maintained for all single element pilot units through the manipulation of feed, recycle, concentrate, and permeate control valves located on the each unit. Target recovery and flux values were 70 percent and 12 gfd, respectively. Concentrate recirculation was utilized throughout the study to maintain minimum concentrate flow requirements. Chemical dosing for all single element units was similar.

4.3.6 Monitoring of Single Element Pilot Units

Operating parameters for each single element pilot unit were recorded twice daily. Feed, permeate, and concentrate pressures were measured from field mounted pressure gauges. The temperature of each of these streams was measured using a portable thermometer. Permeate and concentrate flow rates were measured directly with a 2-liter graduated cylinder and a stopwatch. Cumulative operating time was monitored by a supervisory control and data acquisition (SCADA) system. Raw, feed, permeate, and concentrate samples were collected and analyzed in the field to determine a host of water quality parameters including: pH, conductivity, turbidity, UV-254, color, and monochloramine residual.

4.3.7 Water Quality

Raw, feed, permeate, and concentrate samples were collected from each single element pilot unit on a weekly basis. All samples were transported to the Environmental Systems Engineering Institute (ESEI) at the University of Central Florida for storage and analysis. Water quality parameters of interest included chloride, sulfate, bromide, and silicon, measured by ion chromatography; sodium, calcium, magnesium, strontium, iron, and barium measured by atomic absorption spectrometry; non-purgable dissolved organic carbon (NPDOC) measured by a total organic carbon analyzer; UV-254 measured by a spectrophotometer with a 1-cm path length; total dissolved solids (TDS) measured by summing the concentrations of seven major inorganic ions (calcium, magnesium, sodium, bicarbonate, sulfate, chloride, and silicon), and alkalinity measured by titration.

4.4 Model Development

4.4.1 Data Organization

Filtered water quality data for each pretreatment process (Tables 5 and 6) were analyzed and compared to determine any statistical differences between the two paired data sets. Student T-tests were performed on these data sets assuming equal variance. The results of these statistical analyses (Table 7) indicated that the quality of water produced from either pretreatment process was identical with the exception of organic content and alkalinity. Differences in organic content and alkalinity were attributed to differences in coagulation pH values. Consequently, the data for each membrane type were pooled for model development.

Table 5: Filtered Water Quality for Super Pulsator Pretreatment

Date	NPDOC	TDS	Conductivity	Barium	Calcium	Magnesium	Sodium	Strontium	Silica	Bromide	Chloride	Sulfate	UV-254	Color	pH	Alkalinity
	mg/L	mg/L	uS/cm	ppb	mg/L	mg/L	mg/L	mg/L	mg/L	mg/L	mg/L	mg/L	1/cm	cpu	units	mg/L as CaCO3
4/12/2002	3.7	827	1632	0.08	65.7	26.6	207	1.3	0.5	0.1	358	146	0.046	1	6.7	16
4/19/2002	4	786	1618	0.14	52.4	27.8	156	1.2	0.5	0.1	325	206	0.055	2	7.2	18
4/26/2002	3.6	903	1732	0.12	47.6	26.8	168	1.2	0.5	0.2	353	279	0.046	2	7.1	20
5/3/2002	4.8	871	1874	0.11	32.8	23.5	187	1.8	1	0.9	364	227	0.056	2	7.6	24
5/10/2002	3.4	920	1888	0.09	33.4	23.8	242	1.9	1	0.1	365	246	0.04	1	6.7	6
5/17/2002	3.8	950	2047	0.03	36.1	24.1	257	1.7	4	0.9	381	220	0.04	2	7	18
5/24/2002	1.5	754	1680	0.05	31.7	21.3	200	1.4	5	0.5	236	224	0.025	2	7.4	33
5/31/2002	3.1	1138	1754	0.02	58.2	22.7	238	1.5	1	1	336	450	0.035	3	6.5	24
6/7/2002	2.8	980	1849	0.03	59.4	23.9	219	1.4	6	1	366	265	0.034	3	7	28
6/14/2002	2.3	930	1894	0.01	42.5	23.3	264	1.2	6	0.9	310	246	0.021	1	6.8	27
6/28/2002		811	1250		47.1	17.9	198				266	247	0.025	1	6.7	28
7/12/2002		727	1215		34.3	17.8	189			0.3	229	221	0.113		6.2	29

Table 6: Filtered Water Quality for Zenon Pretreatment

Date	NPDOC	TDS	Conductivity	Barium	Calcium	Magnesium	Sodium	Strontium	Silica	Bromide	Chloride	Sulfate	UV-254	Color	pH	Alkalinity
	mg/L	mg/L	uS/cm	ppb	mg/L	mg/L	mg/L	mg/L	mg/L	mg/L	mg/L	mg/L	1/cm	cpu	units	mg/L as CaCO3
4/12/2002	6.6		1523	0.08	63.7	26.3	209	1.4	0.5	0.1			0.118	3	6.4	7
4/19/2002	7.1	789	1651	0.12	41.7	26.7	167	1.2	0.5	0.1	330	211	0.115	5	6.4	6
4/26/2002	7.5	862	1681	0.11	46.5	26.8	153	1.2	0.5	0.4	358	263	0.126	5	6.6	6
5/3/2002	8	886	1765	0.1	39.3	23.8	163	1.9	2	1	429	211	0.133	5	6.8	7
5/10/2002	7.3	882	1790	0.07	33.7	24	227	1.9	1	0.3	367	222	0.116	5	6.3	3
5/17/2002	7.6	861	1942	0.03	36.1	24.1	242	1.7	4	1.2	354	184	0.116	3	6.3	6
5/24/2002	3.1	703	1603	0.06	35.4	21.7	182	1.5	6	0.9	237	202	0.06	3	8	12
5/31/2002	4.2	898	1614	0.03	57.3	22.6	205	1.5		1	337	272	0.066	4	5.9	3
6/7/2002	5.9	907	1704	0.03	59.4	24.7	195	1.6	5	1.2	381	223	0.107	5	6.5	9
6/14/2002	4.9	955	1866	0.02	54.3	24.8	243	1.2	4	1	341	272	0.08	3	6.4	7
6/28/2002		730	1129		43.7	17.2	162				276	216	0.101	5	6.9	13
7/12/2002		676	1146		37.9	16.8	177			0.3	231	207	0.159		7.1	5

Table 7: T-Test Results for Paired Samples with Equal Variance

Parameter	T-Value	T-Critical	P-Value	Observation	Degrees of Freedom
NPDOC	-4.887	2.101	0	10	18
TDS	1.184	2.08	0.125	12	21
Conductivity	0.825	2.074	0.209	12	22
Barium	0.124	2.101	0.452	10	18
Calcium	-0.145	2.074	0.443	12	22
Magnesium	-0.001	2.074	0.5	12	22
Sodium	1.245	2.074	0.113	12	22
Strontium	-0.354	2.101	0.364	10	18
Silica	-0.107	2.11	0.458	10	17
Bromide	-0.763	2.086	0.227	11	20
Chloride	-0.298	2.08	0.384	12	21
Sulfate	0.962	2.08	0.173	12	21
UV-254	-5.886	2.074	0	12	22
Color	-6.255	2.086	0	11	20
pH	1.443	2.074	0.082	12	22
Alkalinity	6.87	2.074	0	12	22

4.4.2 Productivity Models

Mass loading and resistance models were developed for each of the LPRO membrane elements evaluated in this study and are presented in Tables 8 and 9, respectively. While the statistical differences between the mass loading and resistance models were slight, significant differences were observed between the two models when used to predict solvent mass transfer. When considering the failure of a semi-permeable membrane, a linear increase in solvent mass transfer is observed as the membrane film gradually degrades. The linear increase in productivity continues until the complete failure of the membrane film occurs at which time an exponential increase in solvent mass transfer is observed. The linear nature of a mass loading model is useful when modeling the gradual degradation of a membrane film, however, the

reciprocal nature of a resistance model is useful when modeling the complete failure of a membrane film. While the there is no known method of predicting when complete membrane failure will occur, it is likely that complete membrane failure will occur between the times predicted by the mass loading and resistance models.

Table 8: Mass Loading Models

Membrane	Model Formula	Correlation Coefficient (R^2)
Hydranautics LFC1	$K_w = 1.016^{(T-25)} \times \left[0.013\left(F_w C_{NH_2Cl} t\right) + 0.187\right]$	0.62
Trisep X20	$K_w = 1.014^{(T-25)} \times \left[0.014\left(F_w t\right) + 0.008\left(F_w C_{NH_2Cl} t\right) + 0.164\right]$	0.54
Osmonics SG	$K_w = 1.016^{(T-25)} \times \left[0.158\left(F_w t\right) - 0.894\left(F_w C_{UVA} t\right) - 0.757\left(F_w C_{Turb} t\right) + 0.004\left(F_w C_{NH_2Cl} t\right) + 0.109\right]$	0.93
FilmTec BW30FR	$K_w = 1.014^{(T-25)} \times \left[0.011\left(F_w C_{NH_2Cl} t\right) + 0.143\right]$	0.69

Table 9: Resistance Models

Membrane	Model Formula	Correlation Coefficient (R^2)
Hydranautics LFC1	$K_w = \dfrac{0.191 \times 0.986^{(25-T)}}{1 - 0.051\left(F_w C_{NH_2Cl} t\right) \times 0.986^{25-T}}$	0.61
Trisep X20	$K_w = \dfrac{0.163 \times 0.985^{(25-T)}}{1 - 0.047\left(F_w C_{NH_2Cl} t\right) \times 0.985^{25-T}}$	0.67
Osmonics SG	$K_w = \dfrac{0.112 \times 0.986^{(25-T)}}{1 - \left(0.453 F_w t - 6.058 F_w C_{UVA} t + 0.047 F_w C_{NH_2Cl} t\right) \times 0.986^{25-T}}$	0.93
FilmTec BW30FR	$K_w = \dfrac{0.146 \times 0.979^{(25-T)}}{1 - 0.050\left(F_w C_{NH_2Cl} t\right) \times 0.979^{25-T}}$	0.67

Both mass loading and resistance models accurately predicted solvent mass transfer through each of the membranes tested. Figures 20 through 23 present actual and predicted solvent mass transfer coefficient for the Hydranautics LFC1, Trisep X20, Osmonics SG, and FilmTec BW30FR membranes and clearly illustrate the accuracy of both mass loading and resistance models.

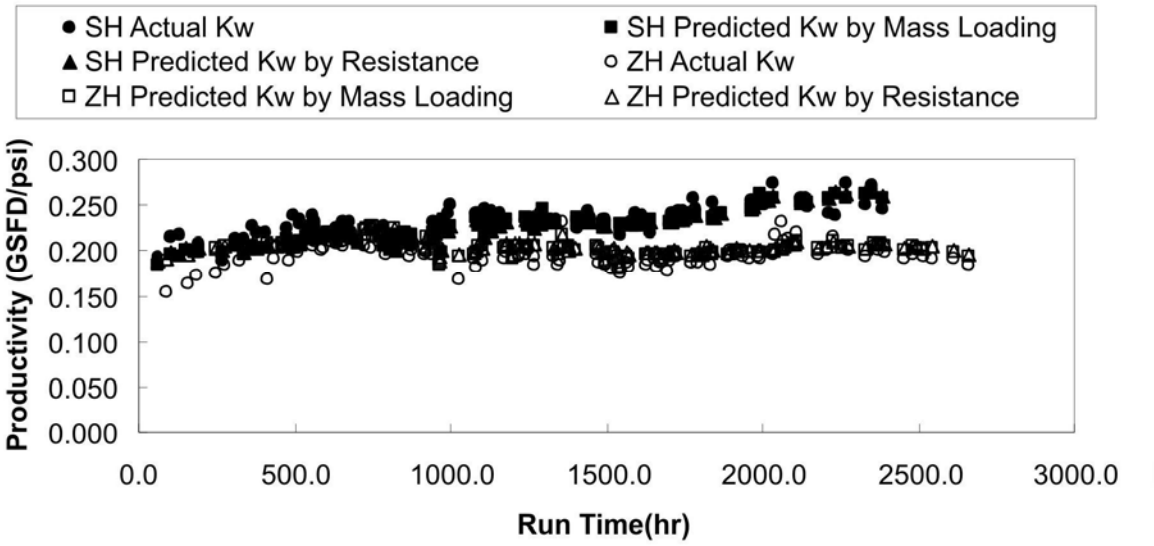

Figure 20: Actual and Predicted Solvent Mass Transfer for Hydranautics LFC1 Membrane

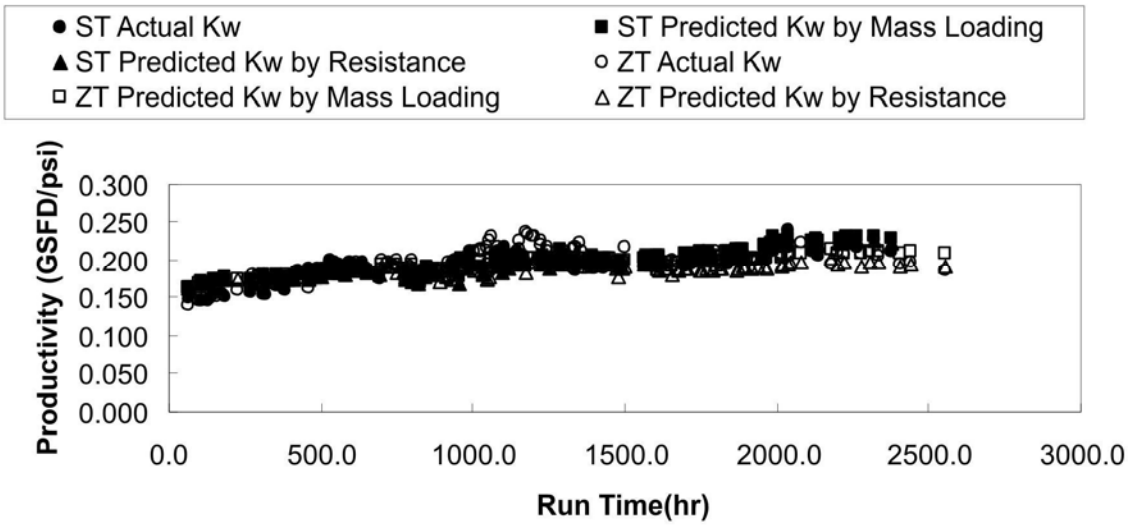

Figure 21: Actual and Predicted Solvent Mass Transfer for Trisep X20 Membrane

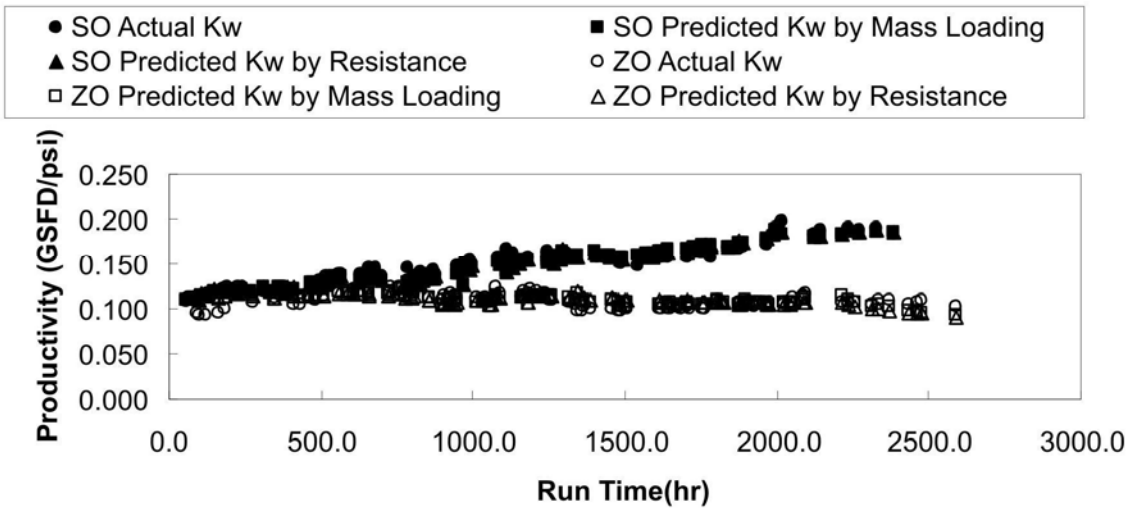

Figure 22: Actual and Predicted Solvent Mass Transfer for Osmonics SG Membrane

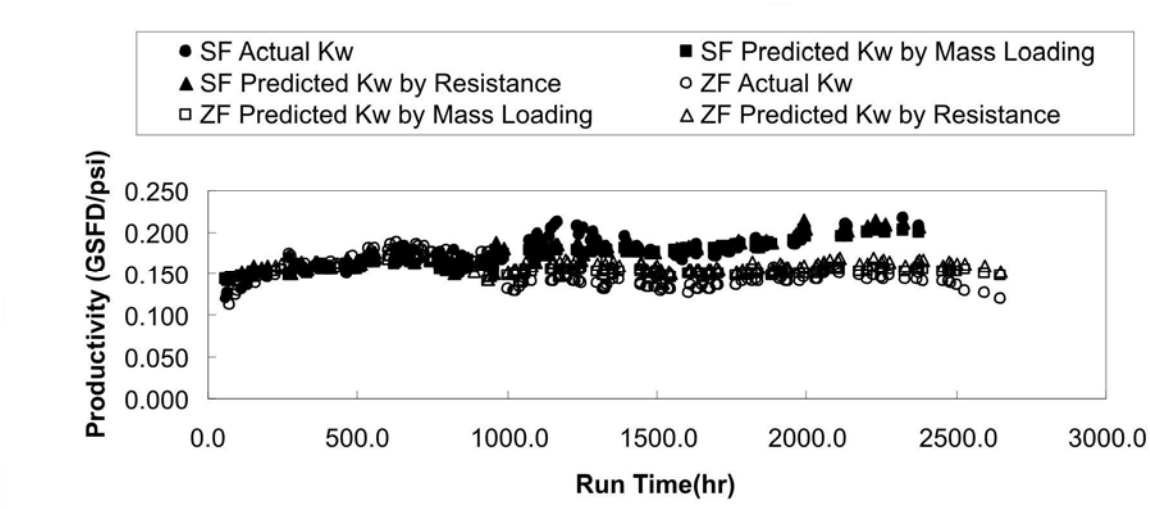

Figure 23: Actual and Predicted Solvent Mass Transfer for FilmTec BW30FR Membrane

4.4.3 Model Predictions

The solvent mass transfer models presented in Tables 8 and 9 were utilized to predict the time to complete membrane failure at standard operating conditions for each of the membranes tested in this study. Standard operating conditions for the duration of this study were: flux = 12 gfd, recovery = 70%, temperature = 28°C, monochloramine concentration = 1 mg/L, UV-254 = 0.087 cm^{-1}, and turbidity = 0.07 NTU. In order to simulate complete membrane failure with respect to ion rejection, mass loading and resistance models were set equal to 1.0 gfd/psi and the equations were solved for time. The time predicted to observe complete membrane failure by each of the models is summarized in Table 10.

Table 10: Predicted Run Time for Membrane Failure

Membrane	Predicted Run Time for Membrane Failure (hr)	
	Mass Loading Model	Resistance Model
Hydranautics LFC1	31,000	8,000
Trisep X20	36,000	9,000
Osmonics SG	40,000	8,000
FilmTec BW30FR	39,000	8,000

4.5 Monochloramine Sensitivity Analyses

Sensitivity analyses were performed for the significant independent variables for each of the mass loading and resistance models presented above. The sensitivity analyses allowed the responsiveness of the mass loading and resistance solvent mass transfer models to each of the independent variables to be determined. The concentration of monochloramine was determined to be a statistically significant independent variable in both mass loading and resistance models for all membranes tested. The results of the monochloramine sensitivity analyses for each membrane are presented and discussed below.

4.5.1 Hydranautics LFC1

The initial solvent mass transfer coefficient, monochloramine concentration and temperature were significant independent variables in both the mass loading and resistance models for the Hydranautics LFC1 membrane. Both models predicted an increase in solvent mass transfer over time with increasing monochloramine concentration and temperature, however, the resistance model predicted accelerated membrane degradation by monochloramine when compared to the mass loading model. The results of the monochloramine sensitivity analyses for the mass loading and resistance models are presented in Tables 11 and 12, respectively. Graphical representations of the sensitivity analysis data are presented in Figures 24 and 25.

Table 11: Hydranautics LFC1 Mass Loading Model Monochloramine Sensitivity Analysis

NH_3Cl (mg/L)	Predicted Mass Transfer Coefficient for Various Membrane Run Times (gfd/psi)					
	0 hrs	1,000 hrs	2,000 hrs	5,000 hrs	10,000 hrs	25,000 hrs
0	0.196	0.196	0.196	0.196	0.196	0.196
1	0.196	0.222	0.248	0.327	0.458	0.850
2	0.196	0.248	0.301	0.458	0.719	1.000
3	0.196	0.275	0.353	0.589	0.981	1.000
4	0.196	0.301	0.405	0.719	1.000	1.000
5	0.196	0.327	0.458	0.850	1.000	1.000
6	0.196	0.353	0.510	0.981	1.000	1.000

Table 12: Hydranautics LFC1 Resistance Model Monochloramine Sensitivity Analysis

NH_3Cl (mg/L)	Predicted Mass Transfer Coefficient for Various Membrane Run Times (gfd/psi)				
	0 hrs	1,000 hrs	2,000 hrs	5,000 hrs	10,000 hrs
0	0.199	0.199	0.199	0.199	0.199
1	0.199	0.221	0.249	0.401	1.000
2	0.199	0.249	0.333	1.000	1.000
3	0.199	0.285	0.503	1.000	1.000
4	0.199	0.333	1.000	1.000	1.000
5	0.199	0.401	1.000	1.000	1.000
6	0.199	0.503	1.000	1.000	1.000

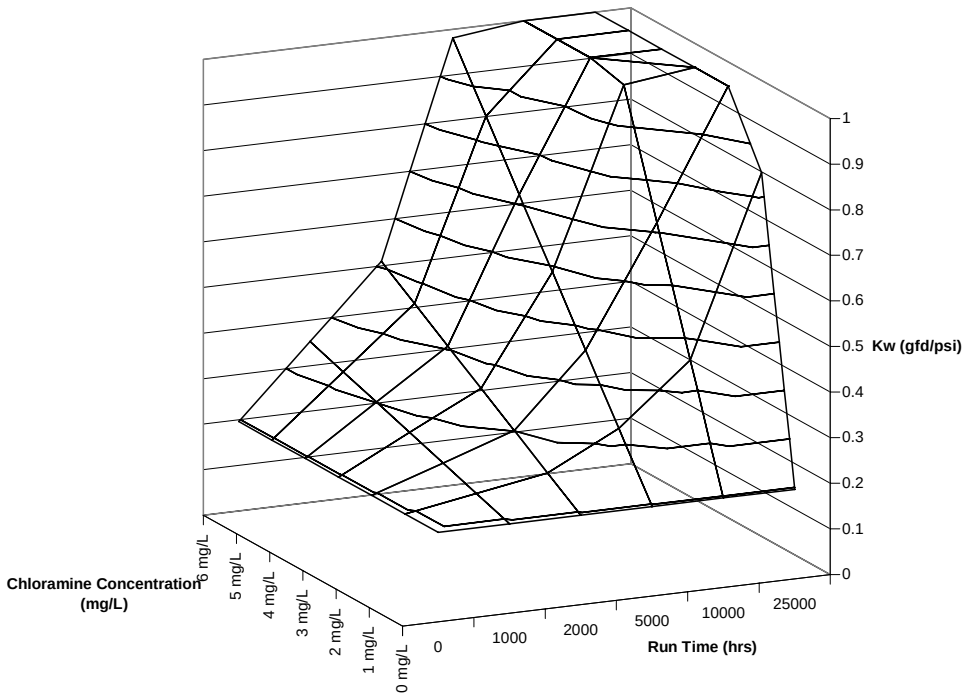

Figure 24: Hydranautics LFC1 Mass Loading Model Monochloramine Sensitivity Analysis

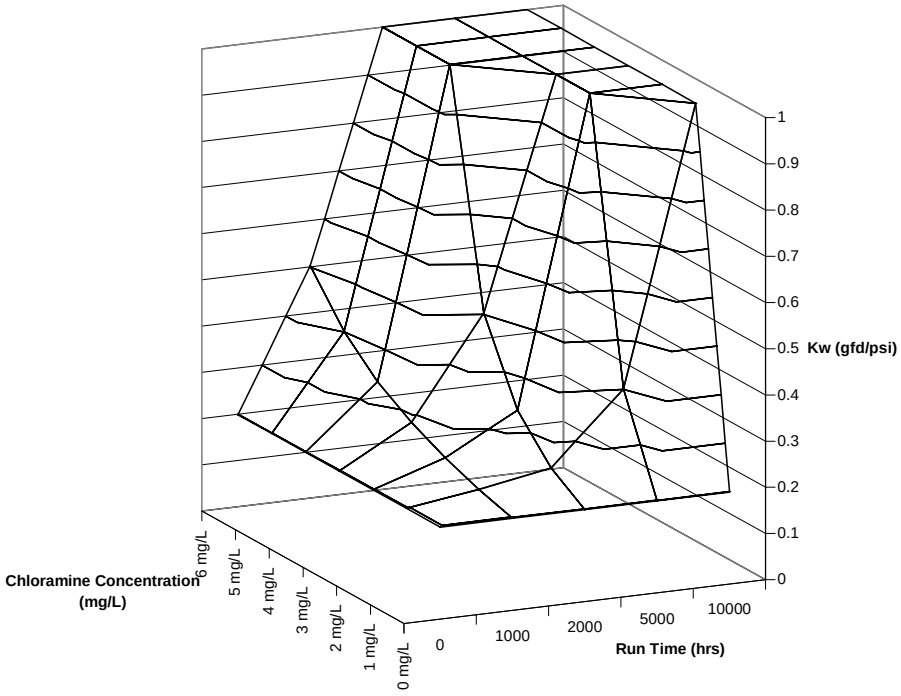

Figure 25: Hydranautics LFC1 Resistance Model Monochloramine Sensitivity Analysis

4.5.2 Trisep X20

Significant independent variables for the mass loading and resistance models for the Trisep X20 membrane included the initial solvent mass transfer coefficient, monochloramine concentration, and temperature. Water loading was also determined to be a significant independent variable for the mass loading model. Increases in solvent mass transfer over time were predicted by both models with increasing monochloramine concentration and temperature, however, the resistance model predicted accelerated monochloramine degradation of the membrane when compared to the mass loading model. While variations in water loading were not significant for the resistance model, increases in the solvent mass transfer coefficient were predicted by the mass loading model with increasing water loading. Tables 13 and 14 summarize the results of the monochloramine sensitivity analyses for both the mass loading and resistance models, respectively, and Figures 26 and 27 present these results graphically.

Table 13: Trisep X20 Mass Loading Model Monochloramine Sensitivity Analysis

NH_3Cl (mg/L)	**Predicted Mass Transfer Coefficient for Various Membrane Run Times (gfd/psi)**					
	0 hrs	**1,000 hrs**	**2,000 hrs**	**5,000 hrs**	**10,000 hrs**	**25,000 hrs**
0	0.171	0.178	0.186	0.207	0.244	0.353
1	0.171	0.194	0.217	0.286	0.402	0.748
2	0.171	0.210	0.249	0.365	0.560	1.000
3	0.171	0.226	0.280	0.444	0.718	1.000
4	0.171	0.241	0.312	0.523	0.875	1.000
5	0.171	0.257	0.343	0.602	1.000	1.000
6	0.171	0.273	0.375	0.681	1.000	1.000

Table 14: Trisep X20 Resistance Model Monochloramine Sensitivity Analysis

NH_3Cl (mg/L)	Predicted Mass Transfer Coefficient for Various Membrane Run Times (gfd/psi)				
	0 hrs	1,000 hrs	2,000 hrs	5,000 hrs	10,000 hrs
0	0.171	0.171	0.171	0.171	0.171
1	0.171	0.189	0.210	0.320	1.000
2	0.171	0.210	0.273	1.000	1.000
3	0.171	0.237	0.387	1.000	1.000
4	0.171	0.273	0.669	1.000	1.000
5	0.171	0.320	1.000	1.000	1.000
6	0.171	0.387	1.000	1.000	1.000

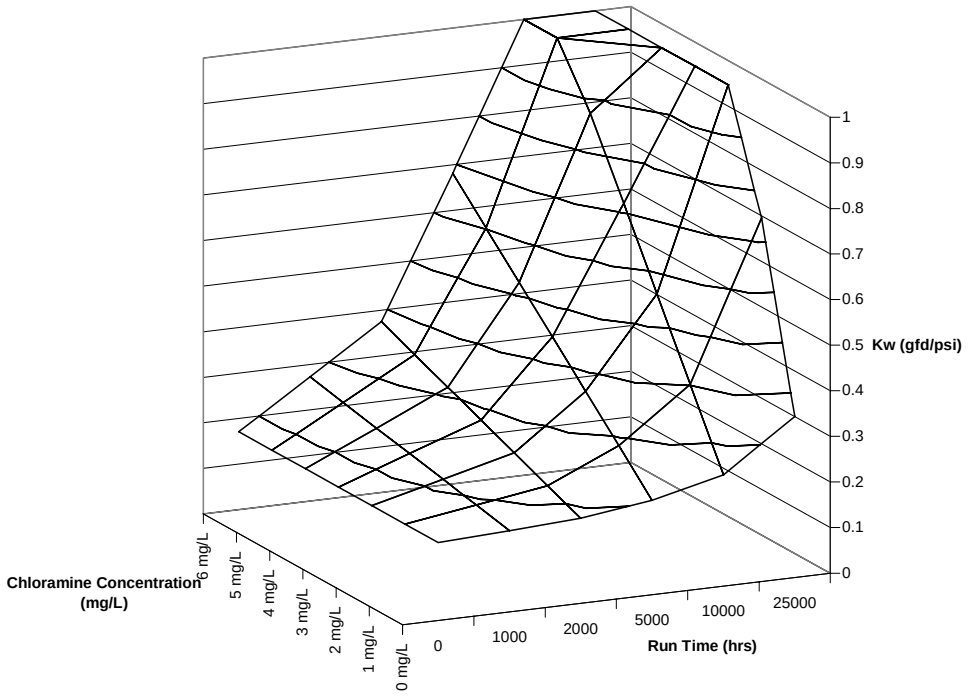

Figure 26: Trisep X20 Mass Loading Model Monochloramine Sensitivity Analysis

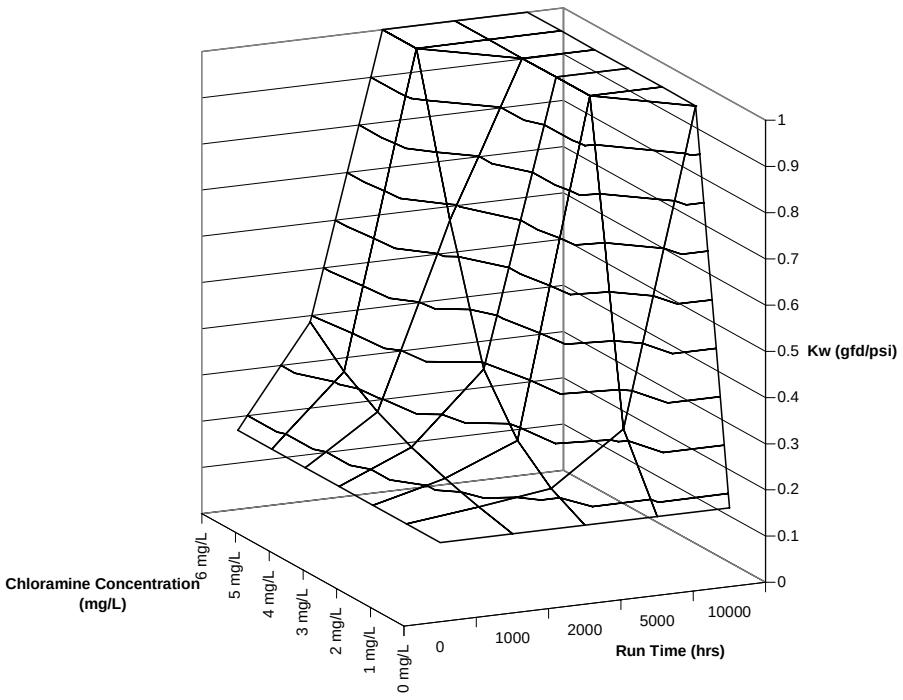

Figure 27: Trisep X20 Resistance Model Monochloramine Sensitivity Analysis

4.5.3 Osmonics SG

Multiple independent variables were determined to be significant in the mass loading and resistance models for the Osmonics SG membrane. Significant independent variables for both models included the initial solvent mass transfer coefficient, water loading, ultraviolet absorbance, monochloramine concentration, and temperature. Turbidity was also determined to be a significant independent variable for the mass loading model. Both models predicted an increase in solvent mass transfer over time with increases in water loading, monochloramine concentration, and temperature. When compared to the mass loading model, the resistance model predicted a more rapid degradation of the membrane by monochloramine. Decreases in solvent mass transfer over time were predicted by both models with increases in ultraviolet absorbance. While variations in turbidity were not significant for the resistance model, decreases

in the solvent mass transfer coefficient were predicted by the mass loading model with increasing turbidity. The results of the monochloramine sensitivity analyses for the mass loading and resistance models are presented in Tables 15 and 16, respectively. Graphical representations of the sensitivity analysis data are presented in Figures 28 and 29.

Table 15: Osmonics SG Mass Loading Model Monochloramine Sensitivity Analysis

NH_3Cl (mg/L)	Predicted Mass Transfer Coefficient for Various Membrane Run Times (gfd/psi)					
	0 hrs	1,000 hrs	2,000 hrs	5,000 hrs	10,000 hrs	25,000 hrs
0	0.114	0.101	0.088	0.049	1.000	1.000
1	0.114	0.109	0.104	0.089	0.063	1.000
2	0.114	0.117	0.120	0.128	0.142	0.184
3	0.114	0.125	0.136	0.168	0.222	0.382
4	0.114	0.133	0.152	0.208	0.301	0.581
5	0.114	0.141	0.168	0.247	0.380	0.779
6	0.114	0.149	0.183	0.287	0.460	0.978

Table 16: Osmonics SG Resistance Model Monochloramine Sensitivity Analysis

NH_3Cl (mg/L)	Predicted Mass Transfer Coefficient for Various Membrane Run Times (gfd/psi)				
	0 hrs	1,000 hrs	2,000 hrs	5,000 hrs	10,000 hrs
0	0.117	0.102	0.091	0.068	0.048
1	0.117	0.110	0.104	0.090	0.073
2	0.117	0.120	0.123	0.134	0.157
3	0.117	0.131	0.150	0.261	1.000
4	0.117	0.145	0.192	1.000	1.000
5	0.117	0.162	0.266	1.000	1.000
6	0.117	0.184	0.432	1.000	1.000

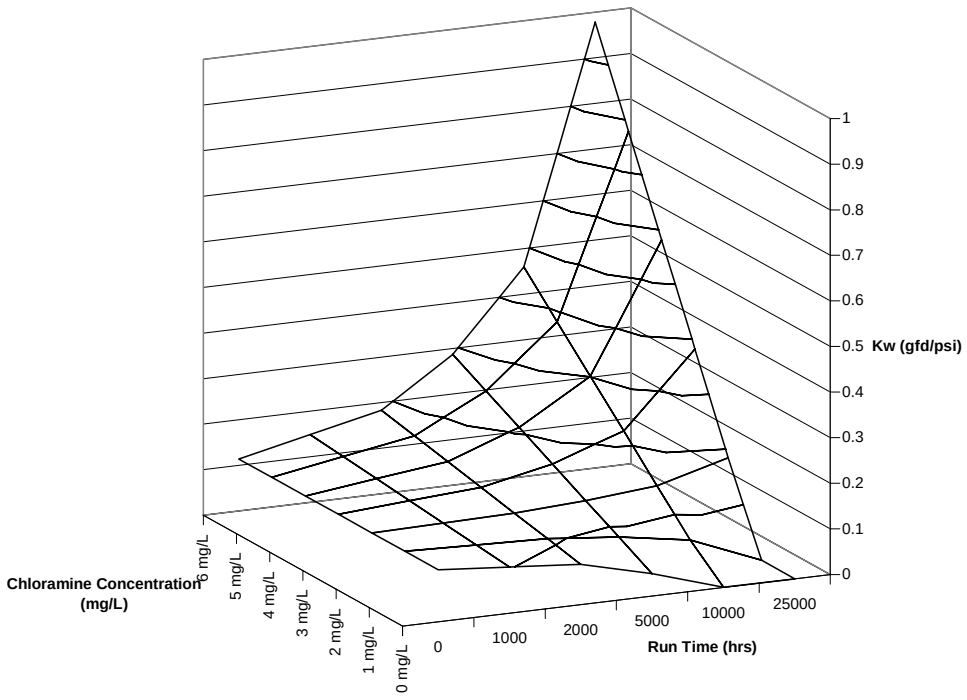

Figure 28: Osmonics SG Mass Loading Model Monochloramine Sensitivity Analysis

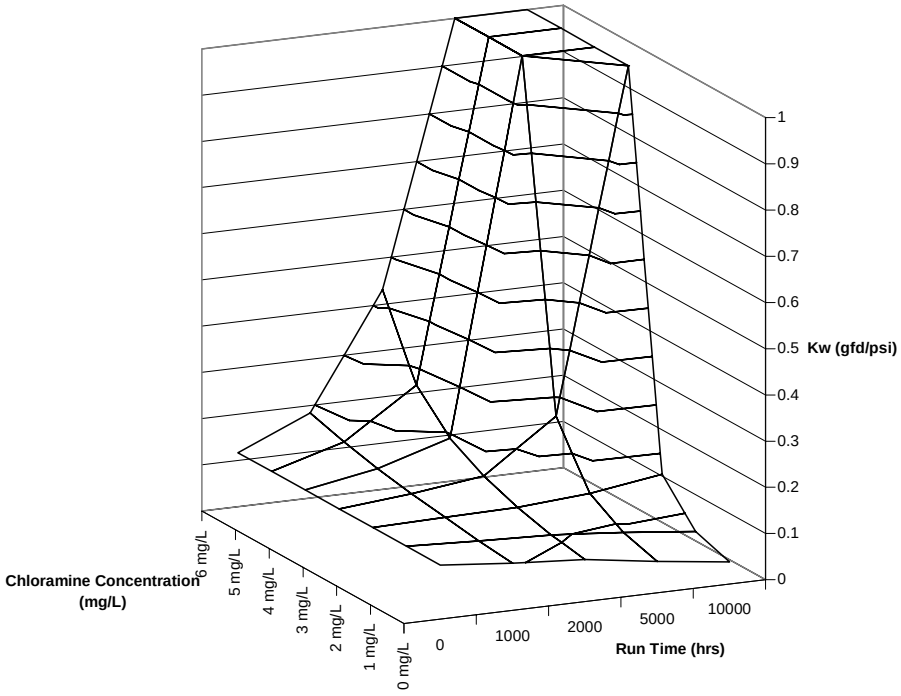

Figure 29: Osmonics SG Resistance Model Monochloramine Sensitivity Analysis

4.5.4 FilmTec BW30FR

The initial solvent mass transfer coefficient, monochloramine concentration and temperature were significant independent variables in both the mass loading and resistance models for the FilmTec BW30FR membrane. Both models predicted an increase in solvent mass transfer over time with increasing monochloramine concentration and temperature, however, the resistance model predicted accelerated membrane degradation by monochloramine when compared to the mass loading model. The results of the monochloramine sensitivity analyses for the mass loading and resistance models are presented in Tables 17 and 18, respectively. Graphical representations of the sensitivity analysis data are presented in Figures 30 and 31.

Table 17: FilmTec BW30FR Mass Loading Model Monochloramine Sensitivity Analysis

NH_3Cl (mg/L)	Predicted Mass Transfer Coefficient for Various Membrane Run Times (gfd/psi)					
	0 hrs	1,000 hrs	2,000 hrs	5,000 hrs	10,000 hrs	25,000 hrs
0	0.149	0.149	0.149	0.149	0.149	0.149
1	0.149	0.171	0.192	0.258	0.366	0.692
2	0.149	0.192	0.236	0.366	0.583	1.000
3	0.149	0.214	0.279	0.475	0.800	1.000
4	0.149	0.236	0.323	0.583	1.000	1.000
5	0.149	0.258	0.366	0.692	1.000	1.000
6	0.149	0.279	0.410	0.800	1.000	1.000

Table 18: FilmTec BW30FR Resistance Model Monochloramine Sensitivity Analysis

NH_3Cl (mg/L)	Predicted Mass Transfer Coefficient for Various Membrane Run Times (gfd/psi)				
	0 hrs	1,000 hrs	2,000 hrs	5,000 hrs	10,000 hrs
0	0.155	0.155	0.155	0.155	0.155
1	0.155	0.172	0.194	0.311	1.000
2	0.155	0.194	0.259	1.000	1.000
3	0.155	0.222	0.390	1.000	1.000
4	0.155	0.259	0.787	1.000	1.000
5	0.155	0.311	1.000	1.000	1.000
6	0.155	0.390	1.000	1.000	1.000

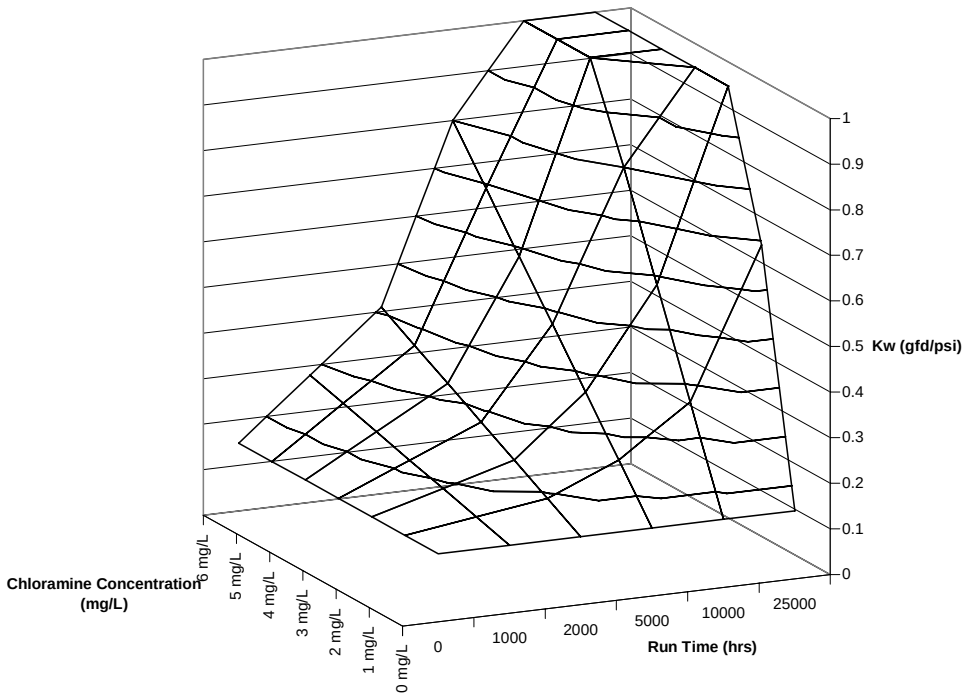

Figure 30: FilmTec BW30FR Mass Loading Model Monochloramine Sensitivity Analysis

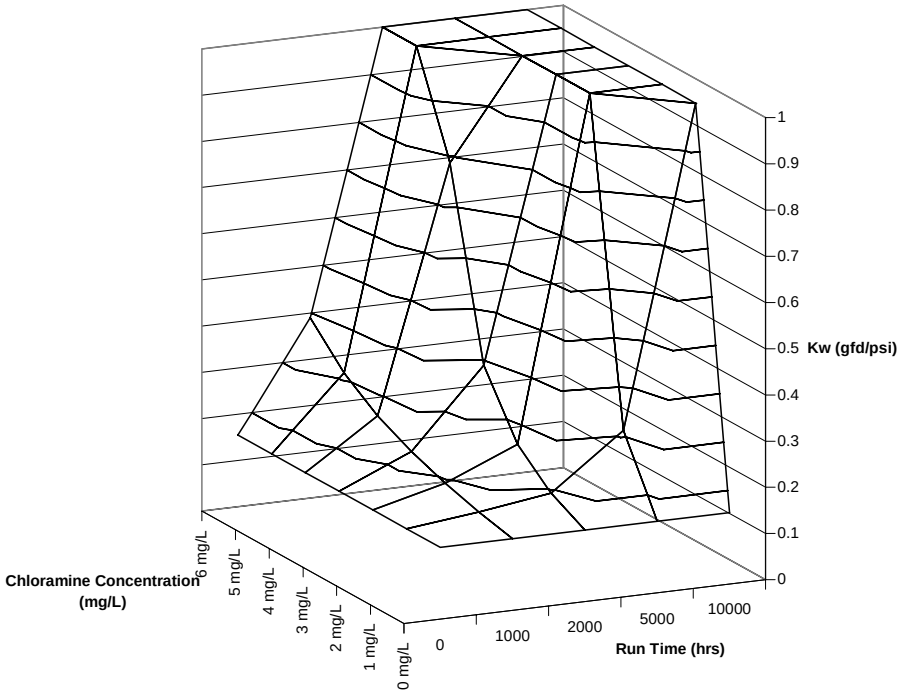

Figure 31: FilmTec BW30FR Resistance Model Monochloramine Sensitivity Analysis

4.6 Conclusions

Primary conclusions from this research are presented below:

1. Accurate mass loading and resistance models were developed to predict solvent mass transfer through diffusion controlled membranes. Independent variables included the initial solvent mass transfer coefficient, water loading, monochloramine concentration, temperature, ultraviolet absorbance, and turbidity.

2. Data collected throughout this study clearly indicated the presence of monochloramine adversely impacted the integrity of the diffusion controlled membranes used throughout this study. All mass loading and resistance models predicted membrane degradation in the presence of monochloramine.

3. Resistance models predicted accelerated membrane degradation by monochloramine when compared to the mass loading models.

4. Predicted run times for complete membrane failure ranged from 31,000 hrs to 40,000 hrs for mass loading models and 8,000 hrs to 9,000 hrs for resistance models. Predicted run times for complete membrane failure were significantly reduced at elevated monochloramine concentrations.

4.7 References

1. Chellam, S.; Jacangelo, J.; and Bonacquisti, T. (1998) Modeling and experimental verification of pilot-scale hollow fiber, direct flow microfiltration with periodic backwashing. Environmental Science and Technology, 32:75-81.

2. Chellam, S. and Wiesner, M. (1997) Evaluation of crossflow filtration models based on shear-induced diffusion and particle adhesion: Complications induced by feed suspension polydispersity. Journal of Membrane Science 3617:1-15.

3. Elimelech, M.; Zhu, X.; Childress, A.; and Hong, S. (1997) Role of membrane surface morphology in colloidal fouling of cellulose acetate and composite aromatic polyamide reverse osmosis membranes. Journal of Membrane Science, 127:101-109.

4. Faibish, R.; Elimelech, M.; and Cohen, Y. (1998) Effect of interparticle electrostatic double layer interactions on permeate flux decline in crossflow membrane filtration of colloidal suspensions: An experimental investigation. Journal of Colloid and Interface Science, 204:77-86.

5. Field, R.; Wu, D.; Howell, J.; and Gupta, B. (1995) Critical flux concept for microfiltration fouling. Journal of Membrane Science, 100:259-272.

6. Gao, S.; Li, C.; Zhang, F.; Zen, H.; and Ye, C. (2006) Pilot testing of outside-in UF pretreatment prior to RO for high turbidity seawater desalination. Desalination, 189:269-277.

7. Gwon, E.; Yu, M.; Oh, H.; and Ylee, Y. (2003) Fouling characteristics of NF and RO operated for removal of dissolved matter from groundwater. Water Research, 37:2989-2997.

8. Hobbs, C.; Hong, S.; and Taylor, J. (2006) Effect of surface roughness on fouling of RO and NF membranes during filtration of a high organic surficial groundwater. Journal of Water Supply, 55:559-570.

9. Hong, S.; Faibish, R.; and Elimelech, M. (1997) Kinetics of permeate flux decline in crossflow membrane filtration of colloidal suspensions. Journal of Colloid and Interface Science, 196:267-277.

10. Jiao, D. and Sharma, M. (1994) Mechanism of cake buildup in crossflow filtration of colloidal suspensions. Journal of Colloid and Interface Science, 162:454-462.

11. Jonsson, A. and Jonsson, B. (1996) Ultrafiltration of colloidal dispersions – A theoretical model of the concentration polarization phenomena. Journal of Colloid and Interface Science, 180:504-518.

12. Lovins, W. (2000) Correlation and modeling of laboratory and field-scale integrated membrane system productivity and water quality. Doctoral Dissertation, University of Central Florida, Orlando.

13. Madaeni, S. and Fane, A. (1996) Microfiltration of very dilute colloidal mixtures. Journal of Membrane Science, 113:301-312.

14. Mulford, L.; Taylor, J.; Nickerson, D; and Chen, S. (1999) NF performance at full and pilot scale, Journal AWWA, 91:64-75.

15. Robert, C. (1999) Resistance modeling of membrane fouling based on water quality mass loading. Doctoral Dissertation, University of Central Florida, Orlando.

16. Romero, C. and Davis, R. (1991) Experimental verification of the shear-induced hydrodynamic diffusion model of crossflow microfiltration. Journal of Membrane Science, 62:249-273.

17. Tarleton, E. and Wakeman, R. (1994) Understanding flux decline in crossflow microfiltration: Part III-Effects of membrane morphology. Trans.IChemE, 72:521-529.

18. USEPA. (1996) ICR manual for bench- and pilot-scale treatment studies. Office of ground water and drinking water. 1-108.

19. Visvanathan, C. and Aim, R. (1989) Studies on colloidal membrane fouling mechanisms in crossflow microfiltration. Journal of Membrane Science, 45:3-15.

20. Welsch, K.; McDonough, R.; Fane, A.; and Fell, C. (1995) Calculation of limiting fluxes in the ultrafiltration of colloids and fine particulates. Journal of Membrane Science, 99:229-239.

21. Zhao, Y. and Taylor, J. (2005) Assessment of ASTM D 4516 for evaluation of reverse osmosis membrane performance. Desalination, 180:231-244.

22. Zhao, Y.; Taylor, J.; and Hong, S. (2005) Combined influence of membrane surface properties and feed water qualities on RO/NF mass transfer, a pilot study. Water Research, 39(7):1233-1244.

23. Zhu, X. and Elimelech, M. (1995) Fouling of reverse osmosis membranes by aluminum oxide colloids. Journal of Environmental Engineering, ASCE, 121:884-892.

CHAPTER 5
MODELING PERFORMANCE OF NANOFILTRATION AND REVERSE OSMOSIS MEMBRANES TREATING FILTERED SECONDARY WASTEWATER EFFLUENT AND IDENTIFICATION OF FOULANTS

5.1 Introduction

Membrane processes have found increasing use in environmental applications (WERF, 2005; Zhao and Taylor, 2005; Zhao et. al., 2005; Chellam et. al., 1998). The use of membrane processes in wastewater treatment is no exception. Presently, over 120 full-scale facilities (design flow rate greater than 0.25 mgd) utilize membrane processes to treat wastewater streams ranging from raw wastewater to secondary effluent. Membrane processes include microfiltration (MF), ultrafiltration (UF), membrane bioreactor (MBR), nanofiltration (NF), and reverse osmosis (RO) (WERF, 2005). However, the reduction of membrane productivity (i.e. membrane fouling) presents significant obstacles for all membrane processes that must be properly managed to maintain system productivity. Membrane fouling originates from the rejection of contaminants contained in the feed stream and the accumulation of these contaminants on the feed side of the membrane. Membrane fouling results in an increased resistance to solvent transport through the membrane and increased operating pressures are required to maintain constant flow rates through the membrane system.

Factors that affect the rate and extent of membrane fouling have been the subject of numerous research studies. These chemical and physical factors can be classified into the following categories: membrane characteristics, particle characteristics, membrane hydrodynamics, and feed solution chemistry. The effects of membrane characteristics, such as

hydrophobicity, surface charge, and surface roughness, on fouling were examined by several researchers through a variety of studies. Madaeni and Fane (1996) investigated the effect of membrane hydrophobicity on fouling and concluded hydrophobic membranes experienced increased fouling when compared to hydrophilic membranes. Studies conducted by Welsh et. al. (1995) and Tarleton and Wakeman (1994) examined the correlation between membrane fouling and surface charge. These researchers determined membrane fouling was reduced when repulsive electrical interactions between the membrane and foulants existed. The effect of membrane surface roughness on fouling was evaluated by Elimelech et. al. (1997) and Hobbs et. al. (2006). Results of both studies indicated membranes with rough surfaces exhibited increased fouling when compared to membranes with smooth surfaces.

Studies have also been conducted to evaluate membrane fouling as a function of particle characteristics, such as size and concentration. The effect of particle size on membrane fouling was studied extensively by numerous researchers. Studies conducted by Hong et. al. (1997), Romero and Davis (1991), Lahoussine-Turcaud et. al. (1990), Jiao and Sharma (1994), Chellem and Wiesner (1997), and Tarleton and Wakeman (1994) clearly demonstrated that the severity of membrane fouling increased with decreasing particle size. Several researchers evaluated the effect of particle concentration on membrane fouling. Increases in membrane fouling resulting from increased particle concentrations were observed by Jonnson and Jonnson (1996), Welsch et. al. (1995), Zhu and Elimelech (1995), and Chudacek and Fane (1984).

The effects of hydrodynamic conditions, including crossflow velocity and permeation velocity, on membrane fouling were evaluated by several researchers through various studies. Chellam and Wiesner (1997), Chen et. al. (1997), and Hong et. al. (1997) all observed increases

in membrane fouling as the crossflow velocity was decreased. Reductions in crossflow velocity increased the thickness of the fouling layer on the surface of the membrane and resulted in increased resistance to permeate flow. Similar studies conducted by Hong et. al. (1997), Faibish et. al. (1998), and Field et. al. (1995) were designed to elucidate the effect of permeation velocity on membrane fouling. Data gathered throughout these studies indicated membrane fouling increased with increasing permeation velocity. Increases in permeation velocity resulted in increased foulant transport to the surface of the membrane and consequently an increase in membrane fouling.

Studies designed to determine the effect of feed solution chemistry (i.e. ionic strength) on membrane fouling were conducted by several researchers. Data collected by Faibish et. al. (1998) Chen et. al. (1997), and Bowen et. al. (1996) indicated membrane fouling increased with increasing feed solution ionic strength. This observation was attributed to two phenomena. First, the increase of the ionic strength of the feed solution decreases the repulsive forces between the foulants and the membrane and results in increased foulant deposition on the surface of the membrane. Second, the reduction in repulsive forces results in a more densely packed foulant layer on the membrane surface and decreases membrane productivity.

While these well controlled laboratory studies contributed significantly to the body of knowledge regarding the fundamental mechanics of membrane fouling, their relevance for predicting long term fouling and performance for membrane systems treating non-synthetic source waters is extremely limited. Consequently, the effects of long-term operation on membrane fouling and performance are often evaluated through pilot studies using natural source waters.

Numerous pilot studies have been conducted on a variety of natural source waters, including: seawater, groundwater, surface water, and secondary and tertiary wastewater effluent (Gao et. al., 2006; Pollice et. al., 2004; and Gwon et. al., 2003). The primary objective of many of these studies was to collect operating data, such as pretreatment requirements, feed pressure requirements, limitations on flux and recovery rates, product water quality, post-treatment requirements, and cleaning frequency, to aid in the design of full-scale facilities. Few pilot studies have been conducted with more fundamental objectives, such as the development of dynamic solvent or solute mass transfer models (Lovins, 2000; Mulford et. al., 1999; Robert, 1999; Chellam et. al., 1998). However, the aforementioned studies were performed utilizing groundwater and surface water supplies. Literature surveys indicated the dynamic mass transfer modeling for diffusion controlled membranes treating wastewater effluent has not yet been addressed.

5.2 Membrane Theory and Model Development

Membrane productivity was evaluated through the calculation of the solvent mass transfer coefficient throughout the study. Figure 32 presents a simplified diagram of a general membrane process. Mass balances for the general membrane process depicted in Figure 32 are presented in Equations 11 and 12.

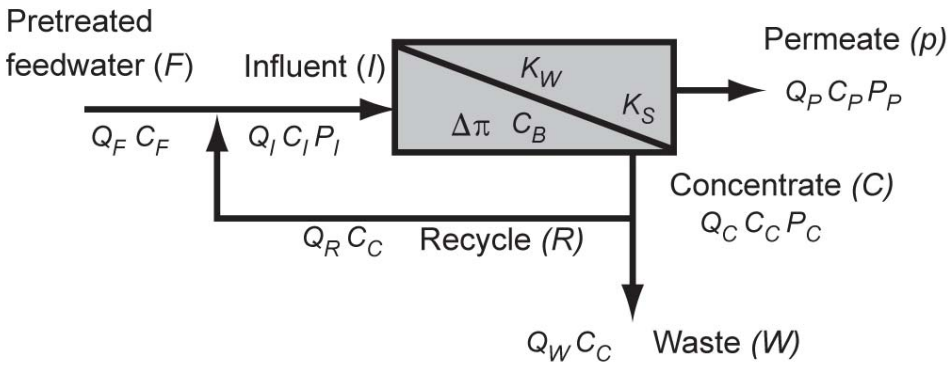

Figure 32: Single Membrane Element Flow Diagram

$$Q_f = Q_p + Q_c \tag{11}$$

$$Q_f C_f = Q_p C_p + Q_c C_c \tag{12}$$

where: Q_f = Feed stream flow rate (L^3/t)

Q_p = Permeate stream flow rate (L^3/t)

Q_c = Concentrate stream flow rate (L^3/t)

C_f = Feed stream solute concentration (M/L^3)

C_p = Permeate stream solute concentration (M/L^3)

C_c = Concentrate stream solute concentration (M/L^3)

Significant equations used in the calculation of the solvent mass transfer coefficient are presented below. The permeate flux of the membrane system was determined by dividing the permeate flow rate by the total membrane surface area available for treatment, as shown in Equation 13. Variations in solvent viscosity due to daily temperature changes were taken into account by normalizing the permeate flux with respect to temperature (Equation 14). The normalized solvent mass transfer coefficient, also referenced as productivity or specific flux, was

determined by dividing the normalized permeate flux by the net driving force applied to the membrane system, as described in Equation 15.

$$F_w = \frac{Q_p}{A} \tag{13}$$

$$F_{w_{Noem}} = \frac{F_w}{1.03^{(T-25)}} \tag{14}$$

$$K_{w_{Norm}} = \frac{F_{w_{Norm}}}{\Delta P - \Delta \Pi} = \frac{F_{w_{Norm}}}{NDF} \tag{15}$$

where: F_w = Permeate flux (L/t)

Q_p = Permeate stream flow rate (L^3/t)

A = Membrane surface area (L^2)

F_{wNorm} = Normalized permeate flux (L/t)

T = Temperature (°C)

K_{wNorm} = Normalized solvent mass transfer coefficient (L^2t/M)

ΔP = Pressure gradient (F/L^2)

$\Delta \Pi$ = Osmotic pressure gradient (F/L^2)

NDF = Net driving force (F/L^2)

As previously stated, the accumulation of contaminants on the feed side of the membrane results in the reduction in membrane productivity with time and several researchers have utilized mass loading and resistance models to dynamically model the solvent mass transfer of a membrane system (Lovins, 2000; Mulford et. al., 1999; Robert, 1999; Chellam et. al., 1998). Details regarding the development of mass loading and resistance models can be found in the aforementioned references. In this study, mass loading and resistance models were developed to

predict solvent mass transfer as a function of various independent variables, including: time, temperature, initial solvent mass transfer coefficient, water loading, total dissolved solids, orthophosphorous, silica, total organic carbon, and turbidity. The general forms of the mass loading and resistance models evaluated in this study are presented in Equations 16 and 17, respectively.

$$K_{w,i} = \Theta^{(T_i - 25)} \times \begin{bmatrix} K_{w_0} + X_1 F_{w,i} t_i + X_2 TDS_i F_{w,i} t_i + \\ X_3 OrthoP_i F_{w,i} t_i + X_4 Silica_i F_{w,i} t_i + \\ X_5 TOC_i F_{w,i} t_i + X_6 Turb_i F_{w,i} t_i \end{bmatrix} \tag{16}$$

$$K_{w,i} = \frac{\Theta^{(T_i - 25)} K_{w_0}}{1 + \left[\Theta^{(T_i - 25)} K_{w_0} \begin{pmatrix} X_1 F_{w,i} t_i + X_2 TDS_i F_{w,i} t_i + \\ X_3 OrthoP_i F_{w,i} t_i + X_4 Silica_i F_{w,i} t_i + \\ X_5 TOC_i F_{w,i} t_i + X_6 Turb_i F_{w,i} t_i \end{pmatrix} \right]} \tag{17}$$

where: $K_{w,i}$ = Predicted solvent mass transfer coefficient at time t (L^2t/M)

Θ = Temperature correction factor

T_i = Temperature at time t (°C)

K_{w0} = Initial solvent mass transfer coefficient (L^2t/M)

X_i = Regression coefficient for parameter i

$F_{w,i}$ = Permeate flux at time t (L/t)

t = Operation time (t)

TDS = Total dissolved solids concentration at time t (M/L^3)

OrthoP = Orthophosphate concentration at time t (M/L^3)

Silica = Silica concentration at time t (M/L^3)

TOC = Total organic carbon concentration at time t (M/L^3)

Turb = Turbidity at time t (NTU)

Non-linear regression techniques provided the means for evaluating the dynamic mass loading and resistance models. All independent variable data were initially regressed against the mass loading and resistance models presented above. Statistically insignificant independent variables were removed from the models, beginning with the least significant variable, one at a time. Regression procedures were repeated until all variables were significant.

5.3 Pilot System

5.3.1 Overview

The source water utilized throughout this study originated from the North Buffalo Water Reclamation Facility (NBWRF), located in Greensboro, North Carolina. Filtered secondary effluent received advanced pretreatment prior to reverse osmosis (RO) and nanofiltration (NF) membrane treatment. Pretreatment processes consisted of microfiltration (MF) and ultrafiltration (UF).

Reverse osmosis and nanofiltration membrane treatment was provided by three different thin film composite membranes: the Hydranautics ESPA2, the Dow/FilmTec NF90, and the Trisep X20. In order to test all three membrane elements simultaneously using both pretreated waters, two multi-skid test units were utilized throughout this study. The process flow diagram for the pilot system is presented in Figure 33.

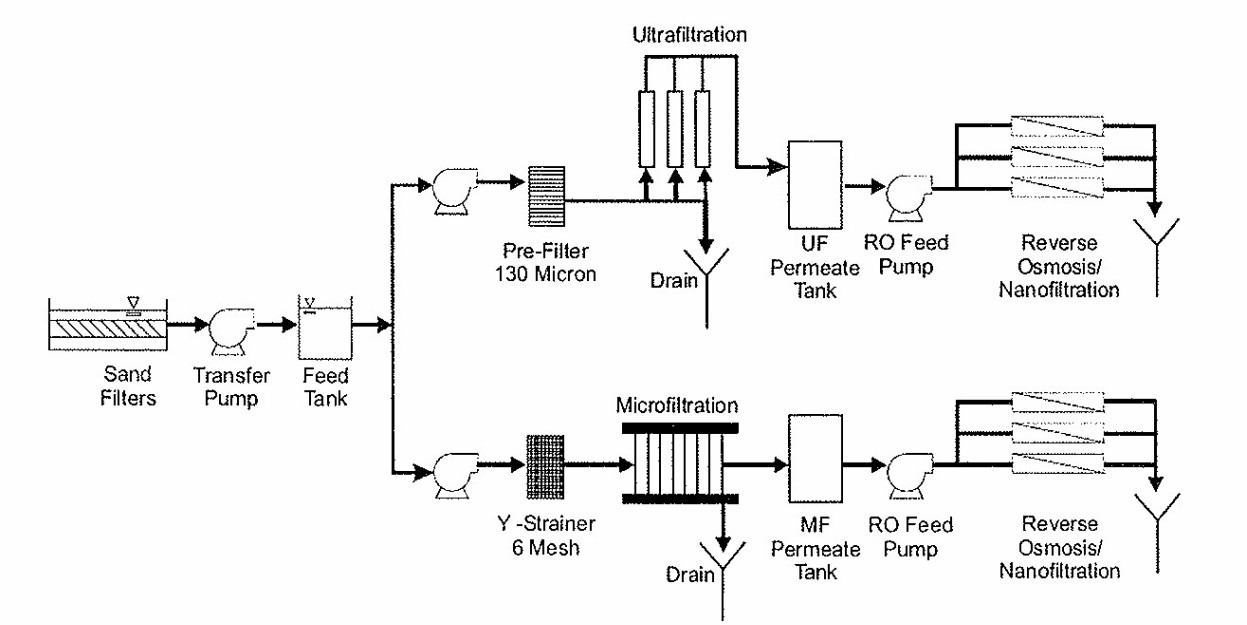

Figure 33: Pilot System Process Flow Diagram

5.3.2 Source Water

Filtered secondary effluent from the NBWRF served as the source water throughout this study. This facility provides treatment for a mixture of domestic, commercial, and industrial wastewaters and has a permitted capacity of 16 mgd annual average daily flow (AADF). Primary treatment consisted of bar screening, grit removal, and primary clarification while secondary treatment consisted of trickling filtration, activated sludge processes, and secondary clarification. Secondary effluent was filtered and disinfected prior to discharge in the North Buffalo Creek. The quality of the filtered secondary effluent is presented in Table 19.

Table 19: Filtered Secondary Effluent Water Quality

Parameter	Average	Standard Deviation
Average Annual Daily Flow	10.3 mgd	1.5 mgd
Biochemical Oxygen Demand (BOD_5)	3.2 mg/L	2.2 mg/L
Total Suspended Solids	4.7 mg/L	3.5 mg/L
Ammonia	1.1 mg/L	0.7 mg/L
Total Phosphorous	1.0 mg/L	0.2 mg/L
Total Organic Carbon	14.9 mg/L	3.2 mg/L
pH	6.6	0.3

5.3.3 Low Pressure Membrane Pretreatment

Microfiltration (MF) and ultrafiltration (UF) processes provided advanced pretreatment of filtered secondary effluent prior to disinfection. The MF unit provided 0.2-um nominal filtration of the effluent and consisted of a feed pump, a 6-mesh (3,350 um) Y-strainer, six outside-in polypropylene US Filter/Memcor M10C modules, and a programmable logic controller to monitor the status of the unit and control automatic processes. The MF unit was operated in a dead-end mode of operation at a constant flux of 16 gallons per square foot per day (gfd). Productivity was maintained through a high pressure air backwash and high velocity feedwater flush sequence which occurred every 20 minutes.

The UF unit provided 0.017-um nominal filtration of the effluent and consisted of a feed pump, a backwash pump, two chemical metering pumps, a 130-um self cleaning Boll strainer, three inside-out polyethersulfone Hydranautics HYDRAcap 60 UF modules, and a programmable logic controller to control automatic processes. The UF unit was operated in a dead-end mode of operation at a constant flux of 30 gfd. In-line coagulation was accomplished through the addition of 4 mg/L of ferric chloride into the feed stream of the unit. Productivity

was maintained through conventional and chemically enhanced backwashing procedures every 25 minutes.

5.3.4 High Pressure Membrane Treatment

Two identical skid mounted pilot units provided simultaneous RO/NF treatment for the pretreated effluent. Each unit contained a single multi-stage centrifugal feed pump equipped with a variable frequency drive; three membrane trains; various pressure gauges, flow meters, and valves to monitor and control the operation of each train. All membrane trains were configured to achieve one-stage operation and consisted of two pressure vessels arranged in series. A total of six 4-inch diameter, 40-inch long membrane elements were installed in each membrane train.

Three different polyamide thin film composite membranes provided RO/NF membrane treatment throughout this study and included the Hydranautics ESPA2, the Dow/FilmTec NF90, and the Trisep X20 membrane elements. Simultaneous side-by-side RO/NF membrane treatment was provided by two skid mounted pilot units and each unit received water from one of the advanced pretreatment processes. The skid mounted pilot unit that received MF pretreated effluent was designated as the MF-RO unit while the unit that received UF pretreated effluent was designated as the UF-RO unit.

5.3.5 Operation of High Pressure Membrane Units

Constant operating conditions for all high pressure membrane trains were maintained through the manipulation of the speed of the feed pumps, feed control valves, and concentrate control valves for the duration of the study. The desired flux and recovery values for all high

pressure membrane trains were 8 gfd and 50 percent, respectively. No physical or chemical treatment beyond that provided during low pressure membrane pretreatment was provided prior to high pressure membrane treatment.

5.3.6 Monitoring of High Pressure Membrane Units

Operating parameters for each high pressure membrane train were recorded every day. Field mounted instrumentation included: an hour meter to monitor the operating time of the unit; pressure gauges to monitor the feed, permeate, and concentrate streams; flow meters to monitor the permeate and concentrate streams; and a pH meter and thermometer to monitor the feed stream. Feed, permeate, and concentrate samples were collected and analyzed in the field to determine the conductivity of each stream.

5.3.7 Water Quality

Samples of the feed, permeate, and concentrate streams were collected from each high pressure membrane train on a bi-weekly basis. Immediately following collection, samples were delivered to Meritech Inc. Environmental Laboratory and the University of North Carolina at Chapel Hill for analysis. Meritech performed the analysis for all inorganic parameters of interest including: ammonia nitrogen, calcium, chloride, nitrate/nitrite nitrogen, orthophosphate, silica, sodium, and total dissolved solids. The University of North Carolina at Chapel Hill determined the total organic carbon concentration of all samples. The method used to determine the concentration of each parameter is summarized in Table 20 below.

Table 20: Methods of Water Quality Analysis

Parameter	Method
Ammonia, Nitrogen	EPA 350.1
Calcium	EPA 200.7
Chloride	EPA 325.3
Nitrate/Nitrite, Nitrogen	EPA 353.2
Orthophosphate	EPA 365.2
Silica	EPA 200.7
Sodium	EPA 200.7
Total Dissolved Solids	EPA 160.1
Total Organic Carbon	Standard Method 5310B

5.3.8 Membrane Autopsy

Autopsies were performed on membrane elements removed from each unit upon the completion of the operational portion of this study. Membrane Forensics of San Diego, California performed loss on ignition (LOI) tests and targeted energy dispersive X-ray analyses (TEDXA) to determine the relative percentages of organic and inorganic foulants on the surface of the membranes and to identify the composition of the inorganic fractions, respectively. The University of North Carolina quantified both the amount of dissolved organic carbon and the amount of polysaccharides that had accumulated on the surface of the membranes during operation.

Samples of the foulant material deposited on the surface of each membrane during operation were collected for analysis. Relative percentages of organic and inorganic foulants for each membrane were determined from Equations 18 and 19 below. Inorganic portions of the foulants were further analyzed by an ETEC Autoscan Scanning Electron Microscope (SEM).

Secondary and backscatter electron images of each sample were used to determine particle structures and elemental compositions.

$$Organic\ \ Foulant\ \ Percentage = \frac{M_{110} - M_{550}}{M_{110}}(100\%) \tag{18}$$

$$Inorganic\ \ Foulant\ \ Percentage = \frac{M_{550}}{M_{110}}(100\%) \tag{19}$$

where: M_{110} = Mass of foulant sample dried at 110°C

M_{550} = Mass of foulant sample after ignition at 550°C

The amount of dissolved organic carbon accumulated on the surface of the membranes was quantified through additional analyses. Foulant material collected from a 100 cm^2 membrane sample was added to 100 mL of ultrapure laboratory grade water and sonicated for 20 minutes. Samples were subsequently filtered through a 0.45 um Durapore PVDF membrane and analyzed by a Shimadzu Total Organic Carbon Analyzer (TOC-5000) using a UV-persulfate digestion method. Similar procedures have been used by other researchers (Croue et. al., 2003).

A phenol-sulfuric acid colorimetric method of analysis was utilized to quantify the amount of polysaccharides deposited on the surface of each membrane (Cho and Fane, 2002; Fonseca, 2002). Small membrane sections (totaling 40 cm^2) were dissolved into 2 mL of a 2.5% phenol solution. Following the dissolution, 10 mL of 98% sulfuric acid was added to the solution and allowed to react for a period of 10 minutes at ambient temperature and 15 minutes at 25°C. The sample absorbance at 488 nm was measured by a Hitachi UV/visible spectrophotometer (U-2000). The absorbance value of each sample was compared against a calibration curve developed with glucose standard solutions.

5.4 Model Development

5.4.1 Data Organization

Water quality data for both the MF and UF filtrate are summarized in Tables 21 and 22, respectively. Analyses were performed on these paired data sets to determine any statistical differences between the pretreated waters. The results of the student T-tests, presented in Table 23, indicated the quality of the pretreated waters was identical with the exception of orthophosphate for the measured parameters. Differences in orthophosphate concentrations were attributed to ferric sulfate addition in the UF pretreatment process. As such, initial models were developed from pooled data from both the MF-RO and UF-RO units for each polyamide thin film composite membrane. Subsequent models were also developed for each membrane from individual data obtained from the MF-RO unit and the UF-RO unit.

Table 21: Filtrate Water Quality for Microfiltration Unit

Date	Chloride (mg/L)	Total Dissolved Solids (mg/L)	Ammonia (mg/L as N)	Nitrate/ Nitrite (mg/L as N)	Ortho Phosphate (mg/L)	Calcium (mg/L)	Silica (mg/L)	Sodium (mg/L)	Total Organic Carbon (mg/L)
4/27/2005	42.4	270	0.2	21.4	0.8	18.1	8.2	56.5	18.5
5/3/2005	43.0	285	0.9	14.8	1.1	17.6	7.4	47.8	13.2
5/11/2005	36.6	260	0.3	13.1	0.9	16.4	6.9	48.1	
5/17/2005	36.4	286	0.1	19.2	0.9	15.8	6.8	51.8	13.1
5/31/2005	34.5	300	0.1	18.0	0.9	17.2	8.0	47.7	13.0
6/14/2005	39.1	263	0.1	18.6	0.9	15.7	7.3	52.7	12.3
7/6/2005	38.6	288	0.1	20.9	0.7	17.4	7.0	52.4	10.7
7/20/2005	40.2	348	0.1	16.8	0.7	15.9	6.6	49.7	12.2

Table 22: Filtrate Water Quality for Ultrafiltration Unit

Date	Chloride (mg/L)	Total Dissolved Solids (mg/L)	Ammonia (mg/L as N)	Nitrate/ Nitrite (mg/L as N)	Ortho Phosphate (mg/L)	Calcium (mg/L)	Silica (mg/L)	Sodium (mg/L)	Total Organic Carbon (mg/L)
4/27/2005	34.3	290	0.3	15.9	0.3	17.7	8.0	52.5	16.9
5/3/2005	34.6	310	1.0	16.8	0.6	17.6	7.4	48.9	12.7
5/11/2005	41.8	249	0.4	12.5	0.5	16.3	7.1	47.4	
5/17/2005	39.2	294	0.1	20.7	0.5	16.4	6.7	52.0	11.1
5/31/2005	42.9	316	0.1	18.0	0.4	17.7	7.4	51.6	12.7
6/14/2005	42.7	329	0.1	18.3	0.4	15.5	7.2	51.6	12.0
7/6/2005	41.2	268	0.1	20.4	0.3	17.5	7.0	53.1	10.6
7/20/2005	39.1	352	0.1	16.1	0.2	16.2	6.9	50.2	11.8

Table 23: T-Test Results for Paired Samples with Equal Variance

Parameter	T-Value	T-Critical	P-Value	Observations	Degrees of Freedom
Chloride	-0.391	2.145	0.351	8	14
TDS	-0.881	2.145	0.197	8	14
Ammonia-N	-0.253	2.145	0.402	8	14
Nitrate/Nitrite-N	0.371	2.145	0.358	8	14
Ortho Phosphate	7.083	2.145	0.000	8	14
Calcium	-0.224	2.145	0.413	8	14
Silica	0.254	2.145	0.402	8	14
Sodium	-0.058	2.145	0.477	8	14
TOC	0.612	2.179	0.276	7	12

5.4.2 Productivity Models Using Pooled Data

Initial mass loading and resistance models were developed for each of the RO/NF membrane models evaluated in this study and are presented in Tables 24 and 25, respectively. Parameters of significance for the mass loading and resistance models for all membranes included the initial solvent mass transfer coefficient and the temperature. Water loading was determined to be significant in only the mass loading model for the Hydranautics ESPA2 membrane.

Table 24: Mass Loading Models Generated from Pooled Data Sets

Membrane	Model Formula	Correlation Coefficient (R^2)
Hydranautics ESPA2	$K_w = 1.001^{(T-25)} \times \left(K_{w_o} - 4.34 \times 10^{-6} F_w t\right)$	0.08
Dow/FilmTec NF90	$K_w = 0.975^{(T-25)} \times \left(K_{w_o}\right)$	0.44
Trisep X20	$K_w = 0.979^{(T-25)} \times \left(K_{w_o}\right)$	0.61

Table 25: Resistance Models Generated from Pooled Data Sets

Membrane	Model Formula	Correlation Coefficient (R^2)
Hydranautics ESPA2	$K_w = \frac{0.981^{(T-25)} K_{w_o}}{1 + 0.981^{(T-25)} K_{w_o}}$	-0.21
Dow/FilmTec NF90	$K_w = \frac{0.991^{(T-25)} K_{w_o}}{1 + 0.991^{(T-25)} K_{w_o}}$	0.52
Trisep X20	$K_w = \frac{0.991^{(T-25)} K_{w_o}}{1 + 0.991^{(T-25)} K_{w_o}}$	0.71

Correlation coefficients for the mass loading and resistance models indicated poor to moderate accuracy when the models were used to predict the solvent mass transfer coefficient of each membrane. Figures 34 through 36 present actual and predicted solvent mass transfer coefficients for the Hydranautics ESPA2, the Dow/FilmTec NF90, and the Trisep X20 membranes, respectively, and illustrate the poor to moderate accuracy of both the mass loading and resistance models developed from the pooled data.

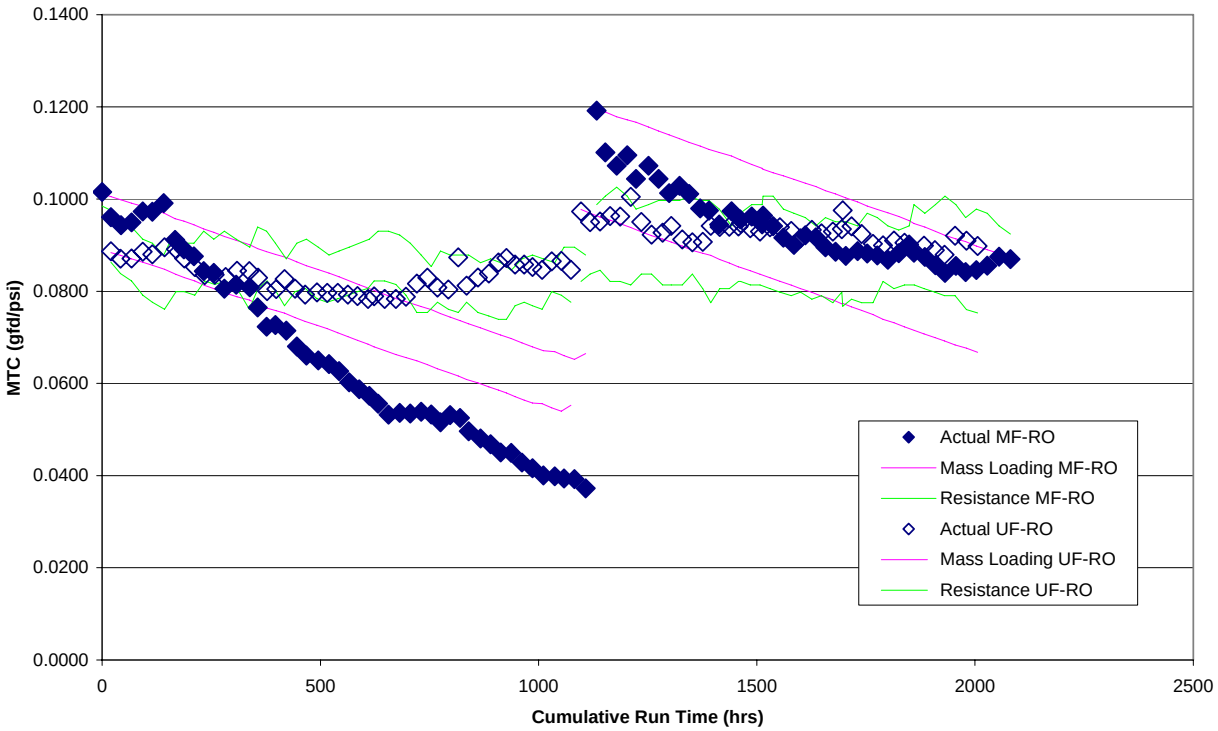

Figure 34: Actual and Predicted Solvent Mass Transfer Coefficient for Hydranautics ESPA2 Membrane Based on Pooled Data

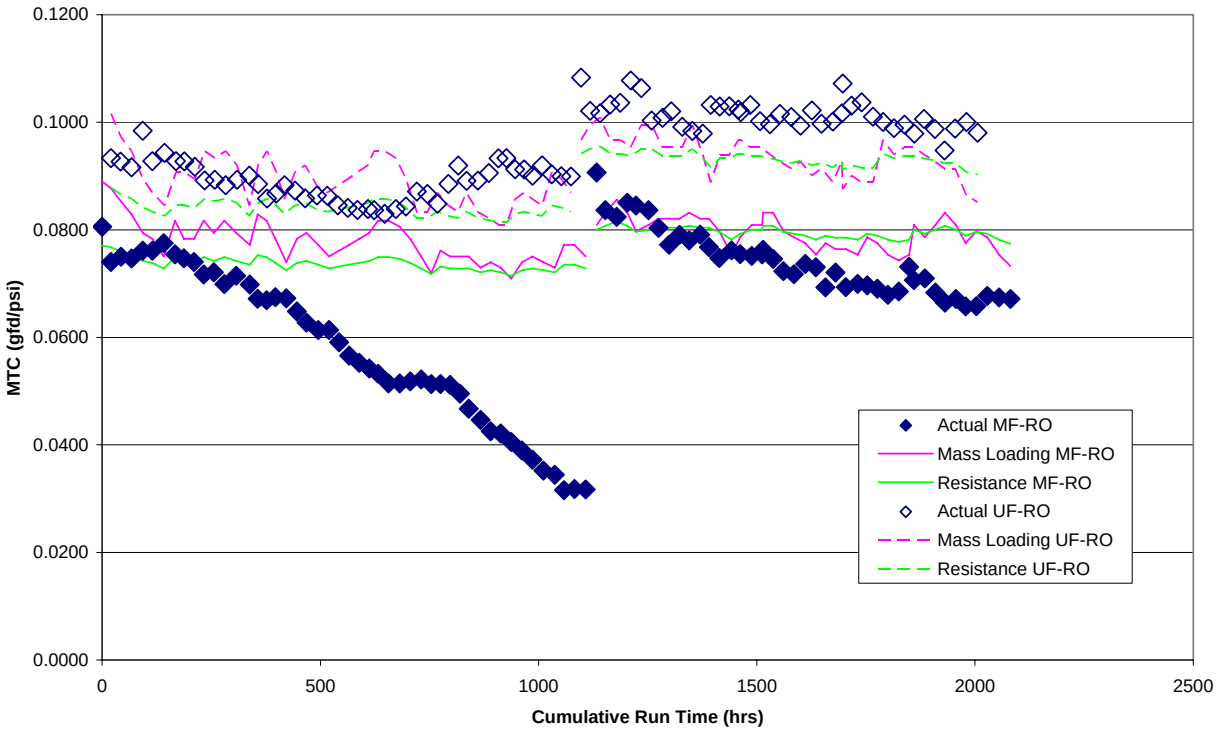

Figure 35: Actual and Predicted Solvent Mass Transfer Coefficient for Dow/FilmTec NF90 Membrane Based on Pooled Data

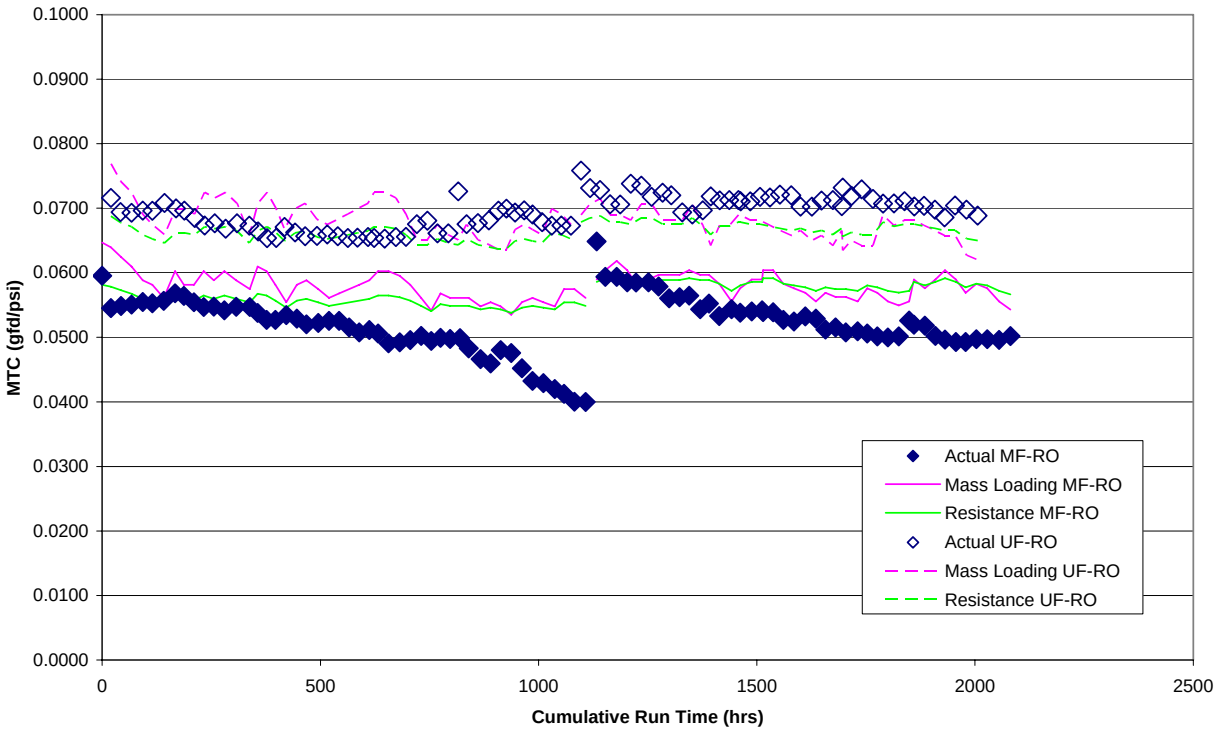

Figure 36: Actual and Predicted Solvent Mass Transfer Coefficient for Trisep X20 Membrane Based on Pooled Data

5.4.3 Productivity Models Using Individual Data

Due to the poor to moderate correlation coefficients for the models developed from the pooled data, additional mass loading and resistance models were developed from individual data obtained from the MF-RO unit and the UF-RO unit. These models are presented in Tables 26 and 27. The initial solvent mass transfer coefficient, temperature, and water loading were determined to be significant parameters in the mass loading and resistance models for all membranes.

Table 26: Mass Loading Models Developed from Independent Data

MF-RO Unit		
Membrane	**Model Formula**	**Correlation Coefficient (R^2)**
Hydranautics ESPA2	$K_w = 1.003^{(T-25)} \times \left(K_{w_o} - 7.38 \times 10^{-6} F_w t\right)$	0.88
Dow/FilmTec NF90	$K_w = 1.004^{(T-25)} \times \left(K_{w_o} - 4.90 \times 10^{-6} F_w t\right)$	0.88
Trisep X20	$K_w = 0.986^{(T-25)} \times \left(K_{w_o} - 1.71 \times 10^{-6} F_w t\right)$	0.72
UF-RO Unit		
Membrane	**Model Formula**	**Correlation Coefficient (R^2)**
Hydranautics ESPA2	$K_w = 1.000^{(T-25)} \times \left(K_{w_o} - 1.07 \times 10^{-6} F_w t\right)$	0.69
Dow/FilmTec NF90	$K_w = 0.995^{(T-25)} \times \left(K_{w_o} - 7.62 \times 10^{-7} F_w t\right)$	0.73
Trisep X20	$K_w = 0.996^{(T-25)} \times \left(K_{w_o} - 6.20 \times 10^{-7} F_w t\right)$	0.15

Table 27: Resistance Models Developed from Independent Data

MF-RO Unit		
Membrane	**Model Formula**	**Correlation Coefficient (R^2)**
Hydranautics ESPA2	$K_w = \frac{1.018^{(T-25)} K_{w_o}}{1 + 1.018^{(T-25)} K_{w_o} \times 0.0011 F_w t}$	0.76
Dow/FilmTec NF90	$K_w = \frac{1.013^{(T-25)} K_{w_o}}{1 + 1.013^{(T-25)} K_{w_o} \times 0.0012 F_w t}$	0.77
Trisep X20	$K_w = \frac{0.989^{(T-25)} K_{w_o}}{1 + 0.989^{(T-25)} K_{w_o} \times 0.0006 F_w t}$	0.76
UF-RO Unit		
Membrane	**Model Formula**	**Correlation Coefficient (R^2)**
Hydranautics ESPA2	$K_w = \frac{1.002^{(T-25)} K_{w_o}}{1 + 1.002^{(T-25)} K_{w_o} \times 0.0002 F_w t}$	0.71
Dow/FilmTec NF90	$K_w = \frac{0.997^{(T-25)} K_{w_o}}{1 + 0.997^{(T-25)} K_{w_o} \times 0.0001 F_w t}$	0.75
Trisep X20	$K_w = \frac{0.997^{(T-25)} K_{w_o}}{1 + 0.997^{(T-25)} K_{w_o} \times 0.0001 F_w t}$	0.18

The correlation coefficients associated with each model generally indicate a high level of accuracy when the models were used to predict the solvent mass transfer coefficient of each membrane. Actual solvent mass transfer coefficients and solvent mass transfer coefficients predicted by models developed from individual data for each membrane are shown in Figures 37 through 39, and illustrate the accuracy of both the mass loading and resistance models developed from individual data obtained from the MF-RO unit and the UF-RO unit.

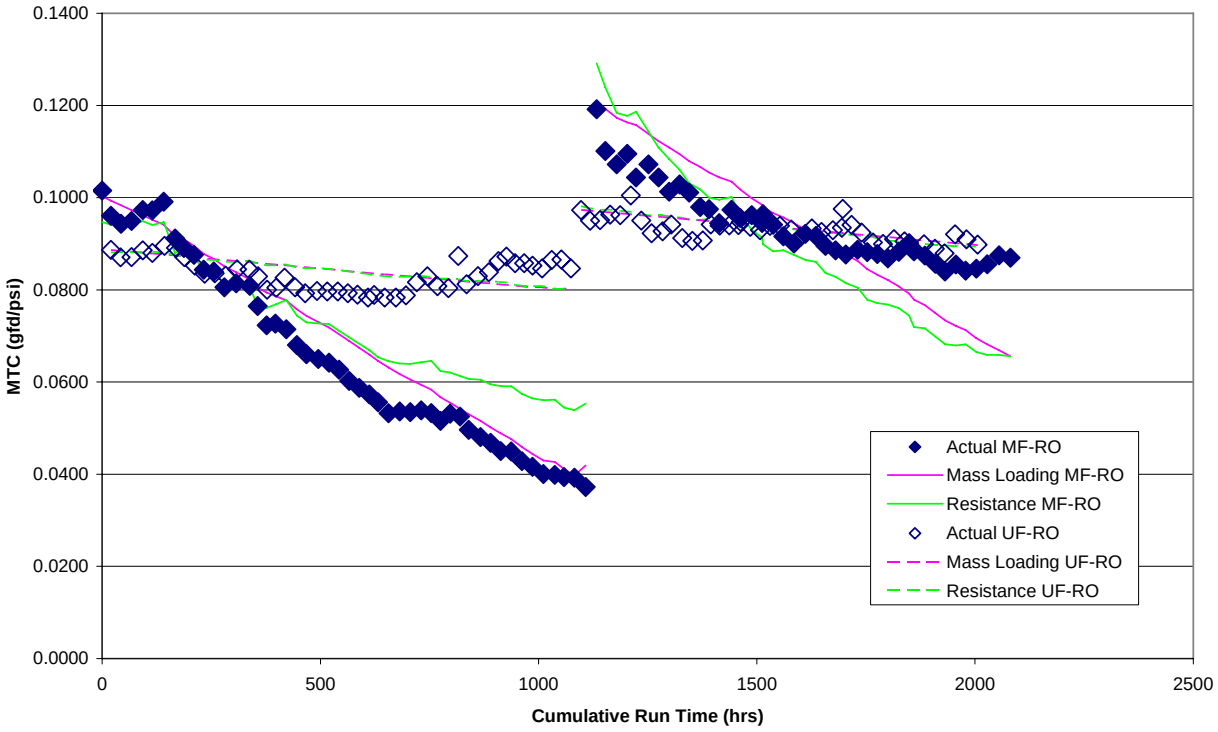

Figure 37: Actual and Predicted Solvent Mass Transfer Coefficient for Hydranautics ESPA2 Membrane Based on Individual Data

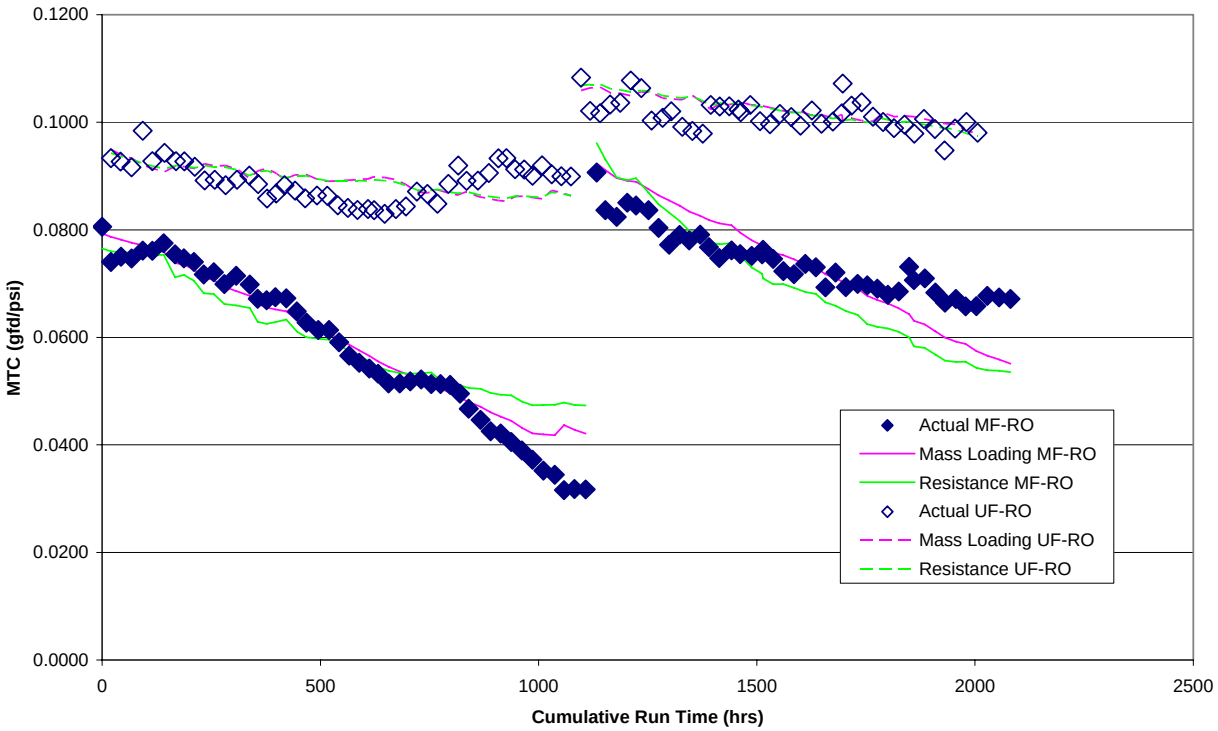

Figure 38: Actual and Predicted Solvent Mass Transfer Coefficient for Dow/FilmTec NF90 Membrane Based on Individual Data

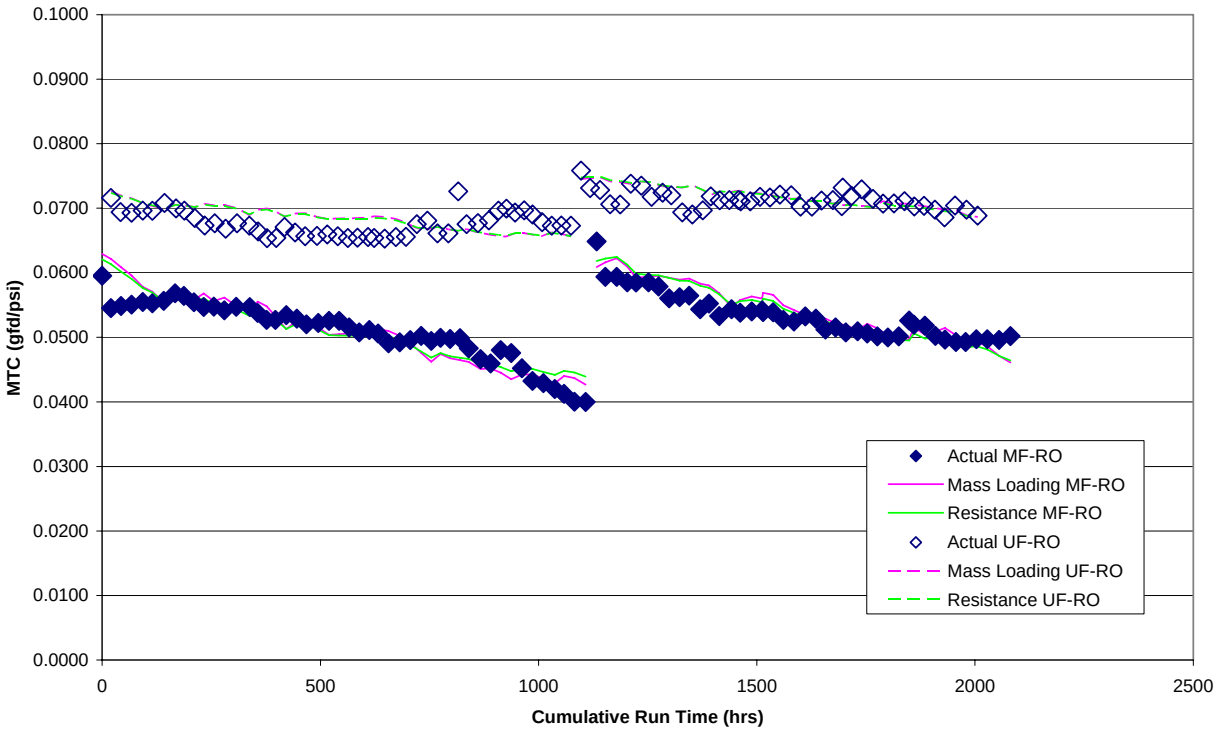

Figure 39: Actual and Predicted Solvent Mass Transfer Coefficient for Trisep X20 Membrane Based on Individual Data

5.5 Membrane Autopsy Results

Data obtained through the autopsy of fouled membrane elements provided valuable insight regarding the nature of the foulants responsible for the significant differences in membrane fouling between the MF-RO and UF-RO units. Loss on ignition results generally indicate inorganic foulants were more prevalent for UF-RO membranes when compared to MF-RO membranes, as shown in Table 28. Furthermore, the percentage of foulants organic in nature was generally higher for MF-RO membranes when compared to UF-RO membranes.

Table 28: Relative Percentage of Organic and Inorganic Foulants

Membrane	MF-RO Unit		UF-RO Unit	
	Organic	Inorganic	Organic	Inorganic
Hydranautics ESPA2	49.6	50.4	43.9	56.1
Dow/FilmTec NF90	43.9	56.1	44.4	55.6
Trisep X20	54.7	45.3	44.4	55.6

The composition of the inorganic fractions of foulants collected from each membrane is presented in Table 29. The composition of inorganic foulants was generally similar for all membranes within each high pressure membrane unit, however, significant differences in inorganic foulant composition existed between membranes that received MF pretreated water and membranes that received UF pretreated water. The element which accounted for the most significant difference between MF-RO and UF-RO inorganic foulants was iron. On average, iron accounted for 4.0 percent and 61.8 percent of the inorganic foulants accumulated on the surface of MF-RO and UF-RO membranes, respectively. Differences in iron percentages were attributed to the addition of 4 mg/L of ferric chloride as part of the UF pretreatment process. Differences in phosphorous percentages (32.6 percent for MF-RO membranes and 21.1 percent for UF-RO membranes) were also attributed to the addition of ferric chloride in the UF feed stream. Notable differences between the composition of MF-RO and UF-RO inorganic foulants were also observed for aluminum, calcium, and manganese.

Table 29: Relative Inorganic Foulant Composition

Element	MF-RO			UF-RO		
	Hydranautics ESPA2	Dow/FilmTec NF90	Trisep X20	Hydranautics ESPA2	Dow/FilmTec NF90	Trisep X20
Aluminum	27.2	22.9	25.8	3.7	3.2	2.7
Calcium	12.9	12.6	15.1	9.2	7.6	9.7
Chloride	0.0	0.2	0.0	1.7	0.7	0.6
Iron	4.2	3.8	4.1	56.4	64.3	64.8
Magnesium	0.1	0.0	0.0	0.4	0.0	0.1
Manganese	15.4	22.6	14.6	0.0	0.0	0.0
Phosphorous	34.6	30.6	32.5	23.8	19.4	20.0
Potassium	0.1	0.1	0.0	0.3	0.5	0.3
Silicon	0.9	2.5	0.8	1.6	1.4	0.3
Sodium	0.0	0.0	0.0	0.9	0.0	0.0
Sulfur	1.6	1.5	2.8	1.4	1.5	1.5
Tin	0.0	0.0	2.2	0.0	0.0	0.0
Titanium	1.8	1.4	1.8	0.6	1.4	0.0
Zinc	1.2	1.8	0.3	0.0	0.0	0.0

The mass of dissolved organic carbon accumulated per unit area on the surface of each membrane is presented in Table 30. These data clearly indicate the membranes that received MF pretreated water accumulated significantly more dissolved organic carbon than the membranes that received UF pretreated water. On average, high pressure membranes installed in the MF-RO unit accumulated 2.0 times the mass of dissolved organic carbon on their surfaces when compared to the membranes installed in the UF-RO unit. Individually, the Hydranautics ESPA2, Dow/FilmTec NF90, and Trisep X20 membranes installed in the MF-RO unit respectively accumulated 1.5, 2.0, and 2.3 times the dissolved organic carbon mass accumulated on the membranes installed in the UF-RO unit.

Table 30: Dissolved Organic Carbon Accumulation

Membrane	**mg Dissolved Organic Carbon/m2**	
	MF-RO Unit	**UF-RO Unit**
Hydranautics ESPA2	43	28
Dow/FilmTec NF90	88	45
Trisep X20	78	34

Results of the polysaccharide analyses are summarized below in Table 31. Pronounced accumulation of polysaccharides was observed for all high pressure membranes, however, membranes installed in the MF-RO unit accumulated approximately 1.5 times the mass of polysaccharides on their surface when compared to those installed in the UF-RO unit. Respective polysaccharide accumulation factors of 1.4, 1.6, and 1.4 were observed for the MF-RO Hydranautics ESPA2, Dow/FilmTec NF90, and Trisep X20 membranes when compared to those installed in the UF-RO unit.

Table 31: Polysaccharide Accumulation

Membrane	mg Polysaccharide (EPS)/m2	
	MF-RO Unit	UF-RO Unit
Hydranautics ESPA2	266	194
Dow/FilmTec NF90	387	240
Trisep X20	287	205

5.6 Observations Regarding Modeling Results

Previous studies have successfully modeled the dynamic nature of solvent mass transfer across semipermeable membranes (Lovins, 2000; Mulford et. al., 1999; Robert, 1999; Chellam et. al., 1998). These models generally considered water quality parameters that represented each of the four major types of membrane fouling: scaling, biological fouling, organic fouling, and particulate fouling. However, when a similar approach was utilized to model the solvent mass transfer coefficient for each membrane using the pooled data collected throughout this study, the resulting models exhibited poor accuracy when compared to actual solvent mass transfer data (Figures 34 through 36). The poor accuracy of the mass loading and resistance models developed using the pooled data was primarily attributed to the inability of a single model to predict the different fouling patterns exhibited by each membrane in the MF-RO and UF-RO units. Furthermore, the insignificance of all parameters with the exception of the initial solvent mass transfer coefficient and temperature for all but one of the models (i.e. models were not dependent on time of operation), cast considerable doubt on the practical applicability of these models.

Considerable improvements in correlation coefficient values were observed when modeling efforts were repeated for each membrane using individual data sets obtained from the MF-RO and UF-RO units (Figures 37 through 39). The increased accuracy of the mass loading

and resistance models developed using these individual data sets was attributed to the development of unique mass loading and resistance models for each membrane which could more accurately predict the decline in solvent mass transfer experienced in each high pressure membrane unit. Parameters of significance for all mass loading and resistance models generated from individual MF-RO and UF-RO data sets included the initial solvent mass transfer coefficient, temperature, and water loading (i.e. time of operation).

The insignificance of all measured water quality parameters in both mass loading and resistance models developed from both pooled and individual data sets is of particular interest. As previously stated, the filtrate produced by both the MF and UF pretreatment units were of identical quality with respect to all measured water quality parameters, with the exception of orthophosphate. Given the dramatically different fouling patterns experienced by membranes installed in the MF-RO and UF-RO units, it is not surprising that water quality parameters typically included in productivity models (total organic carbon, ultraviolet absorbance, turbidity, etc.) were not significant in the models developed in this study. Once orthophosphate was determined to be insignificant in the prediction of solvent mass transfer it was apparent that other parameters were responsible for the differences in membrane fouling observed between the MF-RO and UF-RO units.

The qualitative and quantitative data obtained from the autopsy of fouled membranes, while not definitive, provided a reasonable basis for the following speculation. Despite the fact that MF and UF pretreated waters had statistically equivalent TOC concentrations, the results of the loss on ignition tests suggested that organic fouling was more prevalent for membranes receiving MF pretreated water than for those receiving UF pretreated water. Quantitative results

from the dissolved organic carbon and the polysaccharide analyses further supported this presumption, as MF-RO membranes accumulated 2.0 times the mass of dissolved organic carbon and 1.5 times the mass of polysaccharides when compared to the membranes installed in the UF-RO unit. These data suggest the TOC concentration is not indicative of the organic fouling observed during the nanofiltration or reverse osmosis treatment of wastewater effluent. These data further suggest, specific constituents of the TOC content may be responsible for a majority of the observed organic fouling of NF/RO membranes treating wastewater effluent.

5.7 Conclusions

Accurate mass loading and resistance models were developed to predict the mass transfer of solvent through semipermeable diffusion controlled membranes using independent data sets for each membrane and each pretreatment system. Independent variables included the initial solvent mass transfer coefficient, temperature, and water loading. Measured water quality parameters were not significant in models developed from independent data sets.

The insignificance of all measured water quality parameters in mass loading and resistance models while operating the MF-RO and UF-RO units at identical conditions suggests the different fouling patterns observed between the two units were attributed to differences in water quality parameters other than those measured.

Autopsy results indicated organic fouling was more significant for high pressure membranes receiving MF pretreated water than for those receiving UF pretreated water, as measured by loss on ignition, dissolved organic carbon, and polysaccharide analyses. These data

suggest that total organic carbon may not be a good indicator of organic fouling potential as the total organic carbon concentration of the two pretreated waters were statistically equivalent.

Significant differences in the accumulation of dissolved organic carbon and polysaccharides on the surface of MF-RO and UF-RO membranes suggest that a more refined analysis of specific organic components is warranted for modeling purposes. It is suspected that differences in the concentration of specific organic compounds were responsible for the different fouling patterns observed between the MF-RO and UF-RO units. Monitoring the concentration of these compounds during future studies may result in the identification of additional significant water quality parameters for model development.

Despite the insignificance of orthophosphate in the mass loading and resistance models, inorganic foulant analyses suggest insoluble and sparingly soluble phosphate salts (aluminum phosphate, calcium phosphate, and magnesium phosphate) may have contributed to the rapid decline in the productivity of high pressure membranes in the MF-RO unit when compared to that exhibited by the high pressure membranes in the UF-RO unit.

5.8 References

1. Bowen, W.; Mongruel, A.; and Williams, P. (1996) Prediction of the rate of crossflow membrane ultrafiltration: A colloidal interaction approach. Chem. Eng. Sci., 51:1-13.

2. Chellam, S.; Jacangelo, J.; and Bonacquisti, T. (1998) Modeling and experimental verification of pilot-scale hollow fiber, direct flow microfiltration with periodic backwashing. Environmental Science and Technology, 32:75-81.

3. Chellam, S. and Wiesner, M. (1997) Evaluation of crossflow filtration models based on shear-induced diffusion and particle adhesion: Complications induced by feed suspension polydispersity. Journal of Membrane Science 3617:1-15.

4. Chen, V.; Fane, A.; Madaeni, S.; and Wenten, I. (1997) Particle deposition during membrane filtration of colloids: Transition between concentration polarization and cake formation. Journal of Membrane Science 125:109-122.

5. Chudacek, M. and Fane, A. (1984) The dynamics of polarization in unstirred and stirred ultrafiltration. Journal of Membrane Science 21:145-160.

6. Elimelech, M.; Zhu, X.; Childress, A.; and Hong, S. (1997) Role of membrane surface morphology in colloidal fouling of cellulose acetate and composite aromatic polyamide reverse osmosis membranes. Journal of Membrane Science, 127:101-109.

7. Faibish, R.; Elimelech, M.; and Cohen, Y. (1998) Effect of interparticle electrostatic double layer interactions on permeate flux decline in crossflow membrane filtration of colloidal suspensions: An experimental investigation. Journal of Colloid and Interface Science, 204:77-86.

8. Field, R.; Wu, D.; Howell, J.; and Gupta, B. (1995) Critical flux concept for microfiltration fouling. Journal of Membrane Science, 100:259-272.

9. Gao, S.; Li, C.; Zhang, F.; Zen, H.; and Ye, C. (2006) Pilot testing of outside-in UF pretreatment prior to RO for high turbidity seawater desalination. Desalination, 189:269-277.

10. Gwon, E.; Yu, M.; Oh, H.; and Ylee, Y. (2003) Fouling characteristics of NF and RO operated for removal of dissolved matter from groundwater. Water Research, 37:2989-2997.

11. Hobbs, C.; Hong, S.; and Taylor, J. (2006) Effect of surface roughness on fouling of RO and NF membranes during filtration of a high organic surficial groundwater. Journal of Water Supply, 55:559-570.

12. Hong, S.; Faibish, R.; and Elimelech, M. (1997) Kinetics of permeate flux decline in crossflow membrane filtration of colloidal suspensions. Journal of Colloid and Interface Science, 196:267-277.

13. Jiao, D. and Sharma, M. (1994) Mechanism of cake buildup in crossflow filtration of colloidal suspensions. Journal of Colloid and Interface Science, 162:454-462.

14. Jonsson, A. and Jonsson, B. (1996) Ultrafiltration of colloidal dispersions – A theoretical model of the concentration polarization phenomena. Journal of Colloid and Interface Science, 180:504-518.

15. Lahoussine-Turcaud, V.; Wiesner, M.; and Bottero, J. (1990) Fouling in tangential-flow filtration: The effect of colloid size and coagulation treatment. Journal of Membrane Science, 52:173-190.

16. Lovins, W. (2000) Correlation and modeling of laboratory and field-scale integrated membrane system productivity and water quality. Doctoral Dissertation, University of Central Florida, Orlando.

17. Madaeni, S. and Fane, A. (1996) Microfiltration of very dilute colloidal mixtures. Journal of Membrane Science, 113:301-312.

18. Mulford, L.; Taylor, J.; Nickerson, D; and Chen, S. (1999) NF performance at full and pilot scale, Journal AWWA, 91:64-75.

19. Pollice, A.; Lopez, A.; Laera, G.; Rubino, P.; and Lonigro, A. (2004) Tertiary filtered municipal wastewater as alternative water source in agriculture: A field investigation in southern Italy. Science of the Total Environment, 324:201-210.

20. Robert, C. (1999) Resistance modeling of membrane fouling based on water quality mass loading. Doctoral Dissertation, University of Central Florida, Orlando.

21. Romero, C. and Davis, R. (1991) Experimental verification of the shear-induced hydrodynamic diffusion model of crossflow microfiltration. Journal of Membrane Science, 62:249-273.

22. Tarleton, E. and Wakeman, R. (1994) Understanding flux decline in crossflow microfiltration: Part III-Effects of membrane morphology. Trans.IChemE, 72:521-529.

23. Water Environment Research Foundation (2005) Membrane Treatment of Secondary Effluent for Subsequent Use, Water Environment Research Foundation, Alexandria, Virginia.

24. Welsch, K.; McDonough, R.; Fane, A.; and Fell, C. (1995) Calculation of limiting fluxes in the ultrafiltration of colloids and fine particulates. Journal of Membrane Science, 99:229-239.

25. Zhao, Y. and Taylor, J. (2005) Assessment of ASTM D 4516 for evaluation of reverse osmosis membrane performance. Desalination, 180:231-244.

26. Zhao, Y.; Taylor, J.; and Hong, S. (2005) Combined influence of membrane surface properties and feed water qualities on RO/NF mass transfer, a pilot study. Water Research, 39(7):1233-1244.

27. Zhu, X. and Elimelech, M. (1995) Fouling of reverse osmosis membranes by aluminum oxide colloids. Journal of Environmental Engineering, ASCE, 121:884-892.

CHAPTER 6
VARIATIONS IN BACKWASH EFFICIENCY DURING COLLOIDAL FILTRATION OF HOLLOW-FIBER MICROFILTRATION MEMBRANES

6.1 Introduction

The use of size-exclusion membrane technologies such as microfiltration (MF) and ultrafiltration (UF) has increased dramatically over recent years (Belfort et al, 1994), and MF/UF membranes are now commonplace in numerous industrial processes including wastewater treatment (Bourgeous et al, 2001; Decarolis et al, 2001; Marchese et al, 2000) and drinking water treatment (Hagen, 1998; Lipp et al, 1998). They present a physical barrier to the suspended particles in the feed stream, whereby all particles larger than the pore are retained on the feed side of the membrane. The retained particles, however, accumulate on the surface of the membrane and increase the resistance to water flow across the membrane. As a result, MF/UF membranes must be periodically backwashed by reversing the direction of flow through the membrane to remove the deposited particles. However, backwashing typically recovers only a portion of productivity lost through operation, which results in membrane fouling (e.g., irreversible productivity loss) as shown in Figure 40. The productivity loss due to fouling can be restored only by aggressive chemical cleaning, which significantly increases operating costs.

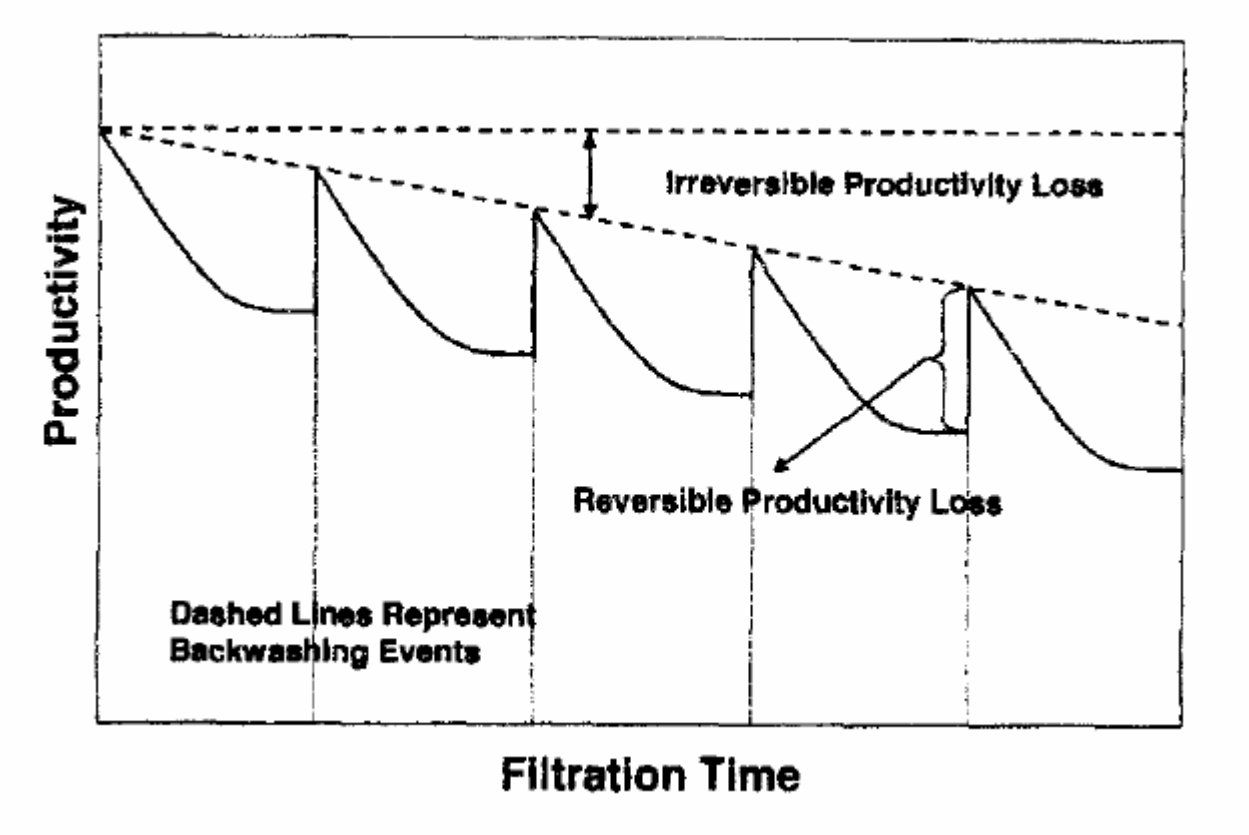

Figure 40: Typical MF Membrane Operations in Various Industrial Separation Processes

The effective control of membrane fouling in MF/UF processes is largely dependent on the mode and efficiency of backwashing. Several pilot-scale studies demonstrated that an increase in backwash frequency (e.g., shorter operation times between backwash cycles) and duration significantly reduced membrane fouling (Bourgeous et al, 2001; Decarolis et al, 2001; Chellam et al, 1998; Hillis et al, 1998; Xu et al, 1995). Other studies investigated variations on the methods of backwashing, such as air sparging (Serra et al, 1999) and backpulsing (Ma et al, 2000). However, there are no systematic studies in the literature which investigated the relationship between various chemical and physical operating conditions and backwashing efficiency.

In this study it is hypothesized that backwashing efficiency can be affected by the structure of particle cake layer formed on the membrane surface. Considering the relative sizes of the membrane pore (d_{pore}) and the colloidal particle ($d_{particle}$), three primary modes of colloidal fouling exist in MF/UF processes (Figure 41): adsorption (Tracey and Davis, 1994; Kim et al, 1992; Clark et al, 1991), pore blocking (Huang and Morrissey, 1998; Koltuniewicz and Field, 1996; Tarleton and Wakeman, 1993; Hermia, 1982), and deposition of a cake layer (Jonsson and Jonsson, 1996; Bacchin et al, 1995; Belfort et al, 1994). Among these mechanisms, cake formation is considered to be the most dominant mode of colloidal fouling, since in a normal membrane filtration, the mean diameter of membrane pores is selected in such a way that a majority of the particles to be separated are larger than the pore size. For dead-end filtration processes, the cake layer grows indefinitely (Chudacek and Fane, 1984), while during cross flow filtration, the growth of the cake layer is limited by the tangential fluid flow in the module (Lojkine et al, 1992; Davis and Birdsell, 1987).

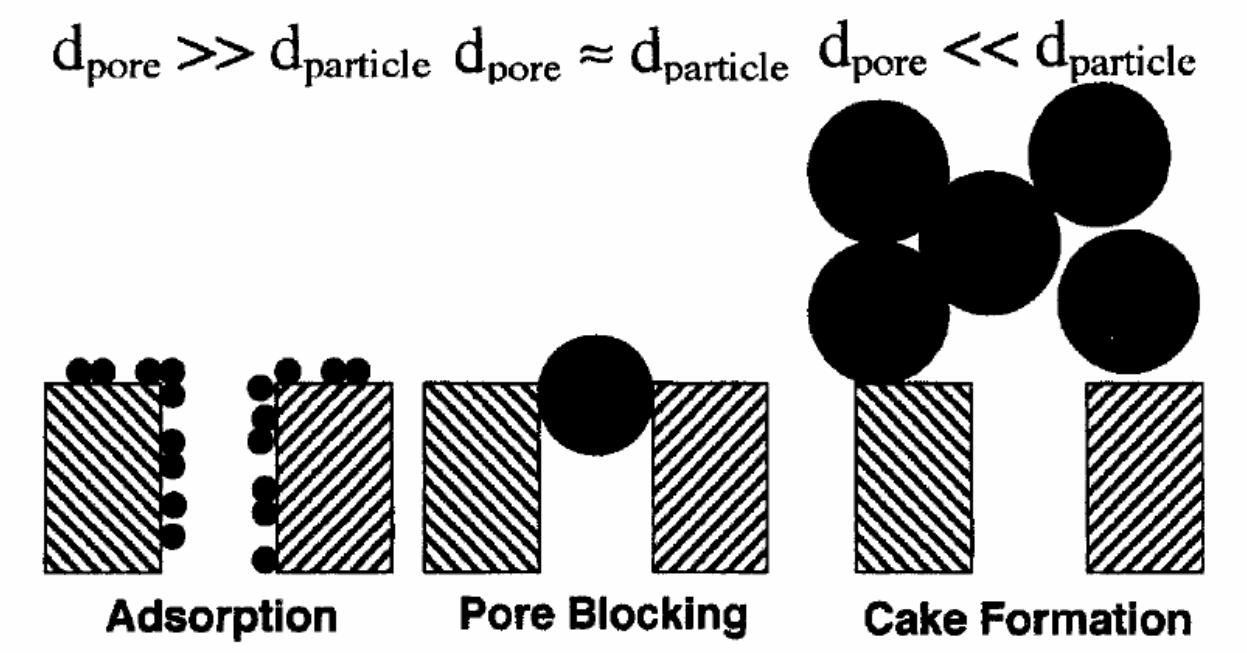

Figure 41: Different Modes of Colloidal Fouling Predominantly Observed in MF Processes

There has been a variety of studies pertaining to elucidation of the structure of the cake layer under the influence of hydrodynamic and colloial interactions. The hydrodynamic interactions among the particles retained in the cake layer have been evaluated by the Happel's cell model, which incorporates the influence of the neighboring particles on the hydrodynamic drag force (Hong et al, 1997; Song and Elimelech, 1995). This approach has often been suggested as a substitute for the Kozeny-Carman equation for evaluating the specific resistance of cake layers. Aside from hydrodynamic interactions, several recent studies have attempted directly to incorporate colloidal interactions in predicting the structure and permeability of the cake layer deposits (Fu and Dempsey, 1998; McDonogh et al, 1992; McDonogh et al, 1989; McDonogh et al, 1984). In such studies, the influence of particle charge, background electrolyte

concentration, and other physicochemical conditions were experimentally assessed and/or theoretically quantified to determine the cake layer structure.

The purpose of this study was to examine the effect of feed water quality and operational parameters on the efficiency of backwashing. In this study, a series of fouling experiments was first performed under various operating conditions. The primary operating parameters varied throughout the experiments were particle concentration, operating pressure and solution ionic strength. A theoretical model for flux decline due to cake formation was evaluated and utilized to determine the structure of the cake layer formed during fouling experiments. Following each fouling experiment, the membrane was backwashed in order to relate the backwash efficiency to both physical and chemical parameters. Finally, a theoretical value for the particle packing density of the cake layer calculated from the model was correlated to the backwash efficiency in order to elucidate the effect of cake structure on the efficiencies of backwashing.

6.2 Experimental

6.2.1 Colloidal Particles

Silica (SiO_2) particles from Nissan Chemical Industries (Houston, TX) were used as model colloids for all of the fouling and backwashing experiments. The particles were received as a stable concentrated (40.7% by weight) aqueous suspension at an alkaline pH. The manufacturer's certificate reported a mean particle diameter of 0.10 ± 0.03 μm (as determined by the centrifugal method) and a specific gravity of 1.301 at 20°C. The size and shape of these model colloids were further verified by a scanning electron microscope (JEOL Model 400, JEOL, Peabody, MA) and by dynamic light scattering (Nicomp Model 380, Particle Sizing

Systems, Santa Barbara, CA). The SEM images and DLS analyses revealed that the model silica particles were monodispersed with a mean particle size of 140 nm. Lastly, the zeta potential of the colloidal silica was determined from electrophoretic mobility measurements (Zeta PALS, Brookhaven Instruments, NY). The results showed the zeta potentials of silica particles to be in the range of -27 to -30 mV at pH 8 and 10^{-2} M NaC1, which were the solution environments employed in the majority of fouling and backwash experiments. More detailed properties of these silica particles are well documented in a paper by Vrijenhoek et al. (2001).

6.2.2 Microfiltration Membranes

All experiments conducted during this study utilized a bench-scale, outside-in, hollow-fine fiber, MF module (SK Chemicals, Seoul, South Korea). Manufacturer's specifications revealed the following physical characteristics of the membrane: nominal pore size of 0.1 μm, inside fiber diameter of 0.7 mm (2.3 x 10^{-3} ft), outside fiber diameter of 1.0 mm (3.3 x 10^{-3} ft), and a fiber length of 520 mm (1.7 ft). Containing a total of 150 hollow-fine fibers, the MF module provided approximately 0.25 m^2 (2.7 ft^2) of membrane area. The average specific flux of this membrane was estimated at 3.55 ± 0.20 lmh/kPa (14.43 ± 0.83 gfd/psi) under given operating conditions.

Prior to all experiments, the operational integrity of the membrane module was verified. This was accomplished by the filtration of a high concentration (0.05% v/v) colloidal silica suspension. During filtration, feed and permeate samples were collected and analyzed for turbidity and total suspended solids (TSS). Results from these tests were then compared to

results obtained through the filtration of a DI (blank) water sample to identify any defects in the membrane module.

6.2.3 Standards and Reagents

All solutions were prepared with ACS-grade $NaHCO_3$ and NaCl (Fisher Scientific, Pittsburgh, PA). These salts were dissolved in DI water (LD5A and MegaPure, Bamstead/Thermolyne, Dubuque, IO). Adjustments in pH, for both zeta potential measurements and fouling studies, were made with ACS-grade HCl. Lastly, all cleaning solutions were made with USP-grade sodium hydroxide and citric acid dissolved in DI water.

6.2.4 Bench-Scale Membrane Filtration Unit

The colloidal suspensions were prepared and stored in a magnetically stirred high-density polyethylene 20-L (5.3 gal) feed reservoir. The temperature of this suspension was maintained at 20°C (68°F) by a Neslab CFT-33 (Portsmouth, NH) digital refrigerated recirculator. The feed suspension was delivered to the MF module by a 6.83 lpm (1.8 gpm) constant flow diaphragm pump (Hydracell, Wanner Engineering, Minneapolis, MN) with a maximum pressure of 3,447 kPa (500 psi). Initial operating conditions (e.g., filtrate flux and cross flow velocity) were set and maintained through the careful manipulation of feed, concentrate, and bypass needle valves (Swagelok, Solon, OH). Feed pressure was monitored by an analog pressure gauge (Dresser Industries, Stratford, CT). Concentrate and filtrate flows were measured both by an in-line flowmeter (Blue-White Industries, Westminster, CA) and by the timed collection of filtrate in a graduated cylinder.

6.2.5 Sequence of Fouling and Backwash Experiments

Prior to each fouling experiment, the benchscale MF unit was thoroughly cleaned by sequentially recirculating sodium hydroxide (pH 11) and citric acid solutions (pH 3) for a minimum of 1 hour. In addition, the module was backwashed with these solutions at a pressure of 68.9 kPa (10 psi). After chemical cleaning was completed, the system was rinsed and flushed with DI water.

An initial clean water test was performed to determine membrane productivity prior to each fouling experiment. Each clean water test was conducted in a dead-end mode of operation at a feed pressure of 41.4 kPa (6 psi) with a background electrolyte solution identical to that which would be used for the ensuing fouling study (e.g., 10^{-3} M $NaHCO_3$ and 10^{-2} M NaC1). A total of 5 L of filtrate was collected, and a stopwatch was used to measure the collection times associated with 1, 2, 3, 4, and 5 L of filtrate accumulated.

Following the initial clean water test, feed, concentrate, and bypass valves were manipulated to achieve the desired initial operating conditions for the fouling study. Once stable operation was attained, the predetermined volume of concentrated silica particles was added to the feed solution to achieve the desired particle concentration. Immediately following the addition of silica particles, 5 L of filtrate was collected, and collection times were measured and recorded for 1, 2, 3, 4, and 5 L.

Once the fouling study was completed, 1 L of DI water was backwashed through the MF module at a pressure of 68.9 kPa (10 psi), and a final clean water test was conducted. Similar to the initial clean water test, the final clean water test was conducted in a dead-end mode of operation at a feed pressure of 41.4 kPa (6 psi) with a background electrolyte solution identical

to that which was used for the previous fouling study. Again, a total of 5 L of filtrate was collected, and a stopwatch was used to measure the collection times associated with 1, 2, 3, 4, and 5L.

Feed and filtrate samples for each fouling study were collected and analyzed for conductivity, pH, and turbidity. Conductivity and pH measurements were made with an Accumet AR-50 conductivity and pH meter (Fischer Scientific, Pittsburgh, PA), and turbidity was determined using a Hach Ratio Turbidimeter (Loveland, CO).

6.2.6 Evaluation of Flux Decline and Backwash Efficiency

In order to compare multiple data sets obtained under various experimental conditions, it was necessary to analyze all experiments on a dimensionless basis. Two parameters of particular interest throughout this study were the normalized flux (J_n) and the backwash efficiency (η). The normalized flux was calculated from Equation 20, as shown below

$$J_n = \frac{J_w}{J_0} \tag{20}$$

where: J_n = normalized flux

J_w = flux after the collection of 5 L of filtrate

J_0 = initial filtrate flux

Similarly, the backwash efficiency (η) was estimated by Equation 21.

$$\eta = \frac{t_i}{t_f} \tag{21}$$

where: t_i = time required to collect 5 L of filtrate during the initial clean water test

t_f = time required to collect 5 L of filtrate during the final clean water test.

6.3 Results and Discussion

6.3.1 Cake Layer Structure

In pressure-driven membrane filtration of colloidal suspensions, particles are transported to the membrane surface by the filtrate flow, which results in the formation of a cake layer on the membrane surface. Particle accumulation in the cake layer provides an additional resistance to filtrate flow and, hence, reduces flux. Resulting pressure drops in the membrane system can be expressed by Equation 22.

$$\Delta P = \Delta P_m + \Delta P_c \tag{22}$$

where: ΔP = applied (transmembrane) pressure drop

ΔP_m = pressure drop across the membrane

ΔP_c = pressure drop across the cake layer

The pressure drop across the membrane (P_m) is simply the product of membrane resistance (R_m) and filtrate flux (J_w) as shown below in Equation 23.

$$\Delta P_m = J_w R_m \tag{23}$$

The pressure drop in the cake layer (ΔP_c) is associated with the frictional drag resulting from the flow of filtrate through the dense layer of accumulated particle as shown in Equation 24.

$$\Delta P_c = \frac{kT}{D} A_s(\theta) J_w M_c \tag{24}$$

where: kT/D = frictional drag coefficient, also equal to $6\pi\mu a_p$

k = Boltzmann constant

T = absolute temperature

D = particle diffusion coefficient

μ = solvent viscosity

a_p = particle radius

M_c = number of particles accumulated in the cake layer per unit area

The $A_s(\theta)$ term is a correction function accounting for the effect of neighboring retained particles and can be evaluated from Happel's cell model, as shown in Equation 25 below.

$$A_s = \frac{1 + \frac{2}{3}\theta^5}{1 - \theta + \frac{3}{2}\theta^5 - \theta^6} \tag{25}$$

where: θ = porosity-dependent variable, also equal to $(1-\varepsilon)^{1/3}$

ε = porosity of the cake layer of accumulated particles

As shown in Equations 23 and 24, the pressure drop across the cake layer is primarily influenced by the structure of the cake layer, as well as particle size and concentration.

The flux decline observed during the membrane filtration of colloidal suspensions can be estimated based on Happel's cell model for the hydraulic resistance of the particle cake layer from Equation 26

$$J_n = \frac{J_w}{J_0} = \left[1 + \frac{3kTA_s(\theta)\Delta PC_0}{2\pi a_p^3 DR_m^2 J_w A} V\right]^{-1/2} \tag{26}$$

where: C_0 = bulk (feed) particle concentration

A = membrane surface area

V = filtrate volume

A detailed theoretical development is well presented in a paper by Hong et al (1997). By utilizing Equation 25, structural characteristics of the cake layer formed under various operating

conditions can be determined from filtration experiments. Specifically, the correction function, $A_s(\theta)$, is estimated first by fitting flux decline experimental data and then the particle packing density (i.e., $1-\varepsilon$) is calculated based on the Happel cell model.

6.3.2 Membrane Integrity and Particle Removal

The results of the membrane integrity tests clearly demonstrated that the membrane fibers were intact and undamaged. Measurements of feed samples (0.05% v/v) revealed that the feed suspension had an average turbidity of 119 NTU. The turbidity was completely removed by filtration as the average turbidity of the permeate samples was 0.02 NTU. These results were further supported by data obtained through TSS measurements. The average TSS of the silica feed suspension was determined to be 0.613 g/L, with a standard deviation of 0.038 g/L. Once again, the silica particles were completely rejected by the membrane as silica permeate samples had insignificant TSS concentrations when compared to both DI feed and DI permeate samples. The TSS values of these three samples were statistically indistinguishable based on hypothesis testing at a 5% level.

Similar to the results of integrity testing, filtrate turbidity was always below the detection limit (~0.02 NTU) regardless of experimental conditions employed in this study. This is due to the fact that the particles used were larger than the membrane pores (approximately 0.14 μm and 0.10 μm, respectively). Thus, all particles were retained on the feed side of the membrane and formed a particle cake layer on the membrane surface as shown in Figure 41.

6.3.3 Particle Loading

As expected from Equation 26, the extent of flux decline in dead-end filtration of colloidal suspensions was directly related to cumulative particle loading to the membrane system (C_0 x V). In this study particle volume concentrations were varied from 0.005% to 0.045% under identical physical and chemical operating conditions. Results of these tests are presented in Figure 42. As shown, the extent of membrane fouling increased with the concentration of colloidal particles. Specifically, after the filtration of 5 L, the averaged normalized flux values were 0.87, 0.79, 0.62, and 0.56 for feed particle concentrations of 0.005%, 0.015%, 0.030%, and 0.045%, respectively. This observation was explained by the concept of mass loading. As more particles were transported to the membrane surface, the resulting cake layer grew and provided greater resistance to filtrate flow and ultimately a more significant decline in flux.

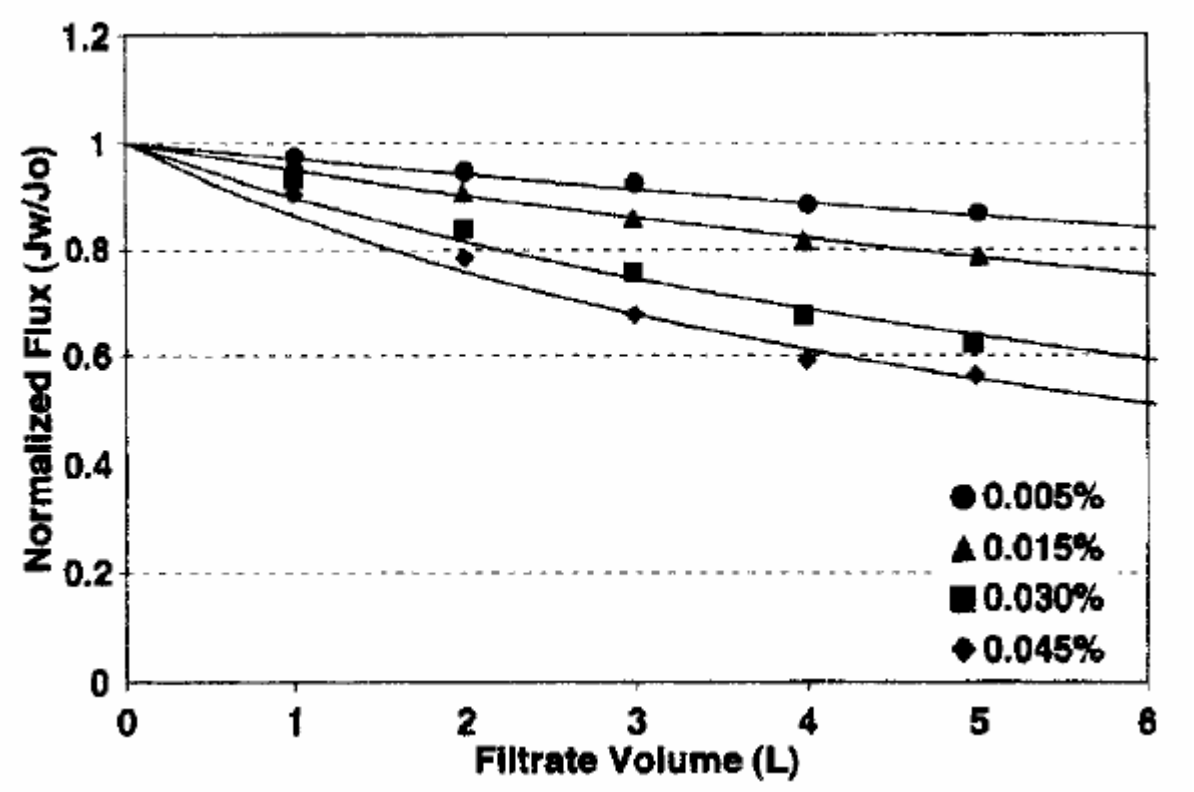

Figure 42: Effect of Colloidal Concentration on Flux Decline of Hollow Fiber MF Membranes

Utilizing the procedures previously described, the structure of each cake layer formed during filtration experiments was determined. These results are presented in Figure 43. As shown, the structure of the cake layer for each particle concentration was relatively consistent, with particle packing density factors ranging from 0.66 to 0.67, which correspond well to random packing density factors (Hong et al, 1997; Song and Elimelech, 1995). This observation suggested that the structure of the cake layer was independent of particle concentration, which is not surprising as all of the operating parameters remained constant except particle concentration, which only affected the thickness of the cake layer, not its structure.

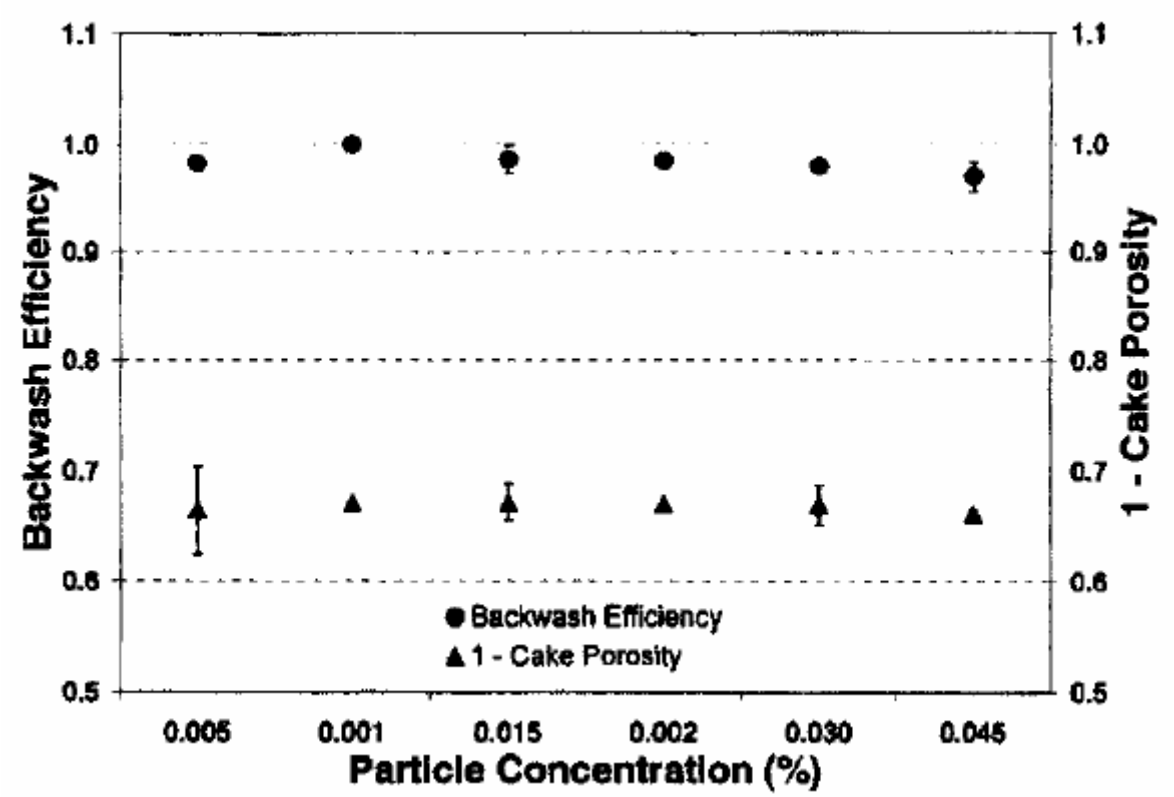

Figure 43: Correlation Between Particle Packing Density and Backwash Efficiency of Hollow-Fiber MF Membranes Under Various Colloidal Concentrations

In addition to fouling experiments, backwashing studies were also conducted to determine the effectiveness of the backwashing under various feed particle concentrations. The results of these experiments are summarized also in Figure 43. The average efficiency of all backwashing procedures ranged from 0.969 to 0.985; however, no clear correlation was observed between particle concentration and backwash efficiency considering variations, although backwash efficiency decreased slightly at high particle concentrations. The apparent lack of dependence of backwash efficiency on particle concentration was in accordance with no changes in particle packing density with feed particle concentrations. Thus, under the given range of

particle loading to the membrane systems, it was hypothesized that the backwash efficiency was more closely related to cake structure than particle mass accumulated on the membrane surface.

6.3.4 Operating Pressure

Filtration experiments were also conducted to determine the effect of operating pressure (or initial flux) on particle fouling. It should be noted that, unlike the previous set of experiments, particle loading per unit membrane surface area was held constant throughout this series of experiments. Thus, the number of particles transported to the surface of the membrane at any given volume of filtrate would be the same, regardless of the initial value of operating pressure. Results are presented for five different values of operating pressures as shown in Fig. 44. After the collection of 5 L of filtrate, operating pressure of 20.7, 34.5, 41.4, 65.6 and 41.4 kPa resulted in average normalized flux values of 0.920, 0.916, 0.867, 0.915, and 0.912, respectively, indicating that particle fouling did not vary significantly with increasing operating pressure, with an exception of 41.4 kPa. It may be expected that, as the operating pressure is increased, the force that transports suspended particles to the membrane surface is also increased, which would cause the formation of a more densely packed and hydraulically resistant cake layer. However, the effect of filtrate drag was not significant under the operating pressure range investigated in this study as shown in the Figure 44.

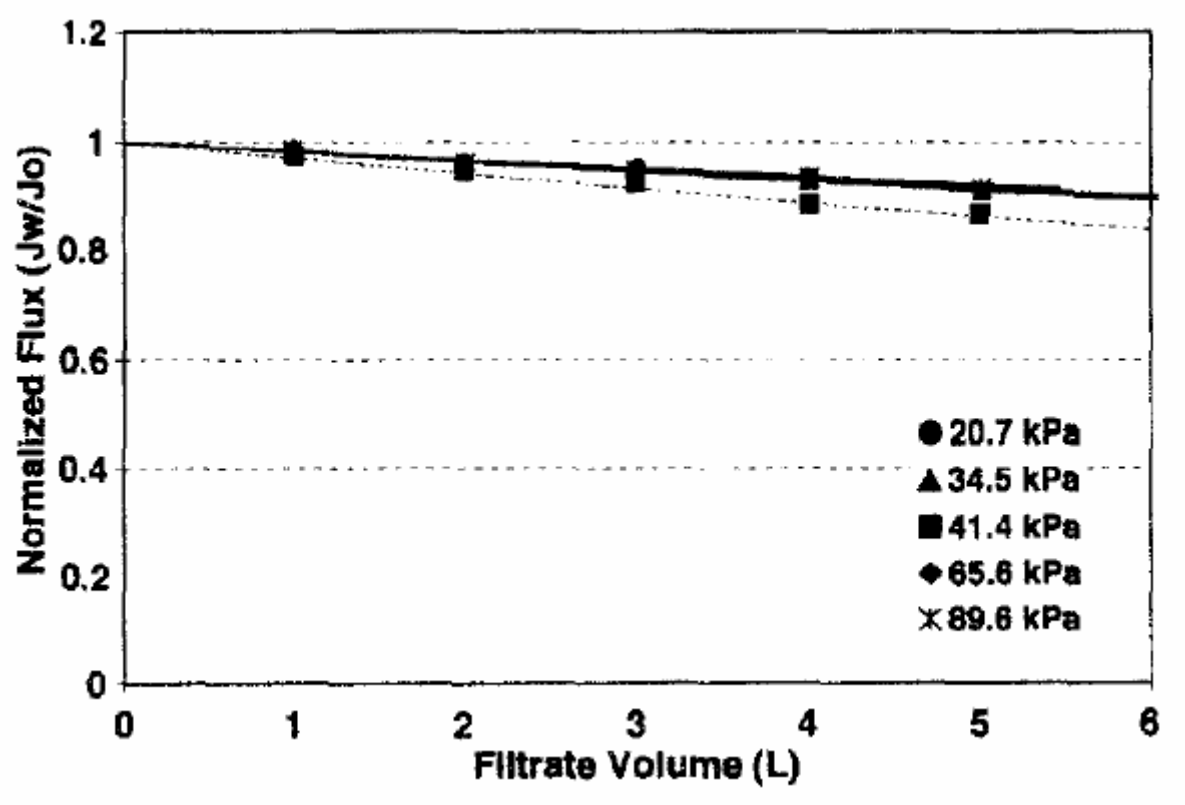

Figure 44: Effect of Operating Pressure on Flux Decline of Hollow-Fiber MF Membranes

Cake layer structures were again determined for each set of experimental conditions. Figure 45 presents these results. As shown, the structure of the cake layer for each operating pressure was relatively consistent, with particle packing density factors ranging from 0.66 to 0.67. Once again, these values are consistent with accepted values of random packing density factors for rigid spherical particles. Since all data points in this figure are within one standard deviation, it may be concluded that the density of the cake structure did not significantly change with increasing operating pressure. While many studies have shown a direct relationship between operating pressure and cake layer density, it is believed that the low pressures used throughout these experiments did not allow for the clear observation of this phenomenon from a statistical

standpoint. However, it should be noted that a direct relationship between operating pressure and cake layer density was observed for average data points.

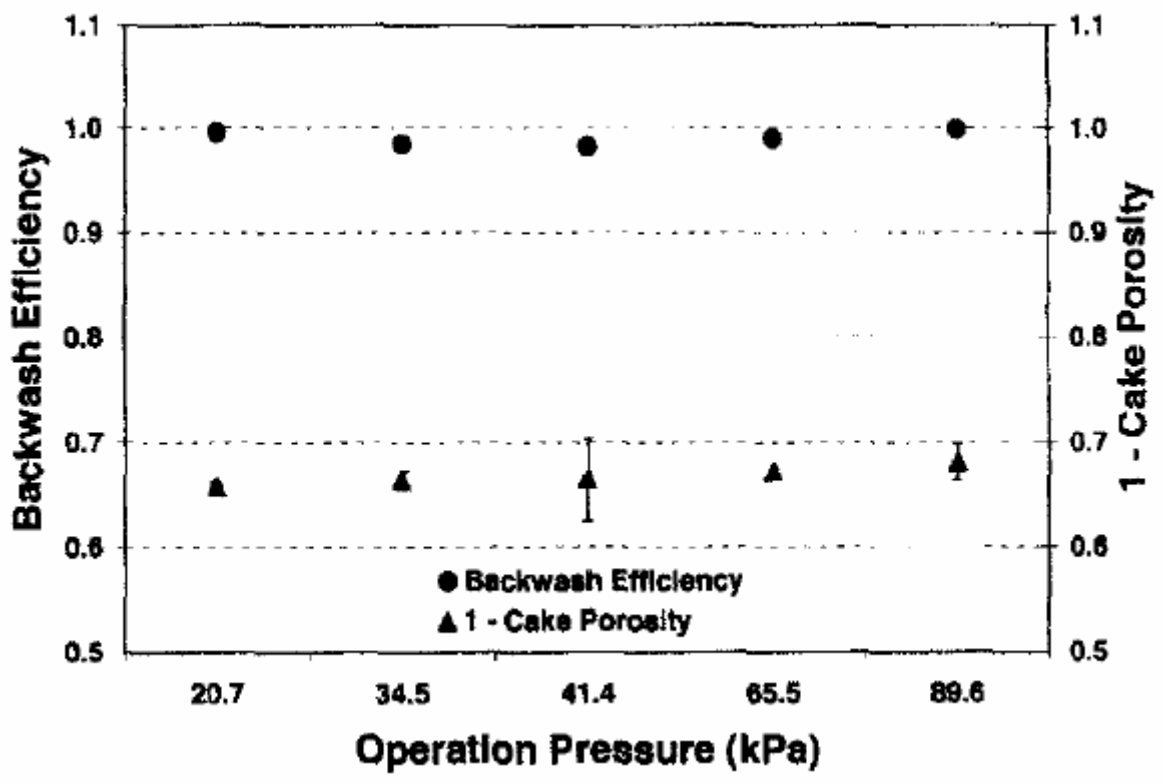

Figure 45: Correlation Between Particle Packing Density and Backwash Efficiency of Hollow-Fiber MF Membranes Under Various Operating Pressures

Upon completion of each fouling run, a backwashing experiment was performed to evaluate the reversibility of fouling experienced during each filtration study. As shown in Figure 45, the average efficiency of the backwashing procedure for each operating pressure value was relatively consistent, with efficiencies ranging from 0.98 to 0.99. This finding was attributed to no significant variation in cake layer structure under given pressure range investigated, again suggesting that backwashing efficiency may be closely related to the structure of the cake layer formed during filtration.

6.3.5 Ionic Strength

The effect of solution chemistry, specifically ionic strength, on the fouling of a hollow-fiber MF module was also investigated. A total of three ionic strengths, spanning two orders of magnitude, were tested; 0.001 M, 0.01 M, and 0.1 M NaCl. Once again, the mass loading of particles on the surface of the membrane was held constant throughout all experiments conducted in this series, as the particle concentration was fixed at 0.005%. Furthermore, the operating pressure was set at 41.4 kPa for all experimental runs. The results of these experiments are shown in Figure 46 and clearly showed that membrane fouling became more severe as the ionic strength of the solution was increased. The average normalized flux values after 5 L of filtrate was collected were 0.97, 0.87, and 0.81, for ionic strengths of 0.001 M, 0.01 M, and 0.1 M NaC1, respectively.

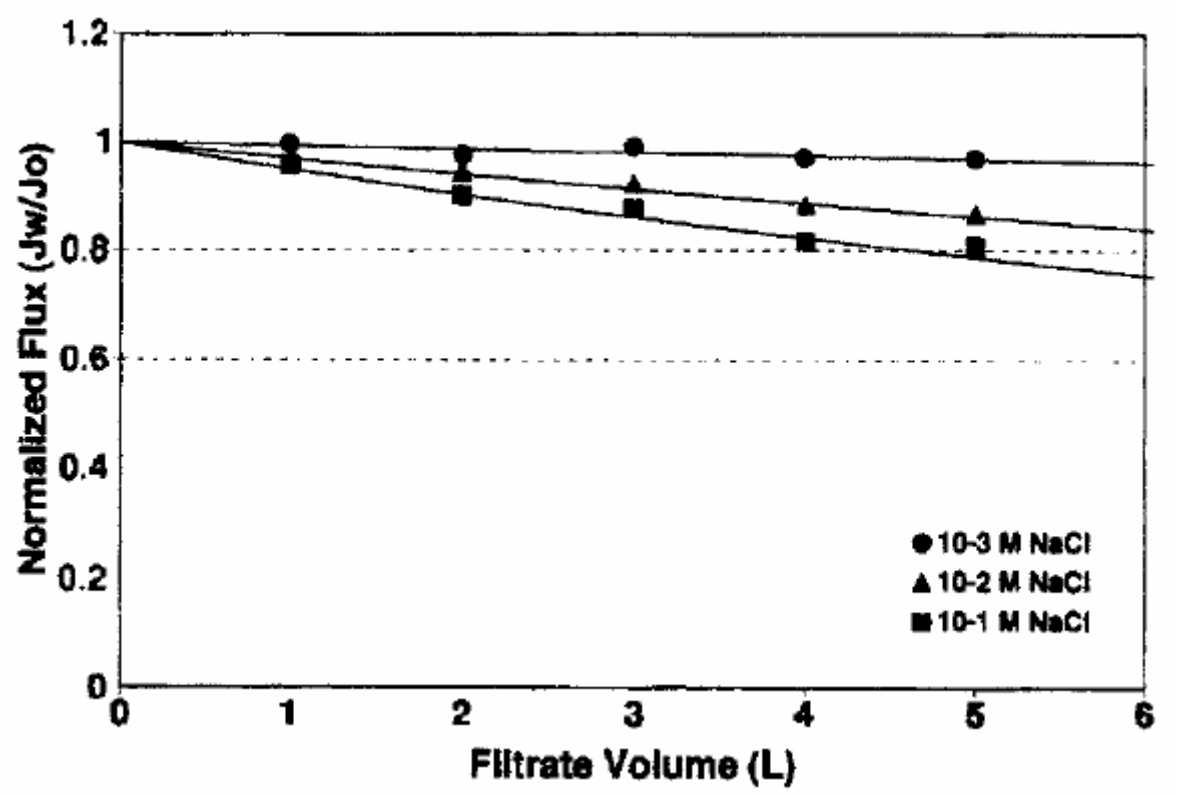

Figure 46: Effect of Ionic Strength on Flux Decline of Hollow-Fiber MF Membranes

According to the classic theory of colloidal interactions, the magnitude of the electrical double layer (EDL) repulsion is inversely proportional to the ionic strength of the solution. The reduction in repulsive forces resulted in the formation of a more densely packed cake layer on the surface of the membrane, which presented a greater resistance to filtrate flow. This finding was further validated through the determination of cake density at various ionic strengths based on the model previously described in Section 5.3.1. The modeling results are summarized in Figure 47 and clearly demonstrated that the density of the cake layer increased with the ionic strength of the particle suspension. However, it should be noted that the packing density for the 0.1 M NaC1 experiment was estimated to be 0.76 which is higher than theoretical values. For

hard spherical particles, theoretical particle volume fractions used in the literature for the cake layer ranged from 0.64 to 0.72, which correspond to random close packed and hexagonal close packed cake structures, respectively (Hong et al, 1997; Bowen and Jenner, 1995; Song and Elimelech, 1995). The high packing density calculated for high ionic strength is likely attributed to additional fouling mechanisms (i.e., adsorption and pore blockage), which were not accounted for by the model. Lastly, backwashing studies were performed to investigate if a relationship exists between the ionic strength of the solution and the efficiency of backwashing events. The results indicated that the average efficiency of backwashing events decreased as the ionic strength of the feed solution increased, as presented in Figure 47. The average backwash efficiency for solution ionic strengths of 0.001 M, 0.01 M, and 0.1 M NaC1 were estimated at 0.986, 0.982, and 0.962, respectively. These findings further suggest that the efficiency of backwashing events is a function of the structure of the cake layer formed during the filtration process. Specifically, the efficiency of backwashing decreased with an increase in the density of the cake layer. At high ionic concentrations, a more densely packed cake layer was formed due to repressed electrostatic interactions among particles, and consequently less flux was recovered per given backwash volume. Particle adsorption and/or pore blockage, as evidenced by the higher packing densities calculated, may also contribute to the reduced backwash efficiencies observed for the high ionic solutions.

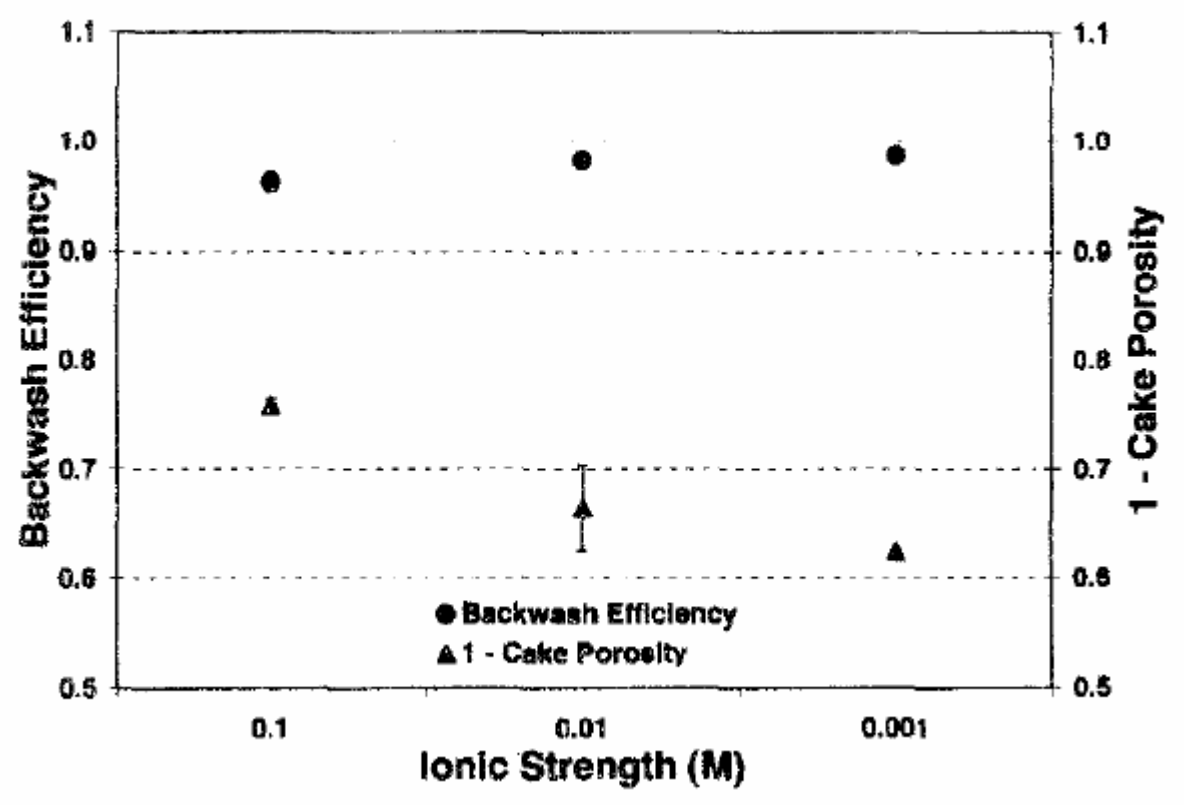

Figure 47: Correlation Between Particle Packing Density and Backwash Efficiency of Hollow-Fiber MF Membranes Under Various Solution Ionic Strengths

6.4 Conclusions

Primary inferences from this research are summarized as follows:

1. An increase in particle concentration resulted in a reduced normalized flux under identical operating conditions, which was attributed to the formation of a thicker cake layer caused by an increase in particle loading. Despite varying degrees of cake thickness, the structure of the cake layer, as determined by the Happel's cell model, did not vary with particle concentration. In addition, the efficiency of the backwashing procedure remained relatively constant throughout all particle concentration experiments, suggesting a close relationship between backwash efficiency and cake structure.

2. Increasing operating pressure under identical particle loading did not cause severe flux decline. The particle packing density remained constant at a random packing density (~0.66-0.67), and thus the compression of the cake layer was not clearly observed for the range of operating pressures investigated in this study. Accordingly, the backwash efficiency was not varied significantly with operating pressures primarily due to similar cake structure.

3. The normalized flux was significantly reduced as the ionic strength of the feed solution increased even when particle loading to the membrane system was kept constant. This was explained by the formation of a more compact cake layer at higher salt concentrations. Modeling data clearly demonstrated a direct relationship between the density of the cake layer and ionic strength, as predicted by the colloidal interactions among the particles accumulated in the cake layer. Furthermore, an inverse relationship was observed between backwash efficiency and the ionic strength of the feed solution, which indicates that the efficiency of backwashing deteriorated as the packing density of the cake layer increased. In addition, particle adsorption and/or pore blockage might contribute to the reduced backwash efficiencies observed for the high ionic solutions.

6.5 References

1. Bacchin, P.; Aimar, P. and Sanchez, V. (1995) Model for colloidal fouling of membranes. American Institute of Chemical Engineers, 41:368-376.

2. Belfort, G; Davis, R; and Zydney, A. (1994) The behavior of suspensions and macromolecular solutions in crossflow microfiltration. Journal of Membrane Science, 96: 1-58.

3. Bourgeous, K.; Darby, J. and Tchobanoglous, G. (2001) Ultrafiltration of wastewater: effects of particles, mode of operation, and backwash effectiveness. Water Resources, 35:77-90.

4. Bowen, W. and Jenner, F. (1995) Dynamic ultrafiltration model for charged colloidal dispersions – a wigner-seitz cell approach. Chemical Engineering Science, 50:1707-1736.

5. Chellam, S.; Jacangelo, J. and Bonacquisti, T. (1998) Modeling and experimental verification of pilot-scale hollow fiber, direct flow microfiltration with periodic backwashing. Environmental Science and Technology, 32:75-81.

6. Chudacek, M. and Fane, A. (1984) The dynamics of polarization in unstirred and stirred ultrafiltration. Journal of Membrane Science, 21:145.

7. Clark, W.; Bansal, A.; Sontakke, M. and Ma, Y. (1991) Protein adsorption and fouling in ceramic ultrafiltration membranes. Journal of Membrane Science, 55: 21-38.

8. Davis, R. and Birdsell, S. (1987) Hydrodynamic model and experiments for cross-flow microfiltration. Chemical Engineering Communications, 49:217-234.

9. Decarolis, J.; Hong, S. and Taylor, J. (2001) Fouling behavior of a pilot scale inside out hollow fiber UF membrane during dead-end filtration of tertiary wastewater. Journal of Membrane Science, 191:165-178.

10. Fu, L. and Dempsey, B. (1998) Modeling the effect of particle size and charge on the structure of the filter cake in ultrafiltration. Journal of Membrane Science, 149:221-240.

11. Hagen, K. (1998) Removal of particles, bacteria and parasites with ultrafiltration for drinking water treatment. Desalination, 119:85-91.

12. Hermia, J. (1982) Constant pressure blocking filtration laws-application to power-law non-newtonian fluids. Trans IChemE, 60:183-187.

13. Hillis, P.; Padley, M.; Powell, N. and Gallagher, P. (1998) Effects of backwash conditions on out-to-in membrane microfiltration. Desalination, 118:197-204.

14. Hong, S.; Faibish, R. and Elimelech, M. (1997) Kinetics of permeate flux decline in crossflow membrane filtration of colloidal suspensions, Journal of Colloid and Interface Science, 196:267-277.

15. Huang, L. and Morrissey, M. (1998) Fouling of membranes during microfiltration of surimi wash water – roles of pore blocking and surface cake formation. Journal of Membrane Science, 144:113-123.

16. Jonsson, A. and Jonsson, B. (1996) Colloidal fouling during ultrafiltration, Separation Science and Technology, 31:2611-2620.

17. Kim, K.; Fane, A.; Fell, C. and Joy, D. (1992) Fouling mechanisms of membranes during protein ultrafiltration, Journal of Membrane Science, 68:79-91.

18. Koltuniewicz, A. and Field, R. (1996) Process factors during removal of oil-in-water emulsions with crossflow microfiltration. Desalination, 105:79-89.

19. Lipp, P.; Baldauf, G.; Schick, R.; Elsenhans, K. and Stabel, H. (1998) Integration of ultrafiltration to conventional drinking water treatment for a better particle removal – efficiency and costs. Desalination, 119:133-142.

20. Lojkine, M.; Field, R. and Howell, J. (1992) Crossflow microfiltration of cell suspensions: a review of models with emphasis on particle size effects. Food and Bioproducts Processing, 70:149-164.

21. Ma, H.; Bowman, C. and Davis, R. (2000) Membrane fouling reduction by backpulsing and surface modification. Journal of Membrane Science, 173:191-200.

22. Marchese, J.; Ochoa, N.; Pagliero, C. and Almandoz, C. (2000) Pilot-scale ultrafiltration of an emulsified oil wastewater. Environmental Science and Technology, 34:2990-2996.

23. McDonogh, R.; Fell, C. and Fane, A. (1984) Surface charge and permeability in the ultrafiltration of non-flocculating colloids. Journal of Membrane Science, 21:285-294.

24. McDonogh, R.; Fell, C. and Fane, A. (1989) Charge effects in the cross-flow filtration of colloids and particulates. Journal of Membrane Science, 43:69-85.

25. McDonogh, R.; Welsch, K.; Fell, C. and Fane, A. (1992) Incorporation of the cake pressure profiles in the calculation of the effect of particle charge on the permeability of filter cakes obtained in the filtration of colloids and particulates. Journal of Membrane Science, 72:197-204.

26. Serra, C.; Durand-Bourlier, L.; Clifton, M.; Moulin, P.; Rouch, J. and Aptel, P. (1999) Use of air sparging to improve backwash efficiency in hollow-fiber modules. Journal of Membrane Science, 161:95-113.

27. Song, L. and Elimelech, M. (1995) Theory of concentration polarization in crossflow filtration, Journal of the Chemical Society, Faraday Transactions, 91:3389-3398.

28. Tarleton, E. and Wakeman, R. (1993) Understanding flux decline in cross-flow microfiltration 1. Effects of particle and pore-size. Chemical Engineering Research and Design, 71: 399-410.

29. Tracey, E. and Davis, R. (1994) Protein fouling of track-etched polycarbonate microfiltration membranes. Journal of Colloid and Interface Science, 167:104-116.

30. Vrijenhoek, E.; Hong, S. and Elimelech, M. (2001) Influence of membrane surface properties on initial rate of colloidal fouling of reverse osmosis and nanofiltration membranes. Journal of Membrane Science, 188:115-128.

31. Xu, Y.; Dodds, J. and Leclerc, D. (1995) Optimization of a discontinuous microfiltration-backwash process. Journal of Chemical Engineering, 57:247-251.

CHAPTER 7
CONCLUSIONS AND OBSERVATIONS

Significant conclusions and observations regarding membrane fouling made during the aforementioned studies are presented below:

- Membrane fouling increased with increasing surface roughness, as measured by the surface area difference, during the reverse osmosis/nanofiltration membrane treatment of a high organic surficial groundwater.
- The presence of monochloramine was determined to adversely impact the integrity of diffusion controlled membranes as determined through non-linear mass loading and resistance modeling of data collected throughout a 2,000 hour pilot study using a highly turbid and organic surface water.
- The results obtained from the analysis of fouled membrane elements treating filtered secondary wastewater effluent indicated organic fouling resulting from dissolved organic carbon and polysaccharides may not be predicted by mass loading and/or resistance models using total organic carbon as an independent variable.
- Increases in the particle packing density of the cake layer formed during the microfiltration of colloidal suspensions resulted in a decrease in the efficiency of backwashing procedures. Increases in the ionic strength of the colloidal suspension increased the density of the cake layer formed during filtration and decreased the efficiency of the backwashing procedures. The density of the cake layer and the

efficiency of backwashing procedures were independent of particle concentrations and operating pressures over the ranges investigated.

- Polyacrylate antiscalants, frequently utilized in full-scale membrane treatment facilities to prevent scaling, increased AOC concentrations which may contribute to the biological fouling of membrane systems. While the hybrid nanofiltration/reverse osmosis water treatment facility examined during this study was capable of removing 63.4 percent of AOC to a level of 60 μg acetate-C/L, it was not capable of producing a biologically stable product water. Biological fouling may be partially responsible for the linear decline in membrane productivity observed in this water treatment facility as AOC concentrations were sufficient to sustain biological activity.